DEVELOPMENT OF HETEROGENEOUS BASE CATALYSTS FOR ALDOL CONDENSATION BETWEEN FURFURAL AND ACETONE AND FOR TRANSESTERIFICATION OF PALM OIL

Narongrit Sosa

A Thesis Submitted in Partial Fulfillment of the Requirements for the

Degree of Doctor of Philosophy in Chemistry

Suranaree University of Technology

Academic Year 2019

การพัฒนาตัวเร่งปฏิกิริยาวิวิธพันธุ์ชนิดเบสสำหรับ
การควบแน่นแบบอัลดอลระหว่างเฟอร์ฟูรัลและอะซิโตน
และสำหรับทรานส์เอสเทอริฟิเคชันของน้ำมันปาล์ม

นายณรงค์ฤทธิ์ โสสะ

วิทยานิพนธ์นี้เป็นส่วนหนึ่งของการศึกษาตามหลักสูตรปริญญาวิทยาศาสตรดุษฎีบัณฑิต
สาขาวิชาเคมี
มหาวิทยาลัยเทคโนโลยีสุรนารี
ปีการศึกษา 2562

DEVELOPMENT OF HETEROGENEOUS BASE CATALYSTS FOR ALDOL CONDENSATION BETWEEN FURFURAL AND ACETONE AND FOR TRANSESTERIFICATION OF PALM OIL

Suranaree University of Technology has approved this thesis submitted in partial fulfillment of the requirements for the Degree of Doctor of Philosophy.

Thesis Examining Committee

_____
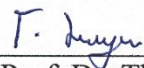
(Asst. Prof. Dr. Thanaporn Manyum)

Chairperson

_____
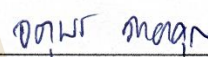
(Prof. Dr. Jatuporn Wittayakun)

Member (Thesis advisor)

_____
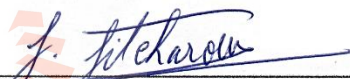
(Asst. Prof. Dr. Juthamas Jitcharoen)

Member

_____

(Assoc. Prof. Dr. Sanchai Prayoonpokarach)

Member

_____

(Assoc. Prof. Dr. Rapee Utke)

Member
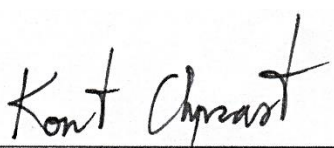
_____
(Assoc. Prof. Flt. Lt. Dr. Kontorn Chamniprasart)

Vice Rector for Academic Affairs

and Internationalization

_____
(Assoc. Prof. Dr. Worawat Meevasana)

Dean of Institute of Science

ฉนรงค์ฤทธิ์ โสสะ : การพัฒนาตัวเร่งปฏิกิริยาวิวิธพันธุ์ชนิดเบสสำหรับการควบแน่นแบบ
อัลดอลระหว่างเฟอร์ฟูรัลและอะซิโตนและสำหรับทรานส์เอสเทอริฟิเคชันของน้ำมัน
ปาล์ม (DEVELOPMENT OF HETEROGENEOUS BASE CATALYSTS FOR
ALDOL CONDENSATION BETWEEN FURFURAL AND ACETONE AND
FOR TRANSESTERIFICATION OF PALM OIL) อาจารย์ที่ปรึกษา : ศาสตราจารย์
ดร.จตุพร วิทยาคุณ, 127 หน้า

วิทยานิพนธ์นี้เกี่ยวข้องกับการปรับปรุงตัวเร่งปฏิกิริยาวิวิธพันธุ์ชนิดเบสบนตัวรองรับที่
แตกต่างกัน ซึ่งเตรียมด้วยวิธีการต่าง ๆ ได้แก่ การตรึงด้วยวิธีดั้งเดิม การใช้อัลตราซาวด์เข้าร่วม และ
การใช้ความร้อน เพื่อการใช้งานในการควบแน่นแบบอัลดอลและทรานส์เอสเทอริฟิเคชัน งานนี้
เริ่มต้นโดยการตรึงอะมิโนโพรพิลไตรเอท็อกซีไซเลน (APTES) กับ SBA-15 ด้วยวิธีดั้งเดิม และ
การยึดติดเพิ่มเติมด้วยวาเนดิลอะซิติลอะซิโตเนต โดยทดสอบตัวเร่งปฏิกิริยาในการควบแน่น
แบบอัลดอลแบบ in situ ระหว่างเฟอร์ฟูรัลและอะซิโตน ปฏิกิริยาที่ถูกเร่งด้วย SBA-15 ที่ตรึงด้วย
APTES เท่านั้นที่แสดงการเกิดเฟอร์ฟูรัลบิวทีโนน (FB) ได้สูงกว่าตัวเร่งปฏิกิริยาที่ยึดติดกับออกโซ
วาเนเดียม เนื่องจากความเป็นเบสที่สูงกว่า นอกจากนี้การเกิดเฟอร์ฟูรัลบิวทีโนนเพิ่มขึ้นตาม
อุณหภูมิ

เพื่อพัฒนากระบวนการตรึงให้ปลอดภัยและใช้เวลาการเตรียมสั้นลง จึงนำเสนอการใช้อัล
ตราซาวด์เข้าช่วยในการตรึงซิลิกาเจลกับ APTES ปริมาณต่าง ๆ ได้แก่ ร้อยละ 20 30 40 และ 50
โดยน้ำหนัก การโซนิเคชันช่วยส่งเสริมการสร้างพันธะระหว่าง APTES และซิลิกาเจล โดยเกิดการ
อุดตันรูพรุนน้อยกว่าวิธีการตรึงแบบดั้งเดิม ความเป็นเบสของตัวอย่างสูงขึ้นตามปริมาณ APTES
จากการรวมตัวแบบอัลดอลระหว่างเฟอร์ฟูรัลและอะซิโตนที่อุณหภูมิ 60 °C ตัวเร่งปฏิกิริยาที่ตรึง
APTES ร้อยละ 30โดยน้ำหนัก ให้ประสิทธิภาพการเร่งปฏิกิริยาดีที่สุด การแปลงผันเฟอร์ฟูรัลและ
ความจำเพาะต่อ FB เพิ่มขึ้นตามเวลาและเข้าสู่ค่าสูงสุดที่ 24 ชั่วโมง

สำหรับทรานส์เอสเทอริฟิเคชันของน้ำมันปาล์ม ได้เตรียมตัวเร่งปฏิกิริยาแคลเซียมจากดิน
สอพองธรรมชาติในประเทศไทยด้วยการใช้ความร้อนที่อุณหภูมิ 600 700 800 900 และ 1000 °C
กระบวนการนี้เปลี่ยนคาร์บอเนตไปเป็นไฮดรอกไซด์ และออกไซด์ที่อุณหภูมิ 800 และ 1000 °C
ตามลำดับ ความเข้มข้นของธาตุแคลเซียมเพิ่มขึ้นตามอุณหภูมิการเผา ทั้งสัณฐานวิทยาและพื้นที่ผิว
ต่างเปลี่ยนไประหว่างการเผา จากการสลายตัวของ 2-เมทิลบิวท์-3-ไอน์-2-ออล (MBOH) ความเป็น
เบสของตำแหน่งเบสบนตัวเร่งปฏิกิริยาแคลเซียมเหล่านี้เพิ่มขึ้นตามอุณหภูมิการเผา   สุดท้ายได้นำ
ตัวเร่งปฏิกิริยาแคลเซียมไปใช้ในทรานส์เอสเทอริฟิเคชันของน้ำมันปาล์ม   กับเมทานอลที่อุณหภูมิ

60 °C เป็นเวลา 3 ชั่วโมง ด้วยการเติมตัวเร่งปฏิกิริยาร้อยละ 1 โดยน้ำหนัก พบว่า ดินสอพองที่ถูกเผา
ที่อุณหภูมิ 800 °C เป็นตัวเร่งปฏิกิริยาที่เหมาะสม
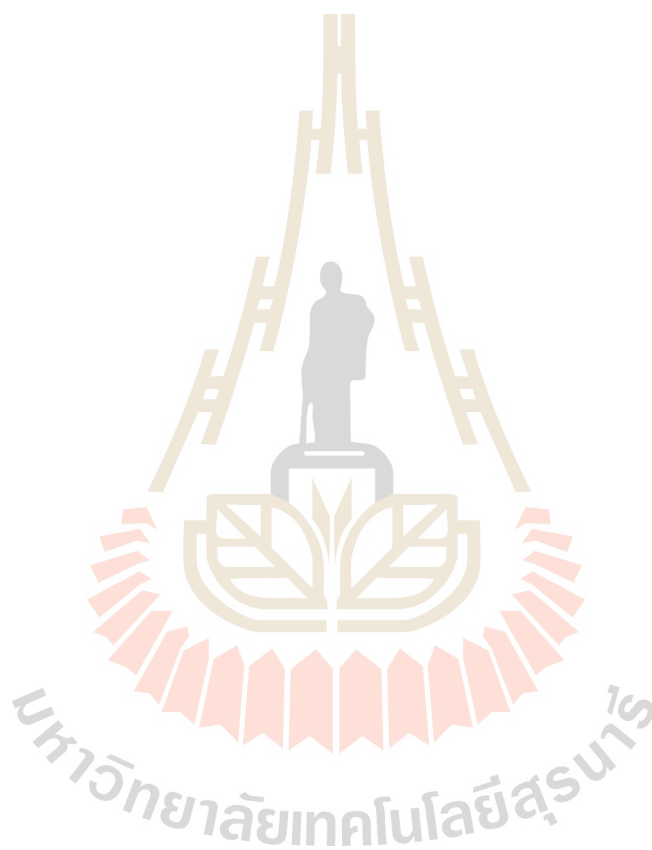
สาขาวิชาเคมี   ลายมือชื่อนักศึกษา _____

ปีการศึกษา 2562   ลายมือชื่ออาจารย์ที่ปรึกษา _____

NARONGRIT SOSA : DEVELOPMENT OF HETEROGENEOUS BASE
CATALYSTS FOR ALDOL CONDENSATION BETWEEN FURFURAL
AND ACETONE AND FOR TRANSESTERIFICATION OF PALM OIL.
THESIS ADVISOR : PROF. JATUPORN WITTAYAKUN, Ph.D. 127 PP.

BASE CATALYST/BASICITY/SBA-15/SILICA GEL/APTES/VANADIUM/
GRAFTING/ULTRASOUND/ALDOL CONDENSATION/FURFURAL/
TRANSESTERIFICATION/CALCITE/CALCIUM/PALM OIL/BIODIESEL

This thesis involves the improvement of heterogeneous base catalysts on different supports prepared by conventional, ultrasound-assisted grafting, and thermal treatment for utilization in aldol condensation and transesterification. This work began with the conventional grafting of aminopropyltriethoxysilane (APTES) with SBA-15 and further anchored by vanadyl acetylacetonate. These catalysts were tested in an in situ aldol condensation between furfural and acetone. Only the reaction catalyzed by SBA-15 grafted by APTES showed more furfurylbutenone (FB) formation than that by oxovanadium-anchored catalyst due to a higher basicity. In addition, the FB formation increased with the temperature.

To further develop the grafting process with a safer and shorter preparation period, ultrasound assistance was proposed in the grafting of silica gel by APTES loading of 20, 30, 40, and 50 wt. %. The sonication facilitated the bond formation between APTES and the silica gel with less pore-blocking than the conventional grafting method. The basicity of the samples increased with the amount of APTES. From aldol condensation between furfural and acetone at temperature of 60 ºC, the

catalyst with 30 wt. % of APTES loading gave the best catalytic activity. The furfural conversion and FB selectivity increased with time and reached the highest value at 24 h.

For the transesterification of palm oil, the calcium catalysts from natural marl in Thailand were prepared by thermal treatment at 600, 700, 800, 900, and 1000 °C. This process converted carbonate species to hydroxide and oxide at 800 and 1000 °C, respectively. The elemental concentration of calcium increased with the calcination temperatures. Both morphologies and surface areas changed during the calcination. From the decomposition of 2-methylbut-3-yn-2-ol (MBOH), the basicity of base sites on these calcium catalysts increased with the calcination temperatures. Finally, the calcium catalysts were employed in the transesterification between palm oil and methanol at temperature of 60 °C for 3 h. With catalyst loading of 1 wt. %, the marl calcined at temperature of 800 °C was the suitable catalyst.
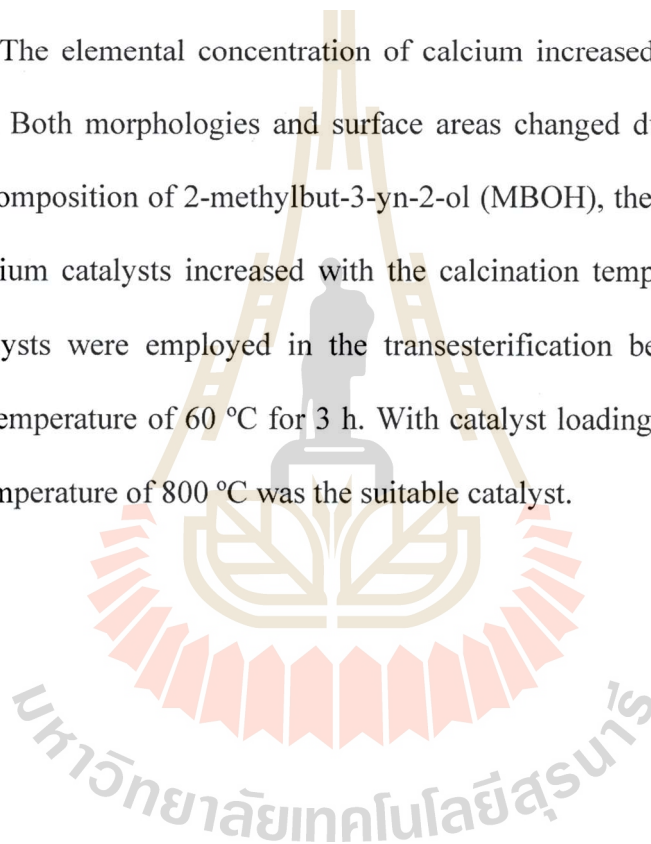
School of Chemistry

Academic Year 2019

Student's Signature _____

Advisor's Signature _____

ACKNOWLEDGEMENTS

Last but not least, this thesis is dedicated to my family for endless love and overwhelming encouragement.

Narongrit Sosa

CONTENTS

CONTENTS (Continued)

CONTENTS (Continued)

CONTENTS (Continued)

CONTENTS (Continued)

LIST OF TABLES

LIST OF FIGURES

LIST OF FIGURES (Continued)

LIST OF FIGURES (Continued)

LIST OF FIGURES (Continued)

LIST OF SCHEMES

CHAPTER I

INTRODUCTION

This thesis focuses on the development of heterogeneous base catalysts for aldol condensation between furfural and acetone and transesterification of palm oil. The thesis is divided into three parts. The first part compares the catalytic performance of mesoporous SBA-15 grafted with aminopropyltriethoxysilane (APTES) and oxovanadium complex for in situ aldol condensation between furfural and acetone. The grafting of these two species was done using a post-synthesis of SBA-15. However, the catalyst preparation has complexity and long operation time. Thus, the second part is designed to simplify the grafting using silica gel instead of SBA-15. This part involves ultrasound-assisted grafting to introduce different amounts of APTES on silica gel which is cheaper than SBA-15 under a shorter operation time and a less toxic system. The catalysts from the developed route were employed in the aldol condensation between furfural and acetone.

Besides aldol condensation, the transesterification of palm oil is studied as a tool to evaluate the strength of base catalysts. The third part of the thesis proposes an approach to determine the base strength of Thai natural marl calcined at different temperatures through the conversion of palm oil. In addition, both chemical and physical properties of as-prepared catalysts were measured by means of various techniques to receive the relevant information for revealing their catalytic roles in such reactions.

1.1 Research objectives

The first part of the thesis aims to graft a mesoporous siliceous SBA-15 support by APTES and oxovanadium complex through a conventional procedure and to study the catalytic activity of as-prepared samples on the in situ aldol condensation between furfural and acetone.

The focus of the second part is to develop the grafting procedure through ultrasound assistance of silica gel with various APTES loading and to investigate the catalytic performance on the aldol condensation between furfural and acetone.

Finally, the last part aims to prepare low-cost calcium catalysts from Thai natural marl calcined at different temperatures and to evaluate the base strength of prepared calcium catalysts by the conversion of palm oil through a transesterification reaction.

1.2 Scope and limitation of the study

In the first part research, the parent and mesoporous SBA-15 support grafted by APTES were synthesized according to the previous procedure by Yang, Hao, Zhang, and Kan (2011). The SBA-15 support grafted by APTES was further functionalized by an oxovanadium complex through the reported method (Pereira, Silva, Carvalho, Pires, and Freire, 2008; Zhu, Li, Zheng, Xu, and Li, 2012). An aldol condensation between furfural and acetone catalyzed by the grafted SBA-15 samples was carried out in in-situ attenuated total reflectance-Fourier transform infrared spectroscopy (ATR-FTIR) available at Vienna University of Technology.

In the second part, a commercial silica gel support was used without further purification. The silica gel was grafted with different APTES contents with the method

from the literature (Quang, Hatton, and Abu-Zahra, 2016) with ultrasound assistance using a probe-type ultrasonicator with a power of 130 W and a frequency of 20 kHz. The aldol condensation between furfural and acetone catalyzed by the grafted silica gel samples was carried out in a classical glassware setup at the operation temperature of 60 °C.

In the last part of the research, commercial Thai natural marl from a convenience store near Suranaree University of Technology was used without further purification. The raw material was calcined with the conditions reported by Ngamcharussrivichai, Nunthasanti, Tanachai, and Bunyakiat (2010). The conversion of palm oil through a transesterification reaction for the evaluation of base strength was monitored by means of thin-layer chromatography (TLC) according to the literature (Manadee et al., 2017)

1.3 References

Manadee, S., Sophiphun, O., Osakoo, N., Supamathanon, N., Kidkhunthod, P., Chanlek, N., Wittayakun, J., and Prayoonpokarach, S. (2017). Identification of potassium phase in catalysts supported on zeolite NaX and performance in transesterification of Jatropha seed oil. **Fuel Processing Technology**. 156: 62-67.

Ngamcharussrivichai, C., Nunthasanti, P., Tanachai, S., and Bunyakiat, K. (2010). Biodiesel production through transesterification over natural calciums. **Fuel Processing Technology**. 91(11): 1409-1415.

Pereira, C., Silva, A. R., Carvalho, A. P., Pires, J., and Freire, C. (2008). Vanadyl acetylacetonate anchored onto amine-functionalised clays and catalytic activity

in the epoxidation of geraniol. **Journal of Molecular Catalysis A: Chemical**. 283(1-2): 5-14.

Quang, D. V., Hatton, T. A., and Abu-Zahra, M. R. M. (2016). Thermally stable amine-grafted adsorbent prepared by impregnating 3-aminopropyltriethoxysilane on mesoporous silica for CO_2 capture. **Industrial & Engineering Chemistry Research**. 55(29): 7842-7852.

Yang, Y., Hao, S., Zhang, Y., and Kan, Q. (2011). Oxovanadium(IV) and dioxomolybdenum(VI) salen complexes tethered onto amino-functionalized SBA-15 for the epoxidation of cyclooctene. **Solid State Sciences**. 13(11): 1938-1942.

Zhu, Y., Li, H., Zheng, Q., Xu, J., and Li, X. (2012). Amine-functionalized SBA-15 with uniform morphology and well-defined mesostructure for highly sensitive chemosensors to detect formaldehyde vapor. **Langmuir**. 28(20): 7843-7850.

CHAPTER II

LITERATURE REVIEW

This literature review focuses on the development of heterogeneous base catalysts for the aldol condensation and the transesterification. The basis of both reactions is shortly presented. For aldol condensation, the properties of catalyst support including SBA-15 and silica gel are mentioned. The development of their basicity by conventional grafting with aminopropyltriethoxysilane (APTES), anchoring by oxo-vanadium complex, and ultrasound assistance are reviewed. For transesterification, the thermal treatment of calcium catalysts from Thai natural marl and the decomposition of 2-methylbut-3-yn-2-ol (MBOH) as a base strength test are also addressed.

2.1 Aldol condensation between furfural and acetone

Aldol condensation is the formation of carbon-carbon bonds through a reaction between two carbonyls such as ketone or aldehyde possessing an α-hydrogen on at least one of carbonyls (West, Liu, Peter, Gärtner, and Dumesic, 2008). This reaction is catalyzed by either acid or base catalysts. Among diverse lignocellulosic biomass-derived compounds, effective and inexpensive feedstocks in aldol condensation are furanic compounds such as furfural, 5-hydroxymethylfurfural (HMF) and methyl tetrahydrofuran (Faba, Díaz, and Ordóñez, 2012; Lange, van der Heide, van Buijtenen, and Price, 2012).

The possible reaction pathways of aldol condensation between furfural and acetone are illustrated in **Scheme 2.1**. The reaction in **equation 2.1** is the key step and desired pathway to produce furfurylbutenone (FB), a C8 condensate which could be used as a fuel intermediate in many applications. This reaction has 2 steps consisting of aldol reaction and condensation. In the first step, furfural is attacked by acetone over a catalyst to generate furfurylhydroxybutanone (FHB), a C8 aldol adduct, possessing both hydroxyl and ketone groups. In the last step, a water molecule is eliminated under the assistance of the catalyst to allow a formation of a C8 condensate or α,β-unsaturated ketone. Reactions in **equation 2.2** to **2.4** are assigned as side reactions.
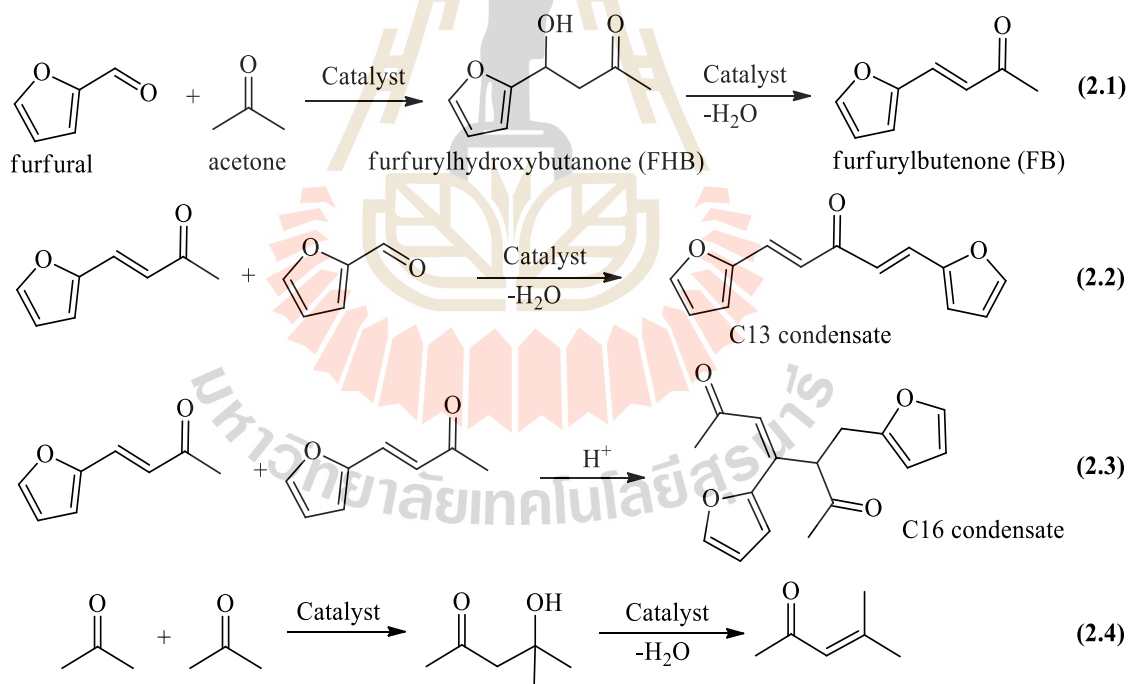
Scheme 2.1 Possible reaction pathways of aldol condensation between furfural and acetone modified from Kikhtyanin, Kubička, and Čejka (2015).

FB can be transformed into a promising platform molecule for the production of a high qualitative fuel through either hydrodeoxygenation or hydrogenation as shown in **Scheme 2.2**. However, such steps are disregarded in this thesis. From a point of view in an industrial application, FB can be utilized not only as a gasoline-engine fuel but also as a monomer in polymerization to produce a furfural-based resin (Fedotov, and Ugryumov, 2014; Olcay et al., 2013).

$$(2.5)$$
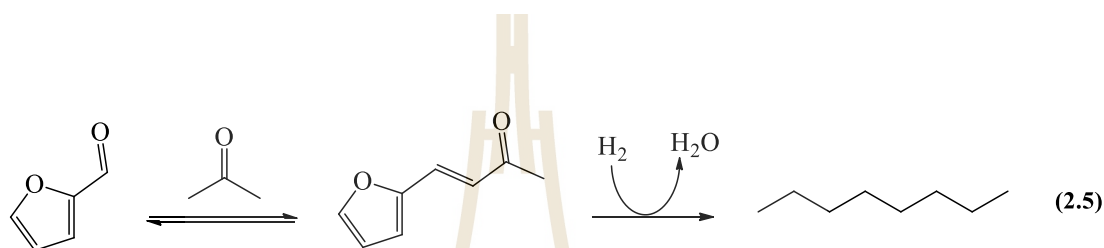
Scheme 2.2 Catalytic conversion of FB as a promising fuel intermediate to a usable liquid fuel via hydrogenation process (Faba, Díaz, and Ordóñez, 2013b).

Currently, research attention has been intensified in aldol condensation between furfural and acetone to obtain a high-quality sustainable petroleum- and chemical-refinery feedstocks. Several research groups have focused on modification and improvement of aldol condensation conditions to gain the optimal selectivity, conversion and other essential parameters of FB production.

2.2 Catalysts for aldol condensation between furfural and acetone

So far, an aldol condensation of lignocellulosic compounds could be achieved in the presence of a homogeneous catalyst such as NaOH and KOH providing a high conversion and yield. However, they have several disadvantages, for example,

corrosion of an operating reactor, difficulty of catalyst separation, poor catalyst reusability and environmental issue. Nowadays, many related works focus on various approaches to overcome such problems. Heterogeneous catalysts are interesting (Faba et al., 2012) because of easy separation and less environmental issue as there is no waste water production from a catalyst removal.

Numerous types of solid base materials such as Mg-Al layered double hydroxide (LDH), magnesia-zirconia (MgO-ZrO$_2$) and calcium oxide-zirconia (CaO-ZrO$_2$) have been used in aldol condensation. However, both leaching of active species and water interaction deactivate these catalysts (Faba, Díaz, and Ordóñez, 2013a). Moreover, the regeneration of spent catalyst requires a high temperature (Sádaba, Ojeda, Mariscal, Richards, and Granados, 2011). Surface functionalization with organic base moieties is proposed for catalyst preparation to solve such drawbacks.

Leaching of active species from a support surface could occur due to a weak interaction. This effect can make the catalyst inactive after regeneration. To avoid this drawback, the surface could be modified with organic molecules can enhance this drawback via a formation of the covalent bond between a desired active group and a modified support. The active site is rigidly immobilized on a surface-modified support and can prevent the leaching. Moreover, catalyst regeneration can be done under a low operating temperature by means of solvent extraction.

There are many ways to immobilize a surface with organic groups, for example, ammonia-amine reaction, nitridization, and co-assembly or organosilanes (Xie et al., 2009). One common grafting is aminoalkoxysilanes. Numerous mesoporous siliceous materials have been used as a support for grafting (Hartmann, 2005), for example, Tech molecular sieves (TMS), hexagonal mesoporous silica (HMS), Mobil composition of

matter (MCM), Santa Barbara amorphous (SBA), and silica gel. Particularly, Santa Barbara amorphous no. 15 (SBA-15) (An et al., 2014; Yang, Hao, Zhang, and Kan, 2011) and Mobil composition of matter no. 41 (MCM-41) (Collier, Ellebracht, Lindy, Moschetta, and Jones, 2016) are interesting because of their large pore, high surface area and thick pore wall (Hess, Hoefelmeyer, and Tilley, 2004; Xie et al., 2009).

In this thesis, siliceous materials are grafted with an aminoalkoxysilane. Both SBA-15 and silica gel are employed as supports due to excellent surface properties. For a grafted SBA-15, a vanadium complex is used for comparison of acid-base properties.

2.2.1 Mesoporous siliceous SBA-15

SBA-15 is an ordered mesoporous silica synthesized with a block-copolymer template composed of poly(ethylene oxide)$_x$-poly(propylene oxide)$_y$-poly(ethylene oxide)$_x$, (PEO)$_x$(PPO)$_y$(PEO)$_x$, (trade name: Pluronic). Its morphology is hexagonally ordered mesopores (Zhao, Huo, Feng, Chmelka, and Stucky, 1998). It has a wall thickness ranging from 3 to 7 nm. A thick wall makes it more stable hydrothermally and thermally than other silica materials. Moreover, the pore size of SBA-15 can be tuned from 6 to 15 nm by changing the template (Taguchi, and Schüth, 2005). Its large pore width can prevent pore-blocking during the grafting with an aminoalkoxysilane or anchoring with a transition metal complex.

2.2.2 Silica gel

Silica gel is a porous material with large surface area, excellent mechanical resistance, and commercially available. Importantly, silica gel surfaces contain silanol groups (Si-OH) which are chemically usable for functionalization by

organic molecules (Li, Li, and Zhang, 2006). From the literature review, the silica gel grafted with APTES and glutaraldehyde in order to further immobilize with a cellulose (Zhang, Hegab, Lvov, Dale Snow, and Palmer, 2016). The APTES species rapidly adsorbed on the surface within several minutes, while the grafting step was completed in 24 hours. Ramasamy, Khan, Repo, and Sillanpää (2017) prepared a silica gel grafting with different aminotrialkoxysilanes. The silica gel was refluxed in a hydrochloric acid solution prior to the grafting in toluene. The report indicated the surface silanols reacted with these precursors to form new functional groups. Additionally, these aminosilanes located on the mesopore walls of the silica gel. Thus, this literature suggests that silica gel is suitable for grafting by aminosilanes.

2.3 Conventional grafting of mesoporous supports by amino-propyltriethoxysilane

Surface functionalization by a grafting method can be classified into two distinct pathways including a direct synthesis, called co-condensation or co-assembly route, and a post-synthesis method, also called grafting (Maria Chong, and Zhao, 2003). The co-condensation method as illustrated in **Figure 2.1(a)** is commonly used to functionalize a mesoporous material via a one-pot synthesis by copolymerization between silica or organosilica and organosilane in the presence of a structure-directing agent (Burleigh, Markowitz, Spector, and Gaber, 2001). The method provides a control of the amount of organic incorporated groups and uniform surface coverage (Malvi et al., 2009). However, some amount of the group could be inserted into the material framework leading to a low active-site distribution. Grafting as illustrated in **Figure 2.1(b)** is an approach to generate amino-modifying species on material surfaces via covalent

bonding between an organosilane and surface silanol groups. The advantages of the method are better-defined structure and hydrolytic stability of the produced materials (Zhu, Li, Zheng, Xu, and Li, 2012). Moreover, the structural framework of these prepared solids can be preserved.

Various organic functional groups have been used for grafting, for example, vinyl (Wach et al., 2015; Wang, Zibrowius, Yang, Spliethoff, and Schuth, 2004), sulfonic acid (Cattaneo et al., 2016; Melero, Bautista, Morales, Iglesias, and Sánchez-Vázquez, 2015), carboxylic acid (Deka et al., 2014; Gao, Zhang, Yang, Gao, and Zhao, 2010) and amines (Yang et al., 2011). Among these organic groups, 3-aminopropyl-triethoxysilane (APTES) is commonly used as an aminosilane group. It provides a less steric hindrance and can facilitate the anchoring with a transition metal complex in SBA-15 surface modification. In this thesis, SBA-15 is grafted with APTES.

a) Co-condensation method   b) Grafting
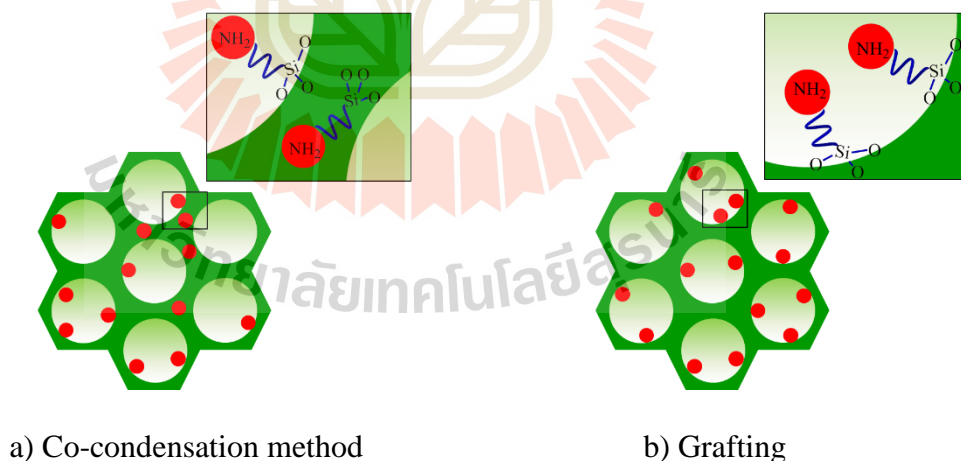
Figure 2.1 Graphical illustration of functionalization on an ordered mesoporous silica via a) co-condensation method and b) grafting.

2.3.1   Anchoring of oxovanadium complex on SBA-15 grafted by APTES

There are considerable research interests on the utilization of transition metal complexes as active catalysts for various homogeneous liquid-phase reactions. Although they can provide efficient catalytic performance, there are several inherent drawbacks, for example, high price, difficult separation from the reaction mixture and low stability. These disadvantages have been solved by means of heterogenization techniques. One of the most common routes is immobilization, also called anchoring, of transition metal compounds. This method makes the material easy to reuse leading to a green catalytic process. The heterogenization strategy can be categorized into two steps. The first step is a synthesis of an anchoring support, also known as a modified material containing an active terminal organic functional group. The last step is an immobilization of the desired transition metal complex on the organo-grafted support.

Heterogenization of oxovanadium based complexes tethered on the modified SBA-15 support is used in many applications such as epoxidation of organic compounds (Grivani, Tahmasebi, Khalaji, Fejfarová, and Dušek, 2013; Jarrais, Silva, and Freire, 2005; Pereira, Silva, Carvalho, Pires, and Freire, 2008). There are a few studies describing the utilization of vanadium phosphate-based catalysts in gas-phase aldol condensation (Tanner et al., 2002; Thomas et al., 2002). Up to date, there are no reports about the catalytic activity of the oxovanadium species anchored on amino-modified SBA-15 for aldol condensation between furfural and acetone. in this thesis, the aldol condensation between furfural and acetone in the liquid phase was catalyzed by oxovanadium complex anchored by APTES as an amino group on modified SBA-15 support.

2.4   Ultrasound-assisted grafting with APTES

Ultrasonic irradiation has been used in many syntheses and modifications of materials because it is environmentally friendly and convenient. With a short operating time, it could be considered as a replacement for conventional power sources (Dinari, and Haghighi, 2018). Ultrasound can be applied in grafting to avoid high temperature, pressure and a long preparation period. The mechanism of ultrasonic irradiation for material modification and synthesis is shown in **Scheme 2.3**. Acoustic cavitation generated from an ultrasonic probe provides formation, growth, and collapse of hot gas bubbles in a liquid system (Mohammadnezhad, Abad, Soltani, and Dinari, 2017). Then, the collapsing bubbles increase temperature and pressure, which enhances the diffusion of a grafting precursor into a support pore and improves surface interaction (Soltani, Dinari, and Mohammadnezhad, 2018; Suslick, and Flannigan, 2008).
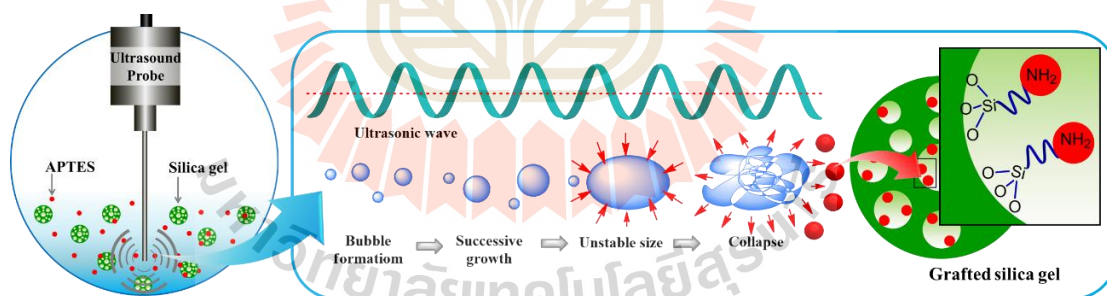
Scheme 2.3 Illustration of ultrasound-assisted grafting of silica gel with APTES.

There are several reports on the utilization of ultrasonication in grafting of silane precursors on siliceous materials. The ultrasound promotes grafting of the aminosilane on the porous support. Mallakpour, Dinari, and Mohammadnezhad (2015) modified the surface of mesoporous SBA-15 by grafting with *N*-trimellitylimido-L-methionine, a

chiral diacid by refluxing in ethanol for 24 hours, followed by irradiating for another 2 hours. They suggested that cavitation from ultrasonic irradiation is a crucial factor in forming the bond between the carbonyl group of the chiral diacid and a silanol group on the SBA-15 surface. Recently, mesoporous MCM-41 was grafted with APTES under refluxing followed by an ultrasound application to exfoliate the agglomerates (Mohammadnezhad et al., 2017; Soltani et al., 2018). They mentioned that the siliceous MCM-41 sample was not only occupied by the silane agent but also deagglomerated after the sonication process.

From the previous research, the ultrasonication for material preparation has used with a refluxing step which leads to an increase in the preparation time. Moreover, there are no reports on grafting of silica gel with APTES via ultrasonication. Thus, the purpose of this work is to compare the properties of base catalysts prepared by ultrasound-assisted with conventional grafting of APTES on silica gel. The physicochemical properties of the samples with various aminopropyl concentrations and catalytic activity in the aldol condensation of furfural and acetone are studied.

2.5 Thermal treatment of calcium catalysts from Thai natural marl for transesterification of palm oil

2.5.1 Thermal treatment of Thai natural marl

Natural marl is a low-cost raw material for the preparation of calcium samples which can be found in many areas of Thailand. It is one of carbonate-rich compounds with a small amount of alumina (Al_2O_3), silica (SiO_2), and other metal oxides. Although calcium carbonate ($CaCO_3$) is a predominant species in the marl sample, it gives a low conversion of triglycerides in a transesterification reaction. It also

requires a high temperature to promote a high reaction activity owing to a low base strength in nature (Ngamcharussrivichai, Wiwatnimit, and Wangnoi, 2007). Thermal treatment is among various routes to improve the basicity of the marl samples. This literature suggested that the base strength of calcium-based catalysts is a predominant effect on the activity of base-catalyzed transesterification. Hence, heterogeneous catalysts require specific and precise techniques to investigate a base property after a preparation process.

2.5.2 Decomposition of 2-methylbut-3-yn-2-ol (MBOH)

According to the limitation of the thermal property of carbonate-rich materials, the basicity could not be measured by temperature-programmed desorption of carbon dioxide (CO_2-TPD) due to the decomposition of the carbonate at a desorption temperature higher than 800 ℃ (Ngamcharussrivichai, Nunthasanti, Tanachai, and Bunyakiat, 2010). Hence, the decomposition of 2-methylbut-3-yn-2-ol (MBOH) has been taken into account as a test reaction to evaluate the base strength by consideration of obtained products catalyzed by different active sites (Kulawong, Prayoonpokarach, Roessner, and Wittayakun, 2015; Supamathanon, Wittayakun, Prayoonpokarach, Supronowicz, and Roessner, 2012). The benefits of this method consist of an operation temperature lower than that of the decomposition of carbonate compounds (less than 180 ℃) and classification of surface-active species in nature.

The MBOH decomposition enables differentiation of acidic, basic active and defect sites (Kulawong et al., 2015) in terms of the selectivity of obtained products as shown in **Scheme 2.4**. For instance, 3-methylbut-3-en-1-yne (MBYNE) and 3-methylbut-2-enal (prenal) are produced from an acid-catalyzed pathway. 3-Methylbut-

3-en-2-one (MIPK) and 3-hydroxy-3-methylbutan-2-one (HMB) are obtained from a defect-site-catalyzed pathway. A base-catalyzed route provides both acetylene and acetone. Thus, the basicity of the marl calcined at different temperatures could be compared directly from the conversion of MBOH and the product selectivity.
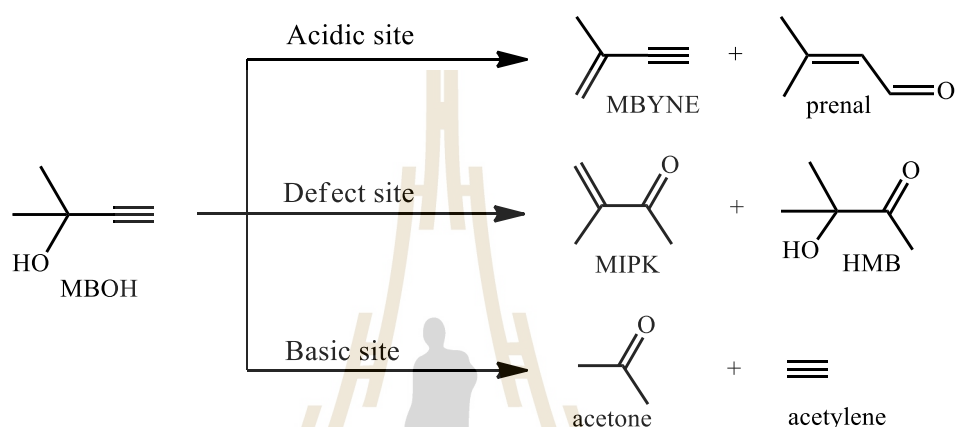
Scheme 2.4 Chemical pathways of MBOH decomposition over different active sites (Supamathanon et al., 2012).

2.5.3 Transesterification of palm oil

Transesterification between triglyceride and methanol has been commonly used to produce biodiesel as an alternative fuel resource as seen in **Scheme 2.5**. Both triglyceride and methanol react to each other under the presence of a base catalyst. Major products from this reaction are composed of methyl esters (ME) and glycerol. In this reaction, palm oil has been chosen as a triglyceride source due to low cost and plenty in Thailand (Ngamcharussrivichai et al., 2010; Roschat, Siritanon, Yoosuk, and Promarak, 2016). Commonly, the transesterification of palm oil could be done under the presence of base catalysts. In addition, the basicity of catalysts is the

predominant effect on the conversion of triglycerides (Manadee et al., 2017; Ngamcharussrivichai et al., 2007). From a point of view, this reaction could be used to evaluate the base strength of catalysts prepared by different conditions.
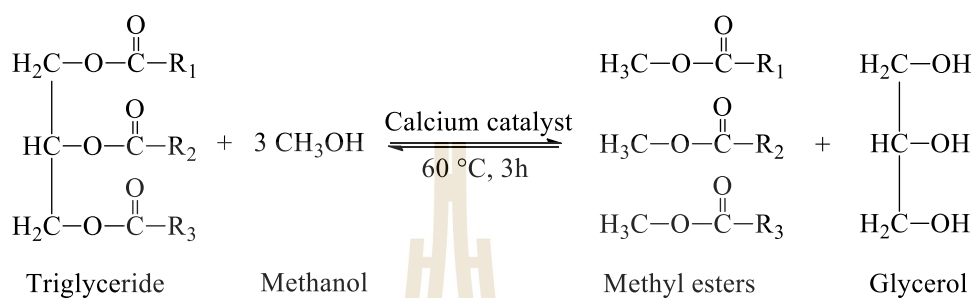
Scheme 2.5 Transesterification between triglyceride and methanol for the production of biodiesel.

2.6   References

An, Z., He, J., Dai, Y., Yu, C., Li, B., and He, J. (2014). Enhanced heterogeneous asymmetric catalysis via the acid–base cooperation between achiral silanols of mesoporous supports and immobilized chiral amines. **Journal of Catalysis**. 317: 105-113.

Burleigh, M. C., Markowitz, M. A., Spector, M. S., and Gaber, B. P. (2001). Direct synthesis of periodic mesoporous organosilicas: functional incorporation by co-condensation with organosilanes. **The Journal of Physical Chemistry B**. 105(41): 9935-9942.

Cattaneo, A. S., Ferrara, C., Villa, D. C., Angioni, S., Milanese, C., Capsoni, D., Grandi, S., Mustarelli, P., Allodi, V., Mariotto, G., Brutti, S., and Quartarone, E. (2016).

SBA-15 mesoporous silica highly functionalized with propylsulfonic pendants: a thorough physico-chemical characterization. **Microporous and Mesoporous Materials**. 219: 219-229.

Collier, V. E., Ellebracht, N. C., Lindy, G. I., Moschetta, E. G., and Jones, C. W. (2016). Kinetic and mechanistic examination of acid–base bifunctional aminosilica catalysts in aldol and nitroaldol condensations. **ACS Catalysis**. 6(1): 460-468.

Deka, J. R., Kao, H.-M., Huang, S.-Y., Chang, W.-C., Ting, C.-C., Rath, P. C., and Chen, C.-S. (2014). Ethane-bridged periodic mesoporous organosilicas functionalized with high loadings of carboxylic acid groups: synthesis, bifunctionalization, and fabrication of metal nanoparticles. **Chemistry – A European Journal**. 20(3): 894-903.

Dinari, M., and Haghighi, A. (2018). Ultrasound-assisted synthesis of nanocomposites based on aromatic polyamide and modified ZnO nanoparticle for removal of toxic Cr(VI) from water. **Ultrasonics Sonochemistry**. 41: 75-84.

Faba, L., Díaz, E., and Ordóñez, S. (2012). Aqueous-phase furfural-acetone aldol condensation over basic mixed oxides. **Applied Catalysis B: Environmental**. 113-114: 201-211.

Faba, L., Díaz, E., and Ordóñez, S. (2013a). Improvement of the stability of basic mixed oxides used as catalysts for aldol condensation of bio-derived compounds by palladium addition. **Biomass and Bioenergy**. 56: 592-599.

Faba, L., Díaz, E., and Ordóñez, S. (2013b). Improvement on the catalytic performance of Mg-Zr mixed oxides for furfural-acetone aldol condensation by supporting on mesoporous carbons. **ChemSusChem**. 6(3): 463-473.

Fedotov, A. A., and Ugryumov, S. A. (2014). Chemical processes of structuring of furfural acetone monomer FA. **Polymer Science Series D**. 7(1): 65-68.

Gao, P., Zhang, T., Yang, H., Gao, C., and Zhao, Y. (2010). Synthesis and characterization of a novel neighboring dicarboxyl-modified SBA-15 via the Diels–Alder reaction. **Materials Letters**. 64(19): 2084-2086.

Grivani, G., Tahmasebi, V., Khalaji, A. D., Fejfarová, K., and Dušek, M. (2013). Synthesis, characterization and crystal structure determination of a new vanadium(IV) Schiff base complex (VOL$_2$) and investigation of its catalytic activity in the epoxidation of cyclooctene. **Polyhedron**. 51: 54-60.

Hartmann, M. (2005). Ordered mesoporous materials for bioadsorption and biocatalysis. **Chemistry of Materials**. 17(18): 4577-4593.

Hess, C., Hoefelmeyer, J. D., and Tilley, T. D. (2004). Spectroscopic characterization of highly dispersed vanadia supported on SBA-15. **The Journal of Physical Chemistry B**. 108(28): 9703-9709.

Jarrais, B., Silva, A. R., and Freire, C. (2005). Anchoring of vanadyl acetylacetonate onto amine-functionalised activated carbons: catalytic activity in the epoxidation of an allylic alcohol. **European Journal of Inorganic Chemistry**. 2005(22): 4582-4589.

Kikhtyanin, O., Kubička, D., and Čejka, J. (2015). Toward understanding of the role of Lewis acidity in aldol condensation of acetone and furfural using MOF and zeolite catalysts. **Catalysis Today**. 243: 158-162.

Kulawong, S., Prayoonpokarach, S., Roessner, F., and Wittayakun, J. (2015). Acidity of modified mordenites synthesized from rice husk silica and catalytic transformation of methylbutynol. **Química Nova**. 38: 191-195.

Lange, J. P., van der Heide, E., van Buijtenen, J., and Price, R. (2012). Furfural-a promising platform for lignocellulosic biofuels. **ChemSusChem**. 5(1): 150-166.

Li, F., Li, X. M., and Zhang, S. S. (2006). One-pot preparation of silica-supported hybrid immobilized metal affinity adsorbent with macroporous surface based on surface imprinting coating technique combined with polysaccharide incorporated sol-gel process. **Journal of Chromatography A**. 1129(2): 223-230.

Mallakpour, S., Dinari, M., and Mohammadnezhad, G. (2015). Ultrasonic assisted organo-modification of mesoporous SBA-15 with *N*-trimellitylimido-L-methionine and preparation of the poly(amide-imide)/SBA nanocomposites. **Progress in Organic Coatings**. 78: 300-306.

Malvi, B., Sarkar, B. R., Pati, D., Mathew, R., Ajithkumar, T. G., and Sen Gupta, S. (2009). "Clickable" SBA-15 mesoporous materials: synthesis, characterization and their reaction with alkynes. **Journal of Materials Chemistry**. 19(10): 1409-1416.

Manadee, S., Sophiphun, O., Osakoo, N., Supamathanon, N., Kidkhunthod, P., Chanlek, N., Wittayakun, J., and Prayoonpokarach, S. (2017). Identification of potassium phase in catalysts supported on zeolite NaX and performance in transesterification of Jatropha seed oil. **Fuel Processing Technology**. 156: 62-67.

Maria Chong, A. S., and Zhao, X. S. (2003). Functionalization of SBA-15 with APTES and characterization of functionalized materials. **The Journal of Physical Chemistry B**. 107(46): 12650-12657.

Melero, J. A., Bautista, L. F., Morales, G., Iglesias, J., and Sánchez-Vázquez, R. (2015). Acid-catalyzed production of biodiesel over arenesulfonic SBA-15: insights into the role of water in the reaction network. **Renewable Energy**. 75: 425-432.

Mohammadnezhad, G., Abad, S., Soltani, R., and Dinari, M. (2017). Study on thermal, mechanical and adsorption properties of amine-functionalized MCM-41/PMMA and MCM-41/PS nanocomposites prepared by ultrasonic irradiation. **Ultrasonics Sonochemistry**. 39: 765-773.

Ngamcharussrivichai, C., Nunthasanti, P., Tanachai, S., and Bunyakiat, K. (2010). Biodiesel production through transesterification over natural calciums. **Fuel Processing Technology**. 91(11): 1409-1415.

Ngamcharussrivichai, C., Wiwatnimit, W., and Wangnoi, S. (2007). Modified dolomites as catalysts for palm kernel oil transesterification. **Journal of Molecular Catalysis A: Chemical**. 276(1-2): 24-33.

Olcay, H., Subrahmanyam, A. V., Xing, R., Lajoie, J., Dumesic, J. A., and Huber, G. W. (2013). Production of renewable petroleum refinery diesel and jet fuel feedstocks from hemicellulose sugar streams. **Energy & Environmental Science**. 6(1): 205.

Pereira, C., Silva, A. R., Carvalho, A. P., Pires, J., and Freire, C. (2008). Vanadyl acetylacetonate anchored onto amine-functionalised clays and catalytic activity in the epoxidation of geraniol. **Journal of Molecular Catalysis A: Chemical**. 283(1-2): 5-14.

Ramasamy, D. L., Khan, S., Repo, E., and Sillanpää, M. (2017). Synthesis of mesoporous and microporous amine and non-amine functionalized silica gels for the application of rare earth elements (REE) recovery from the waste water-

understanding the role of pH, temperature, calcination and mechanism in Light REE and Heavy REE separation. **Chemical Engineering Journal**. 322: 56-65.

Roschat, W., Siritanon, T., Yoosuk, B., and Promarak, V. (2016). Biodiesel production from palm oil using hydrated lime-derived CaO as a low-cost basic heterogeneous catalyst. **Energy Conversion and Management**. 108: 459-467.

Sádaba, I., Ojeda, M., Mariscal, R., Richards, R., and Granados, M. L. (2011). Mg–Zr mixed oxides for aqueous aldol condensation of furfural with acetone: effect of preparation method and activation temperature. **Catalysis Today**. 167(1): 77-83.

Soltani, R., Dinari, M., and Mohammadnezhad, G. (2018). Ultrasonic-assisted synthesis of novel nanocomposite of poly(vinyl alcohol) and amino-modified MCM-41: A green adsorbent for Cd(II) removal. **Ultrasonics Sonochemistry**. 40(Pt A): 533-542.

Supamathanon, N., Wittayakun, J., Prayoonpokarach, S., Supronowicz, W., and Roessner, F. (2012). Basic properties of potassium oxide supported on zeolite Y studied by pyrrole-TPD and catalytic conversion of methylbutynol. **Química Nova**. 35: 1719-1723.

Suslick, K. S., and Flannigan, D. J. (2008). Inside a collapsing bubble: sonoluminescence and the conditions during cavitation. **Annual Review of Physical Chemistry**. 59(1): 659-683.

Taguchi, A., and Schüth, F. (2005). Ordered mesoporous materials in catalysis. **Microporous and Mesoporous Materials**. 77(1): 1-45.

Tanner, R., Gill, P., Wells, R., Bailie, J. E., Kelly, G., Jackson, S. D., and Hutchings, G. J. (2002). Aldol condensation reactions of acetone and formaldehyde over

vanadium phosphate catalysts: comments on the acid-base properties. **Physical Chemistry Chemical Physics**. 4(4): 688-695.

Thomas, L., Tanner, R., Gill, P., Wells, R., Bailie, J. E., Kelly, G., Jackson, S. D., and Hutchings, G. (2002). Aldol condensation reactions of acetone over alkali-modified vanadium phosphate catalysts. **Physical Chemistry Chemical Physics**. 4(18): 4555-4560.

Wach, A., Drozdek, M., Dudek, B., Biazik, M., Łątka, P., Michalik, M., and Kuśtrowski, P. (2015). Differences in catalytic activity of poly(vinylamine) introduced on surface of mesoporous SBA-15 by grafting from and grafting onto methods in Knoevenagel condensation. **The Journal of Physical Chemistry C**. 119(34): 19954-19966.

Wang, Y., Zibrowius, B., Yang, C.-M., Spliethoff, B., and Schuth, F. (2004). Synthesis and characterization of large-pore vinyl-functionalized mesoporous silica SBA-15. **Chemical Communications**. (1): 46-47.

West, R. M., Liu, Z. Y., Peter, M., Gärtner, C. A., and Dumesic, J. A. (2008). Carbon–carbon bond formation for biomass-derived furfurals and ketones by aldol condensation in a biphasic system. **Journal of Molecular Catalysis A: Chemical**. 296(1-2): 18-27.

Xie, Y., Sharma, K. K., Anan, A., Wang, G., Biradar, A. V., and Asefa, T. (2009). Efficient solid-base catalysts for aldol reaction by optimizing the density and type of organoamine groups on nanoporous silica. **Journal of Catalysis**. 265(2): 131-140.

Yang, Y., Hao, S., Zhang, Y., and Kan, Q. (2011). Oxovanadium(IV) and dioxomolybdenum(VI) salen complexes tethered onto amino-functionalized

SBA-15 for the epoxidation of cyclooctene. **Solid State Sciences**. 13(11): 1938-1942.

Zhang, D., Hegab, H. E., Lvov, Y., Dale Snow, L., and Palmer, J. (2016). Immobilization of cellulase on a silica gel substrate modified using a 3-APTES self-assembled monolayer. **SpringerPlus**. 5(1): 48.

Zhao, D., Huo, Q., Feng, J., Chmelka, B. F., and Stucky, G. D. (1998). Nonionic triblock and star diblock copolymer and oligomeric surfactant syntheses of highly ordered, hydrothermally stable, mesoporous silica structures. **Journal of the American Chemical Society**. 120(24): 6024-6036.

Zhu, Y., Li, H., Zheng, Q., Xu, J., and Li, X. (2012). Amine-functionalized SBA-15 with uniform morphology and well-defined mesostructure for highly sensitive chemosensors to detect formaldehyde vapor. **Langmuir**. 28(20): 7843-7850.
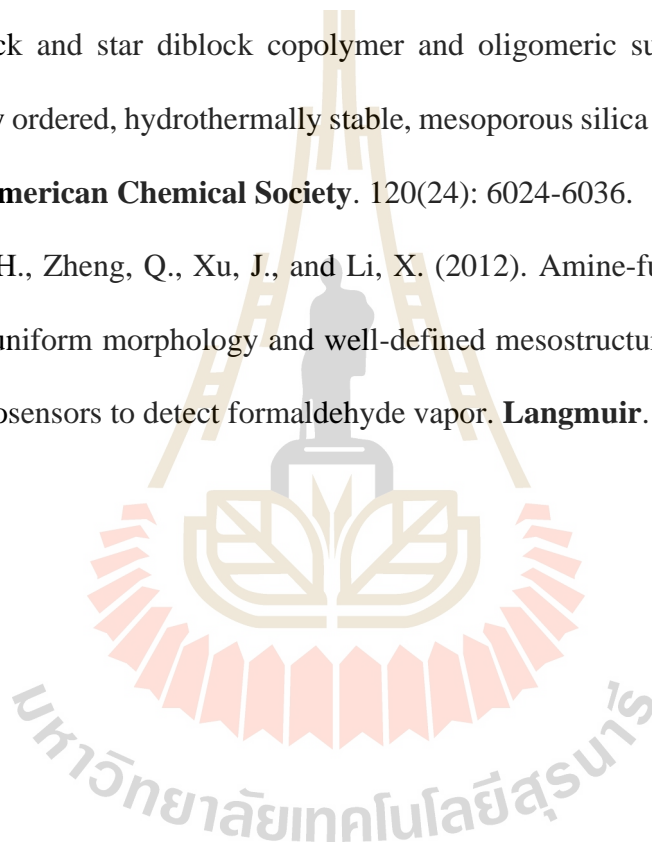
CHAPTER III

CONVENTIONAL GRAFTING OF SILICEOUS SBA-15 BY AMINOPROPYLTRIETHOXYSILANE AND OXOVANADIUM COMPLEX FOR IN SITU ALDOL CONDENSATION OF FURFURAL AND ACETONE

3.1 Abstract

This chapter compares the activity of the mesoporous siliceous SBA-15 support grafted with aminopropyltriethoxysilane (APTES) against vanadyl acetylacetonate ($VO(acac)_2$) in an in situ aldol condensation between furfural and acetone. The SBA-15 grafted with APTES (AP-SAB-15) was prepared by a conventional method before further anchoring by $VO(acac)_2$ to produce VAP-SBA-15. These samples were analyzed by XRD, N_2 sorption analysis, FE-SEM, TEM, FTIR, XPS, and UV-vis. The grafting facilitates the formation of covalent bonds between surface silanol of the SBA-15 and APTES precursor. After the anchoring process, an acetylacetonate ligand is chemically tethered by surface aminopropyl species. The chemical changes do not affect the morphology of SBA-15, but the surface areas decrease due to the presence of grafted moieties. The reaction testing was done in an in situ reactor monitored by ATR-FTIR technique. Because of higher basicity, the AP-SBA-15 showed more furfurylbutenone (FB) formation than that of the VAP-SBA-15. Additionally, the FB formation increased with the temperature on the AP-SBA-15.

3.2   Introduction

Transformation of biomass-derived compounds to transportation fuels has been widely considered as an alternative method among various promising technologies for sustainable petrol production. This methodology can enhance carbon efficiency, decrease an environmental carbon crisis and provide a renewable fuel resource (Bohre, Dutta, Saha, and Abu-Omar, 2015). Biomass conversion can be achieved under different strategies such as chemical, thermal, biological or enzymatic processes. Chemical transformation is used extensively because of the abundance of lignocellulosic feedstock and low operation cost (Faba, Díaz, and Ordóñez, 2012).

Furanic compounds such as furfural and 5-hydroxymethylfurfural (HMF) are promising biomass-based chemicals to produce fuels or other valuable chemicals. Importantly, the use of these chemicals does not compete with the needs of food crops, fodder, and natural habitat. Among such furanic compounds, furfural has been used as a platform molecule in various biomass conversions. Moreover, acetone as a by-product of phenol production has been commonly used. Both furfural and acetone are cheap and commercially available. Hence, they can be converted to value-added chemicals such as jet or diesel fuel intermediates via a conventional aldol condensation (Huang et al., 2012).

Aldol condensation has been widely exploited to convert biomass to desired chemicals through the formation of carbon-carbon (C-C) bonds. The reaction can be operated in either gas or liquid phase in the presence of an acid or base catalyst. According to many researches, the reaction has been carried out in the presence of a homogeneous catalyst which is difficult to regenerate. To solve this drawback, the procedure could be carried out with a heterogeneous solid catalyst.

For an excellent activity, catalysts for the aldol condensation should possess both acidic and basic active sites. Particularly, acid-base bi-functionalized mesoporous SBA-15 catalysts, prepared by a reaction between a silanol surface and aminoalkoxysilane coupling reagents, are commonly used (An et al., 2014). However, amino-imprinted catalysts provide an inactive surface species in the aldol condensation owing to imine formation between a terminal surface amine with a ketone (Lauwaert et al., 2015). To prevent the inactive imine appearance, anchoring of a transition metal complex is used. Schiff base group is generated from a reaction between a carbonyl group contained in a ligand and the surface amine group. A transition metal complex could be anchored on those groups. For example, copper bidentate Schiff base ligand supported on zeolite NaY is employed in aldol condensation of cyclohexanone and benzaldehyde (Mobinikhaledi, Zendehdel, and Safari, 2014).

Up to date, there are no reports on an oxovanadium complex tethered on amino-imprinted supports for aldol condensation between furfural and acetone. This work investigates the feasibility of upgrading furfural via catalytic aldol condensation over oxovanadium Schiff base complex tethered on amino-modified mesoporous SBA-15 in liquid phase.

3.3   Experimental

3.3.1   Preparation of SBA-15 as a siliceous mesoporous support

SBA-15 was prepared according to the method reported by Yang, Hao, Zhang, and Kan (2011). Pluronic® P123 (average molecular weight of 5800, Sigma-Aldrich) as an organic template, 7.48 g, was dissolved in 305.2 mL of 1.5 M HCl in a 500-mL three-neck round-bottom flask connected with a glass condenser. The template

solution was stirred in an oil bath at 40 ℃ for 24 h. Tetraethyl orthosilicate (TEOS, 98.0%, Fluka Chemika) as a silica source, 17.4 mL, was slowly dropped into the template solution (about 80 min). The colloidal mixture was further stirred at 40 ℃ for 5 h. Then, the mixture was divided into two portions and transferred to 270 mL and 275 mL of Teflon-lined stainless-steel autoclaves. They were aged without stirring at 100 ℃ for 24 h and quenched with tap water. The solid products were centrifuged at a speed of 4000 rpm for 3 min, washed by deionized water until the pH became 5.5 and dried under a hot air oven at 60 ℃ for 12 h. Finally, the samples were calcined at 550 ℃ for 16 h with a heating rate of 1 ℃/min.

3.3.2 Conventional grafting of SBA-15 with 50 wt. % of APTES

SBA-15 was grafted by APTES with the method by Yang et al. (2011) as shown in **Scheme 3.1**. The desired amount of SBA-15 support was dried at 120 ℃ for 2 h to remove adsorbed water. Then, the dried powder, 1.00 g, was suspended into 100 mL of toluene (99.5%, QRëC^{TM}) in a 100-mL round bottom flask, equipped with a glass condenser under N_2 gas flow for 30 min. APTES (99%, Acrōs Organics) of 50 wt. %, 0.54 mL (2.3 mmol), was added dropwise via a 1-mL plastic syringe with a needle under N_2 gas flow. The suspension was stirred at room temperature for 24 h, filtered through a thimble, washed by absolute ethanol (99.9%, Carlo Erba), extracted via a Soxhlet extractor using absolute ethanol for 12 h and dried at 80 ℃ for 12 h. This as-prepared sample was named AP-SBA-15.
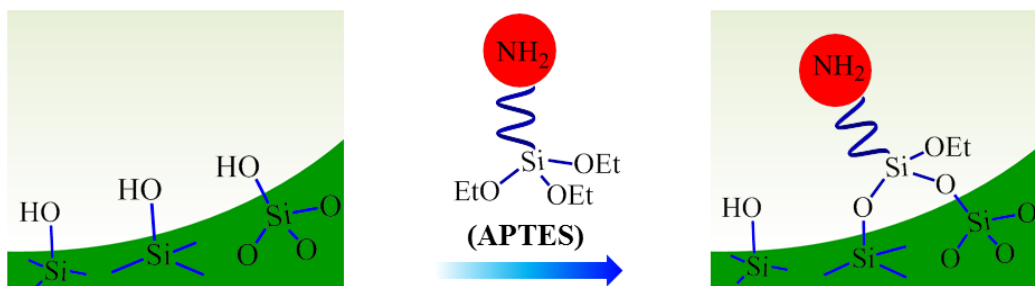
Scheme 3.1 An illustration of the possible functionalization through a conventional grafting of APTES on surface silanol groups of the mesoporous siliceous SBA-15.

3.3.3 Modification of AP-SBA-15 by anchoring oxovanadium complex

AP-SBA-15 by anchoring the oxovanadium complex was prepared from a method from the literature (Li et al., 2012; Pereira, Silva, Carvalho, Pires, and Freire, 2008) as illustrated in **Scheme 3.2**. Vanadyl(IV) acetylacetonate (99%, Acrōs Organics), 0.308 g (1.15 mmol), was dissolved in 25 mL of dried toluene, stirred at 80 ºC for 3 h, filtered to remove undissolved solids. AP-SBA-15, 0.500 g, was loaded to 15 mL of dried toluene in a 100-mL three-neck round bottom flask, equipped with a glass condenser, and stirred at 80 ºC for 3 h under N_2 flow. The filtered blue solution was transferred to a 25-mL dropping glass funnel prior to being added dropwise to the suspension. Toluene, 10 mL, was added to wash the remaining solution in the funnel. The mixture was refluxed at 110 ºC for 24 h, filtered, purified by a Soxhlet extractor with ethanol for 12 h and dried in a hot air oven at 80 ºC for 12 h. This sample was called VAP-SBA-15.
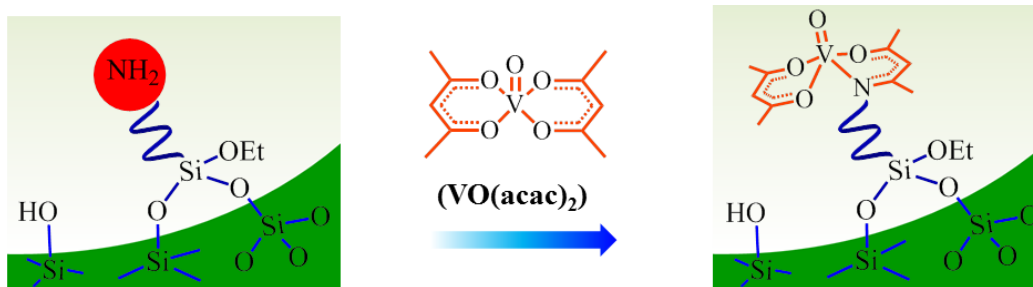
Scheme 3.2 The illustration of anchoring of vanadyl acetylacetonate on AP-SBA-15.

3.3.4 Materials characterization of SBA-15 grafted by APTES and oxovanadium complex

X-ray diffraction (XRD) patterns were obtained using a Bruker XRD-D8 Advance with Cu-K$_\alpha$ (1.54 Å) radiation operated at a voltage of 40 kV and current of 40 mA. The detector was LYNXEYE. The scan 2θ range was from 0.5 to 5.0º with a step size of 0.02º and time per step of 1.2 s. Both interplanar spacing of the plane (100), (d$_{(100)}$) and unit cell parameter (A$_o$) of the prepared samples were calculated from the following equations.

$$d_{(100)} = \frac{\lambda}{2 \sin \theta} \tag{3.1}$$

$$A_o = \frac{2d_{(100)}}{\sqrt{3}} \tag{3.2}$$

All morphological images were recorded from field emission scanning electron microscopy (FE-SEM) using a Zeiss AURIGA FE-SEM/FIB/EDX with an upper electron detector operating at an accelerated voltage of 10 kV with a working

distance of 8.9 mm. Each sample was placed on a carbon tape adhered to a copper stub and then coated by gold, using an operating current at 10 mA under an argon atmosphere for 5 minutes. A particle size distribution was processed by an ImageJ software version 1.49.

TEM images and SAED were obtained from an FEI Tecnai G^2 transmission electron microscope operated at an accelerating voltage of 200 kV in bright field mode. For sample preparation, a small amount of each sample was first dispersed in 1 mL of absolute ethanol, sonicated for a minute and then dropped repeatedly on a carbon-coated copper grid at least 5 times. The sample was dried under a desk lamp in air before the analysis. Pore diameter and wall thickness distribution were evaluated by ImageJ software version 1.49.

Nitrogen (N_2) adsorption-desorption isotherms were obtained at a temperature of -196 ℃ using a BELSORP-mini II. Prior to a measurement, samples were degassed at 120 ℃ for 24 h. Both specific surface area and pore volume were calculated by a Brunauer-Emmett-Teller (BET) method. Pore size and pore size distribution were computed from the adsorption branch using a Barrett-Joyner-Halenda (BJH) method.

FTIR spectra were collected using a Bruker Vertex 70+RamII FTIR spectroscopy equipped with an FT-Raman instrument manipulated in an attenuated total reflectance (ATR) mode. The condition was as follows: a signal amplitude at 3638 (in absolute value), a range of wavenumber from 400 to 4000 cm^{-1}, a resolution of 4 cm^{-1}, a scan number of 64.

Chemical states of surface species were identified by X-ray photo-electron spectroscopy (XPS) using a ULVAC-PHI PHI5000 VersaProbe II operating at

a pressure of 1.2×10^{-7} Pa using Al K_α at 1486.6 eV as a conventional X-ray source. The XPS data interpretation was processed with MultiPak 9.0 using a combined Gaussian-Lorentzian function with a Shirley background correction (Acres et al., 2012). All peaks of binding energy (BE) were calibrated corresponding to the peak of standard C 1s at 284.8 eV from an adventitious carbon (Jakša, Štefane, and Kovač, 2013; Qiao, Wang, Gao, and Jin, 2015; Shircliff et al., 2011).

UV-visible spectra were recorded using an Agilent Varian Cary 300 Scan UV-visible spectrophotometer with a diffuse reflectance (DR) mode operating at a wavelength from 800 to 200 nm with a resolution of 1 nm, a scan rate of 600 nm/min and a scan number of 3. $BaSO_4$ powder was employed as a non-absorbing reference material.

3.3.5 Catalytic testing of aldol condensation between furfural and acetone by in situ ATR-FTIR

In situ ATR-FTIR technique is used as a real-time analysis for an in situ aldol condensation of furfural and acetone. ZnSe was employed as an internal reflectance element. Before starting the reaction testing, the catalyst powder was dried under a hot air oven at 80 ℃ for 3 h. The pre-dried catalyst of 10 mg was dispersed in ethanol, sonicated for several minutes, and deposited on the ZnSe surface. Afterward, the ZnSe plate was fixed on a cell holder. The mixture of furfural and acetone with the mole ratio of 1:10 was dissolved in the solution of water and ethanol with the volume ratio of 4:1. Then, the solution was introduced through the cell aligned in the in situ instrument at room temperature. IR spectra were recorded and defined.

3.4   Results and discussion

3.4.1   Characterization results of AP-SBA-15 and VAP-SBA-15

XRD patterns of all samples are shown in **Figure 3.1**. The SBA-15 shows three characteristic peaks at 0.83, 1.44, and 1.64º which correspond to the plane (100), (110) and (200), respectively, of SBA-15 (Yang et al., 2011). The XRD patterns of both AP-SBA-15 and VAP-SBA-15 have lower intensity than that of the parent. There are slight changes in XRD peaks to a higher degree. Both interplanar spacing and wall thickness are listed in **Table A.1** in Appendix A. These parameters of SBA-15 decreased after grafting with APTES and additional anchoring with VO(acac)$_2$. These implied that the grafted bulky species did not change the SBA-15 structure. This finding is similar to the works of Yang et al. (2011) and Li et al. (2012).
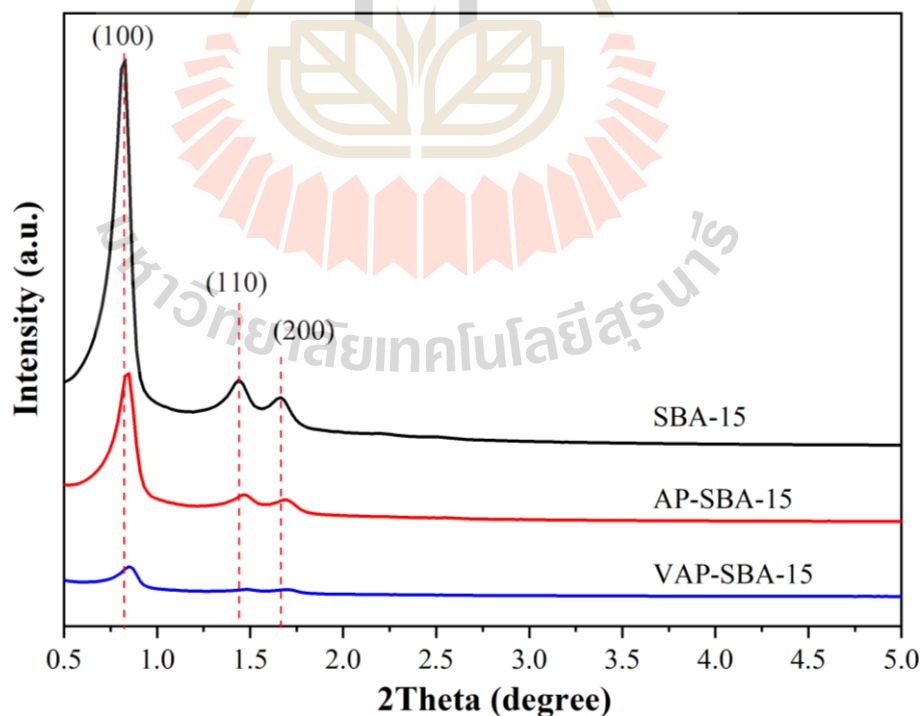
Figure 3.1 XRD patterns of the parent SBA-15, AP-SBA-15, and VAP-SBA-15.

SEM images and particle-size distribution of the as-prepared samples are shown in **Figure 3.2**. Morphologies of these materials are rope-like shape with a particle size around 1.4 µm. Some particles aggregated to form a wheat-like structure related to the previous literature by Zhao et al. (1998). After the surface modification of SBA-15 by either grafting with APTES or anchoring with the oxovanadium complex, the identical morphology did not change related to the remained geometry confirmed by XRD results. In addition, the morphological result is in accordance with the research by Li et al. (2012).

To further understand pore topology and crystallinity of the parent and AP-SBA-15 and VAP-SBA-15, both TEM micrographs and selected-area electron diffraction (SAED) are depicted in **Figure 3.3**. The result indicated that the parent and grafted SBA-15 had an ordered mesoporous topology arranged in a two-dimensional direction (Lowe, and Baker, 2014) as seen in **Figure 3.3(a-c)**. Additionally, SAED patterns in **Figure 3.3(d-f)** exhibit a broad diffuse ring indicating that all SBA-15 samples were amorphous materials with the short-range atomic order from the ordered pore walls (Morsi, and Mohamed, 2018). From **Figure A.1** in Appendix A, pore size distribution and wall thickness slightly change after surface modification.
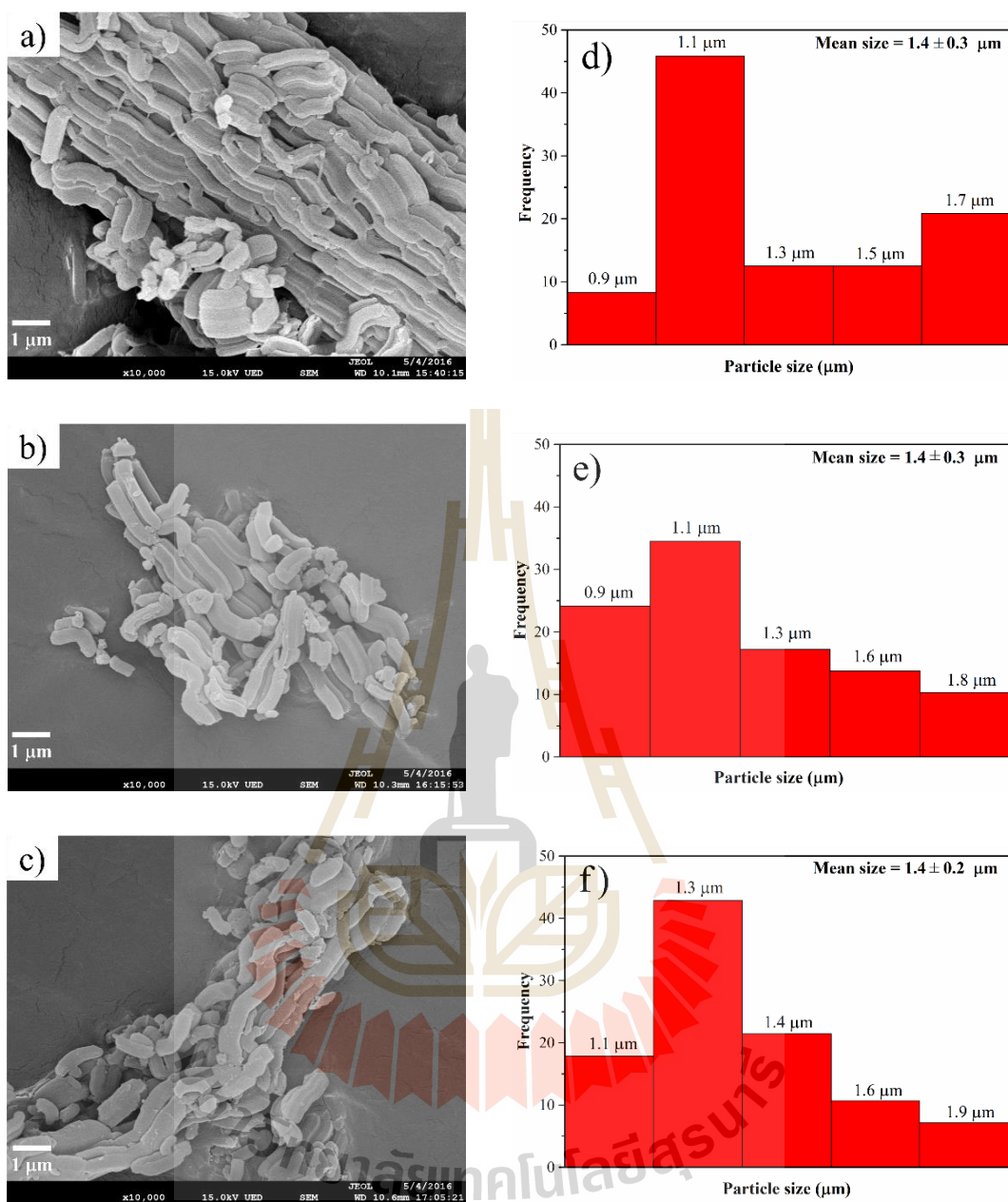
Figure 3.2 SEM images of a) SBA-15, b) AP-SBA-15 and c) VAP-SBA-15; and a

particle size distribution of d) SBA-15, e) AP-SBA-15 and f) VAP-SBA-15.
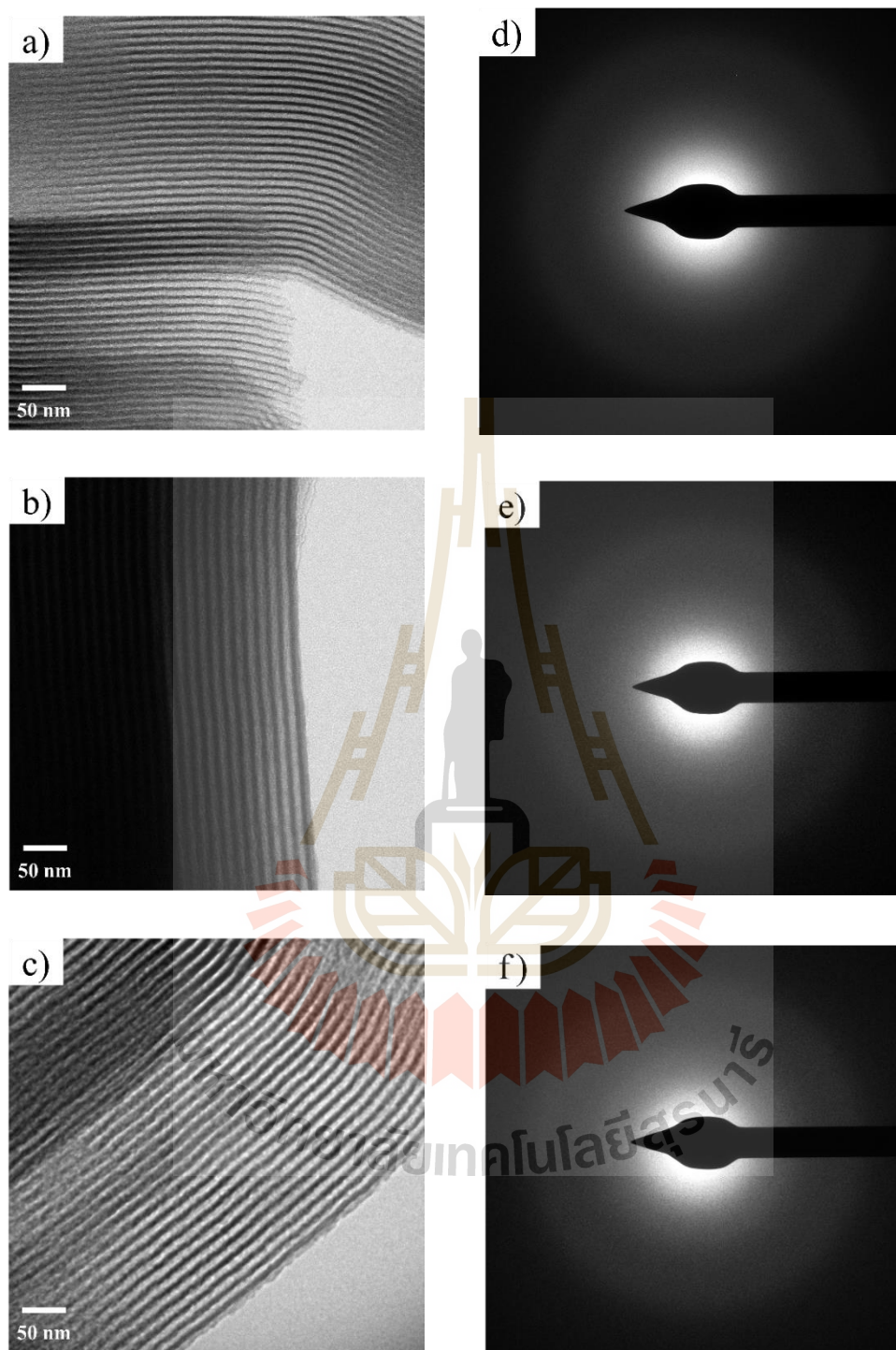
Figure 3.3 TEM images of a) SBA-15, b) AP-SBA-15 and c) VAP-SBA-15; and patterns of selected-area electron diffraction (SAED) of d) SBA-15, e) AP-SBA-15 and f) VAP-SBA-15.

N$_2$ adsorption-desorption isotherms of all samples are shown in **Figure 3.4(a)**. Isotherms from all samples are type IV(a) according to the IUPAC classification (Thommes et al., 2015). It is characteristic adsorption of mesoporous materials including the formation of monolayer and multilayer on the mesopore walls before the pore condensation. In addition, all samples exhibit a type H1 hysteresis loop which indicates a narrow range of uniform mesopores wider than 4 nm (Thommes et al., 2015). In **Figure 3.4(b)**, AP-SBA-15 and VAP-SBA-15 have a lower range of pore size distribution than the parent SBA-15. This could imply that either ATPES or oxovanadium complex were tethered on the SBA-15 walls.

The summary of textural properties consisting of surface area, porosity, and pore-wall thickness of all as-prepared samples are listed in **Table 3.1**. Both surface area and porosities of the grafted samples are smaller than that of the parent SBA-15 indicating the formation of new surface components on the support surface. Moreover, the presence of new grafted species consisting of either APTES or oxovanadium slightly increased the pore-wall thickness of the SBA-15 support according to the XRD peak shift. These results are in good agreement with the literature (Yang et al., 2011).
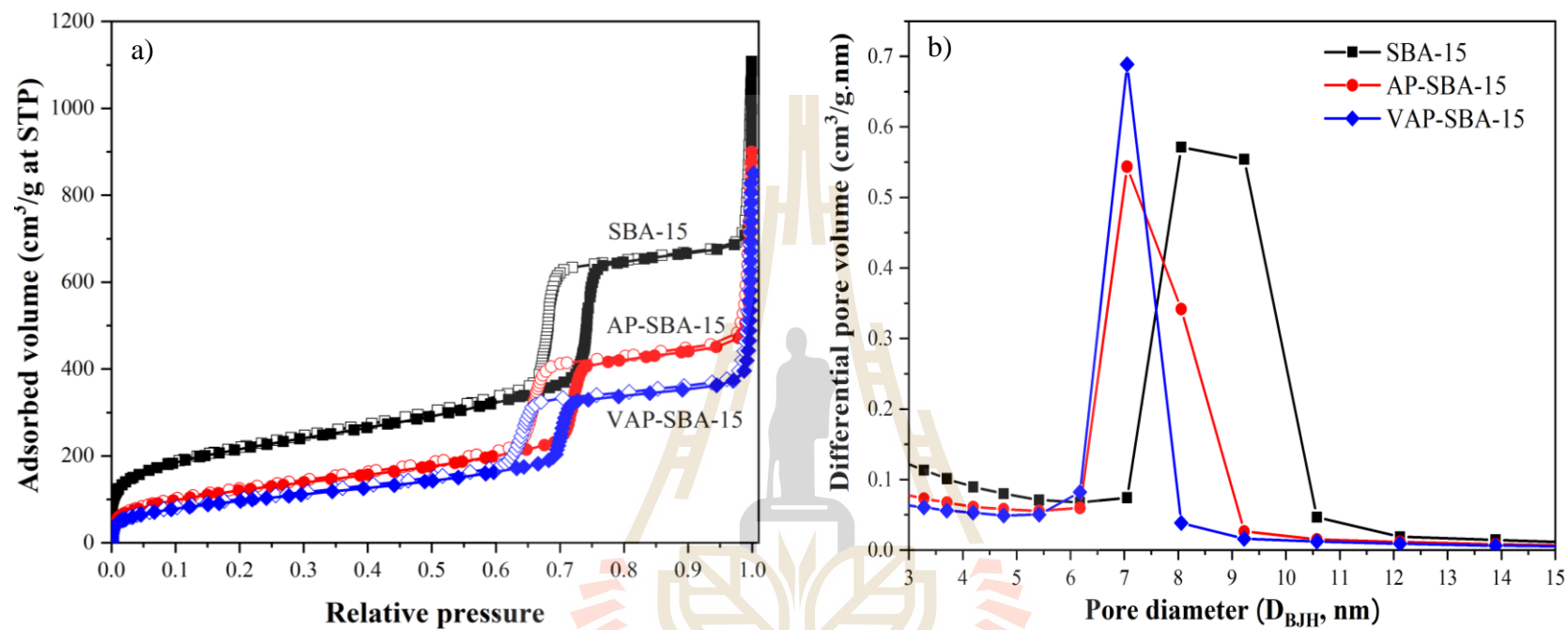
Figure 3.4 N$_2$ adsorption-desorption isotherms (a) and pore size distribution (b) of the parent and SBA-15 grafted by APTES (AP-SBA15) and oxovanadium complex (VAP-SBA15) (Filled symbol = adsorption branch and hollow symbol = desorption branch).

Table 3.1 Surface area, mesopore volume, pore diameter, and wall thickness of parent and SBA-15 grafted with APTES and further anchored by oxovanadium complex.

Sample	S_{BET} (m^2/g) [a]	V_{BJH} (cm^3/g) [b]	D_{BJH} (nm) [c]	$d_{(100)}$ (nm) [d]	A_o (nm) [e]	W (nm) [f]
SBA-15	786	1.00	8.06	10.67	12.32	4.26
AP-SBA-15	434	0.77	7.06	10.41	12.02	4.96
VAP-SBA-15	346	0.63	7.06	10.17	11.74	4.68

[a] S_{BET} is a surface area calculated by a BET method using an adsorption branch.

[b] V_{BJH} is a pore volume calculated by a BJH method.

[c] D_{BJH} is a pore diameter calculated by the BJH method.

[d] $d_{(100)}$ is interplanar spacing at (100) plane calculated from equation 3.2.

[e] A_o is a unit cell parameter calculated from equation 3.1.

[f] W is wall thickness calculated from $W = A_o - D_{BJH}$.

To further confirm the presence of new functional groups of all materials, FTIR spectra and peak assignments are illustrated in **Figure 3.5**. Vibrational bands and their assignments are also summarized in **Table A.3** in Appendix A. The parent SBA-15 shows the characteristic vibration modes including stretching and bending of silanol group (ν(Si-O-H) and δ(O-H), respectively) and the stretching of siliceous framework (ν(Si-O-Si)) (Di Giuseppe et al., 2013). The AP-SBA-15 shows several new vibrational bands consisting of the stretching and bending of the hydrocarbon chain belonged to aminopropyl (ν(C-H) and δ(Si-C), respectively). Obviously, the peak intensity of the silanol group decreases indicating the chemical bond formation through the condensation between the APTES and surface silanol of the support similar to the work by Pereira et al. (2008).

The AP-SBA-15 displays additional peaks including the stretching of vanadyl group (ν(V=O) and the vibration of Schiff base or imine ligands (ν(C=N)). Pereira et al. (2008) have explained that these peaks are from a new bond between the surface aminopropyl (-NH$_2$) and the carbonyl (C=O) of an acetylacetonate ligand within the further anchoring process. Hence, these FTIR results confirmed the presence of new surface moieties including either APTES or the oxovanadium species on the SBA-15 surface through a chemical bond formation. This finding is in accordance with the literature (Li et al., 2012; Pereira et al., 2008; Yang et al., 2011).
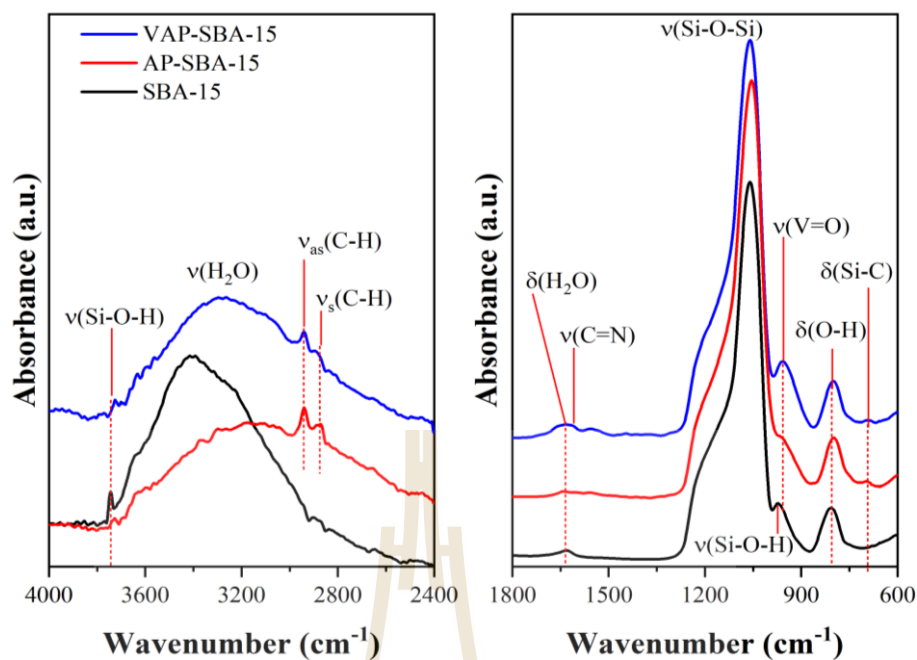
Figure 3.5 FTIR spectra and assignment of the parent and SBA-15 grafted with

APTES (AP-SBA-15) and successively anchored by oxovanadium (VAP-SBA-15).

To further confirm the new functional groups, XPS spectra of Si 2p, O 1s, C 1s,

N 1s, and V 2p for all samples are depicted in **Figure 3.6**. The wide-scan spectra of all

as-prepared samples and of reference vanadium species are also shown in **Figure A.2**

and **A.3**, respectively, in Appendix A. After the surface functionalization, the XPS

peaks of Si 2p and O 1s of the prepared samples shifted to lower binding energy

compared to those of SBA-15 indicating the presence of new chemical bonding (Jakša

et al., 2013). The shift of C 1s might relate to the appearance of different

electronegativities of carbonaceous species. Remarkably, the N 1s peak of the AP-SBA-

15 sample shifts to lower binding energy implying the bond formed between the surface

amine and acetylacetonate ligand. In addition, the V 2p peak of VAP-SBA-15 is

different from that of the VO(acac)$_2$, confirming the chemical anchoring of the complex on the AP-SBA-15. These results agree with the FTIR results.
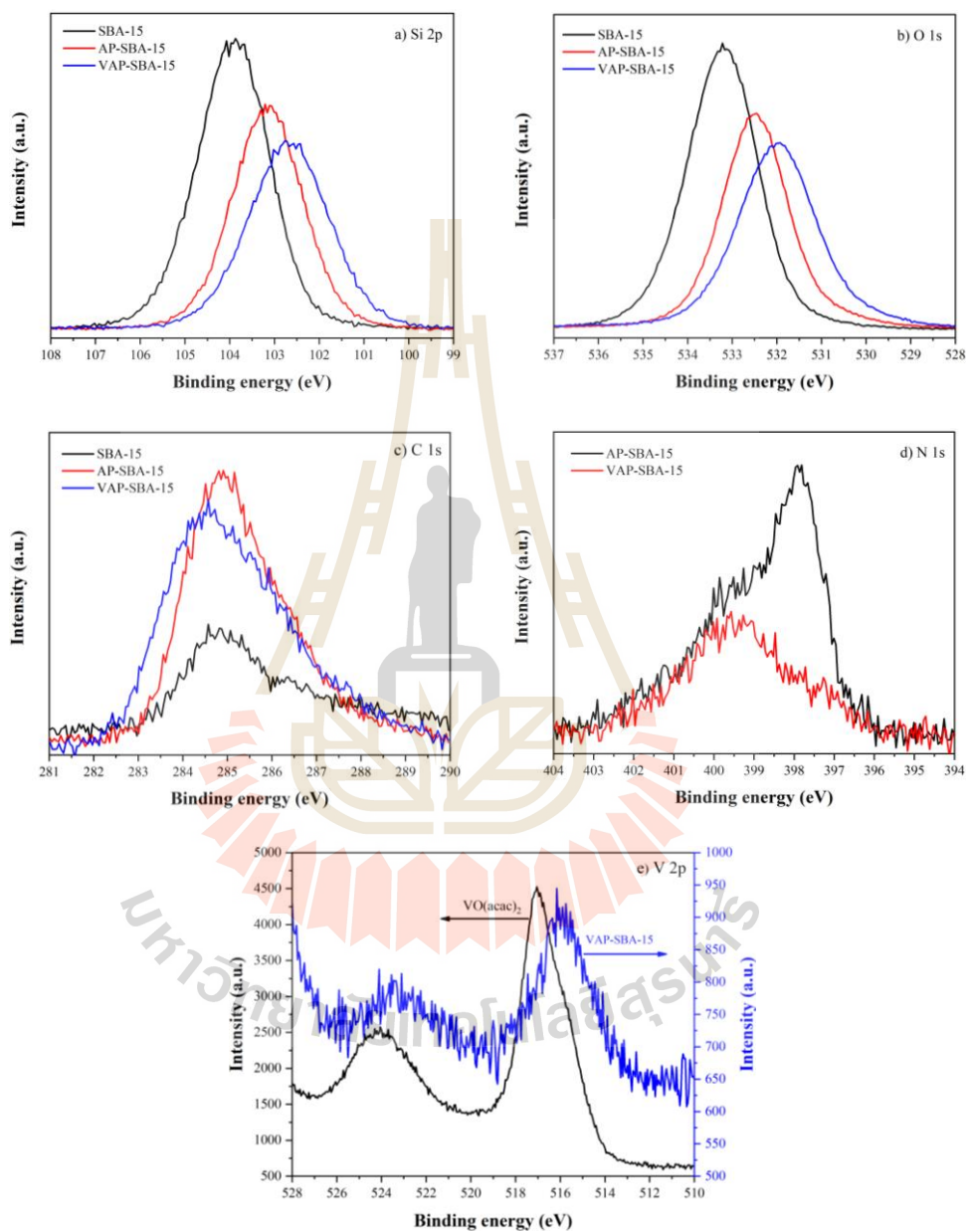
Figure 3.6 XPS spectra of the parent and SBA-15 grafted with APTES (AP-SBA-15) and further anchored by oxovanadium complex (VAP-SBA-15) including a) Si 2p, b) O 1s, c) C 1s, d) N 1s, and e) V 2p.

To confirm the presence of oxovanadium species, the samples were analyzed by UV-visible spectrometry. The results are shown in **Figure 3.7**. The AP-SBA-15 sample shows two absorption bands at 205 and 244 nm which are the characteristic of SBA-15 (Shylesh, and Singh, 2004). The VAP-SBA-15 sample shows a new broadband in the region from 260 to 360 nm. Yang et al. (2011) and Li et al. (2012) have explained that the band corresponding to n-π* and π-π* ligand charge transfer to a central oxovanadium atom. The absorption band with the peak at 349 nm was assigned to the low charge transfer of $(\pi)t_1$ to $(d)e$ from V=O to tetrahedral V(V) species (Shylesh, and Singh, 2006). These results confirmed the chemical anchoring of the oxovanadium complex on the amino-grafted SBA-15. This finding agrees with the FTIR and XPS results.
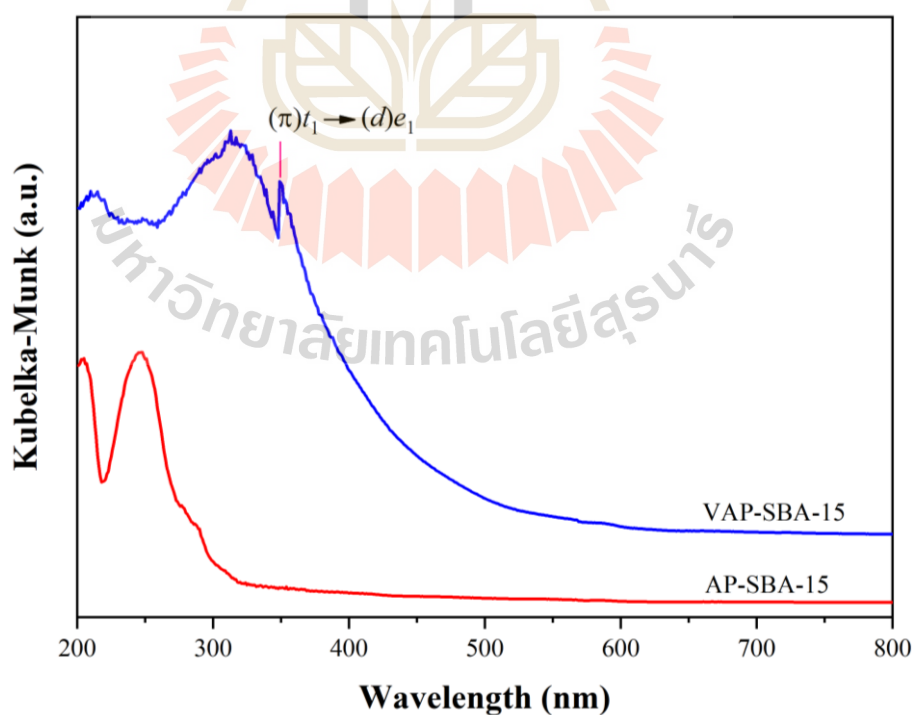
Figure 3.7 UV-visible spectra of AP-SBA-15 and VAP-SBA-15.

3.4.2 In situ aldol condensation between furfural and acetone

3.4.2.1 Effect of surface species on catalytic activity

The aldol condensation between furfural and acetone was monitored by in situ ATR-FTIR measurements at 60 °C up to 9 h. The spectra of the reaction solution under the presence of SBA-15, AP-SBA-15, and VAP-SBA-15 are shown in **Figure 3.8**. Two peaks at 1284 and 1278 cm^{-1} were assigned to the fingerprint of the starting reagents and furfurylbutenone (FB) as the desired product, respectively in aqueous solution. SBA-15 shows only the peak of the starting agents implying that it is not active. SBA-15 only contained a weak base from the surface silanol group (Shi, Ji, Gao, and Wang, 2005). In a similar manner, VAP-SBA-15 shows a low catalytic activity implying low basicity of vanadyl group contained Lewis acid sites (Cashin et al., 2002). Remarkably, AP-SBA-15 provided the highest activity in terms of the FB formation due to sufficient base strength to generate an enolate from acetone corresponding to the work of Lauwaert et al. (2015). They explained that a basic amine site affected the nucleophilic addition of acetone to form an enamine intermediate before reacting with another carbonyl. These results suggested that the aldol condensation between furfural and acetone required base catalysts to facilitate the FB formation at the mild reaction temperature. Because AP-SBA-15 gave the best FB formation, it was further studied to determine the optimal temperature.
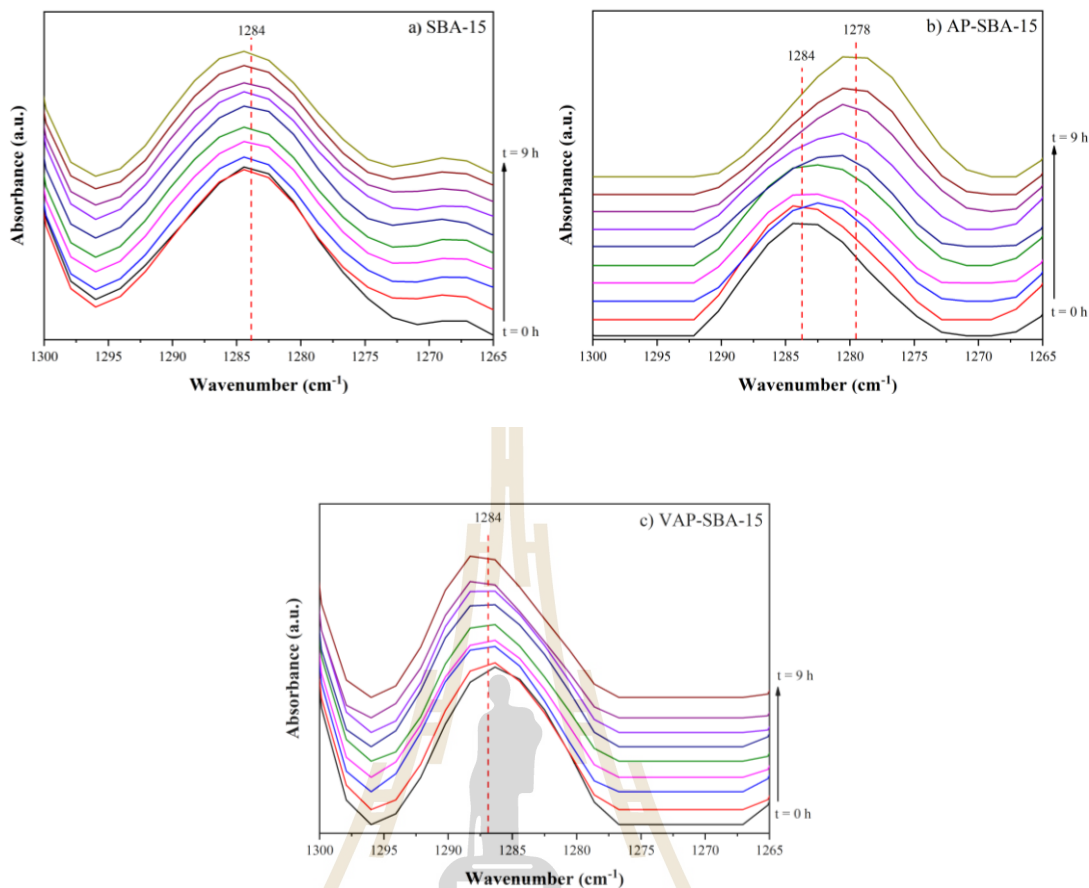
Figure 3.8 In situ IR spectra of reaction solution under the presence of SBA-15, AP-SBA-15, and VAP-SBA-15 during the aldol condensation between furfural and acetone at 60 ℃.

3.4.2.2 Effect of reaction temperature on the formation of furfurylbutenone in an in situ aldol condensation

In situ IR spectra of reaction solution from the aldol condensation between furfural and acetone catalyzed by AP-SBA-15 are shown in **Figure 3.9**. The results show that the temperature of at least 40 ℃ enables the shift of the peak at 1284 to 1278 cm^{-1} indicating the effect of temperature could facilitate the FB formation in the aqueous solution. Moreover, the longer reaction time gives the

higher peak intensity at 1278 cm^{-1} implying the larger FB formation was obtained. In addition, these FTIR spectra were deconvoluted to differentiate the effect of the reaction temperature in detail.
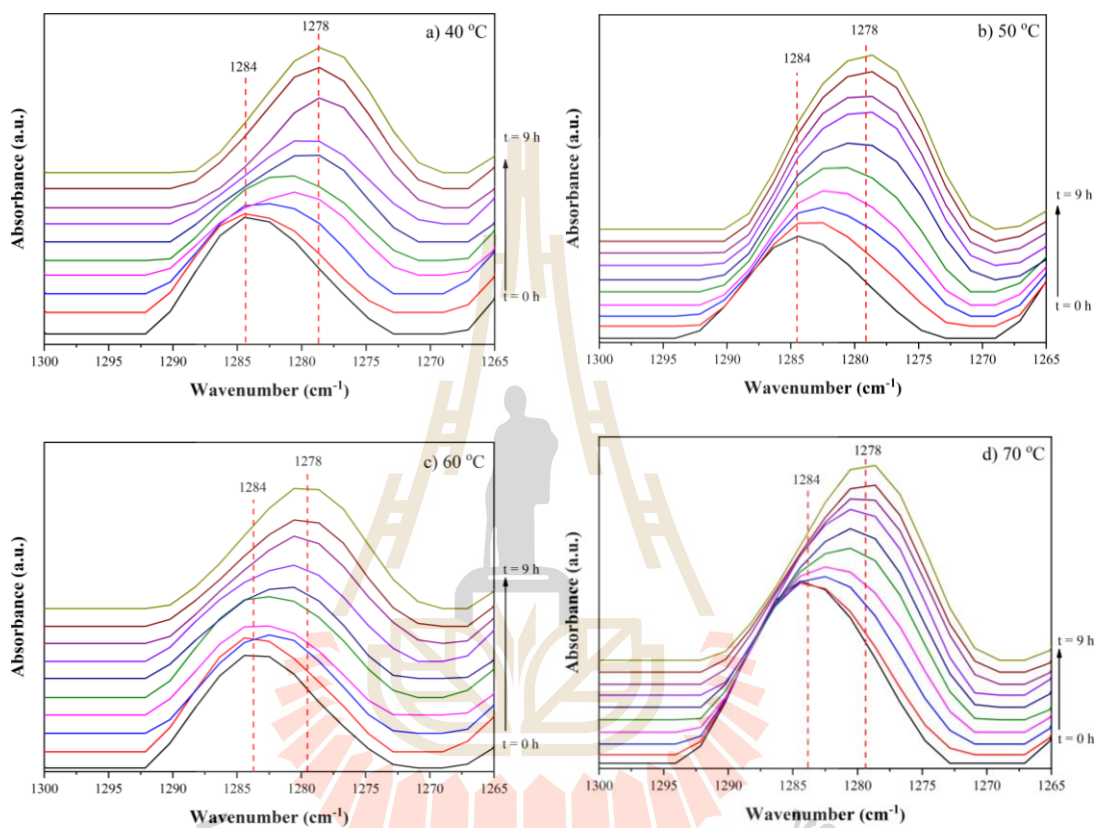
Figure 3.9 In situ IR spectra of reaction solution under the presence of AP-SBA-15 during the aldol condensation between furfural and acetone at various temperatures against the reaction time up to 9 h.

The relative peak area curves of furfurylbutenone at different reaction temperatures against the reaction time are shown in **Figure 3.10**. Reaction temperatures affected not only the catalytic activity but also the equilibrium of FB

formation. From the curves, the FB formation increased with a reaction time until they reached 6 h. At the temperature above 50 ℃, the formation became nearly constant after 6 h. In contrast, at 40 ℃, the formation still increased. These results confirmed that the reaction depended on the temperature. This finding agrees with the literature by Heynderickx (2019) studying the kinetics of aldol condensation between benzaldehyde and heptanal. It was proposed that the reaction reached equilibrium more quickly at higher temperatures.
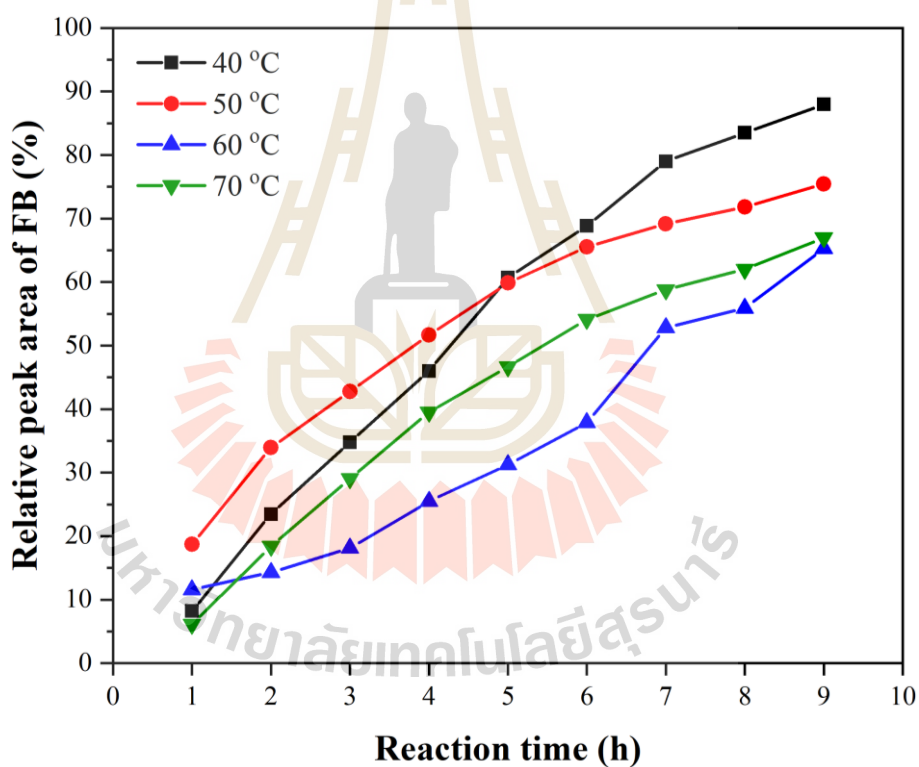
Figure 3.10 Relative peak area of furfurylbutenone (FB) from the deconvolution results of the peak at 1278 cm^{-1} during in situ aldol condensation between furfural and acetone at various reaction temperatures.

3.5   Conclusions

Mesoporous SBA-15 was grafted with aminopropyltriethoxysilane (APTES), producing AP-SBA-15 and successively anchored by vanadyl acetylacetonate, producing VAP-SBA-15. From XRD results, the conventional preparation did not affect the characteristic geometry of SBA-15. The morphologies and pore topologies by SEM and TEM imaging of SBA-15 were still observed. From N_2 sorption analysis, both grafted moieties consisting of APTES and the oxovanadium complex were on the pore walls of SBA-15. It was confirmed by FTIR and XPS that the grafting and anchoring species chemically bonded with the silanol groups on the SBA-15 surface. The presence of oxovanadium species chemically tethered on the amino-grafted SBA-15 was confirmed by UV-vis spectroscopy. It was tested for in situ aldol condensation between furfural and acetone. The catalytic activity of all as-prepared samples was evaluated in aldol condensation between furfural and acetone monitored by the in situ ATR-FTIR spectroscopy. AP-SBA-15 gave the highest degree of the formation of furfurylbutenone, while VAP-SBA-15 less affected the reaction activity. The FB formation increased with the reaction time. The optimal reaction temperature for the in situ aldol condensation was 40 ºC. Thus, the amino-grafted SBA-15 was proposed as a promising catalyst for the upgrading of furfural.

3.6   References

Acres, R. G., Ellis, A. V., Alvino, J., Lenahan, C. E., Khodakov, D. A., Metha, G. F., and Andersson, G. G. (2012). Molecular structure of 3-

aminopropyltriethoxysilane layers formed on silanol-terminated silicon surfaces. **The Journal of Physical Chemistry C**. 116(10): 6289-6297.

An, Z., He, J., Dai, Y., Yu, C., Li, B., and He, J. (2014). Enhanced heterogeneous asymmetric catalysis via the acid–base cooperation between achiral silanols of mesoporous supports and immobilized chiral amines. **Journal of Catalysis**. 317: 105-113.

Bohre, A., Dutta, S., Saha, B., and Abu-Omar, M. M. (2015). Upgrading furfurals to drop-in biofuels: an overview. **ACS Sustainable Chemistry & Engineering**. 3(7): 1263-1277.

Cashin, B., Cunningham, D., Daly, P., McArdle, P., Munroe, M., and Ní Chonchubhair, N. (2002). Donor properties of the vanadyl ion: reactions of vanadyl salicylaldimine β-ketimine and acetylacetonato complexes with groups 14 and 15 lewis acids. **Inorganic Chemistry**. 41(4): 773-782.

Di Giuseppe, A., Di Nicola, C., Pettinari, R., Ferino, I., Meloni, D., Passacantando, M., and Crucianelli, M. (2013). Selective catalytic oxidation of olefins by novel oxovanadium(IV) complexes having different donor ligands covalently anchored on SBA-15: a comparative study. **Catalysis Science & Technology**. 3(8): 1972-1984.

Faba, L., Díaz, E., and Ordóñez, S. (2012). Aqueous-phase furfural-acetone aldol condensation over basic mixed oxides. **Applied Catalysis B: Environmental**. 113-114: 201-211.

Heynderickx, P. M. (2019). Activity coefficients for liquid organic reactions: towards a better understanding of true kinetics with the synthesis of jasmin aldehyde as showcase. **International Journal of Molecular Sciences**. 20(15): 3819.

Huang, X.-m., Zhang, Q., Wang, T.-j., Liu, Q.-y., Ma, L.-l., and Zhang, Q. (2012). Production of jet fuel intermediates from furfural and acetone by aldol condensation over MgO/NaY. **Journal of Fuel Chemistry and Technology**. 40(8): 973-978.

Jakša, G., Štefane, B., and Kovač, J. (2013). XPS and AFM characterization of aminosilanes with different numbers of bonding sites on a silicon wafer. **Surface and Interface Analysis**. 45(11-12): 1709-1713.

Lauwaert, J., De Canck, E., Esquivel, D., Van Der Voort, P., Thybaut, J. W., and Marin, G. B. (2015). Effects of amine structure and base strength on acid–base cooperative aldol condensation. **Catalysis Today**. 246: 35-45.

Li, Z., Liu, L., Hu, J., Liu, H., Wu, S., Huo, Q., Guan, J., and Kan, Q. (2012). Epoxidation of styrene with molecular oxygen catalyzed by a novel oxovanadium(IV) catalyst containing two different kinds of ligands. **Applied Organometallic Chemistry**. 26(5): 252-257.

Lowe, J. B., and Baker, R. T. (2014). Deformation of ordered mesoporous silica structures on exposure to high temperatures. **Journal of Nanomaterials**. 2014: 1-13.

Mobinikhaledi, A., Zendehdel, M., and Safari, P. (2014). Preparation and characterization of a novel host (zeolite NaY)/guest (copper(II) complex of a new bidentate Schiff base ligand) nanocomposite material (HGNM): a comparison between catalytic reactivity of free and encapsulated complexes in oxidation of benzyl alcohol and aldol condensation. **Journal of Porous Materials**. 21(5): 565-577.

Morsi, R. E., and Mohamed, R. S. (2018). Nanostructured mesoporous silica: influence of the preparation conditions on the physical-surface properties for efficient organic dye uptake. **Royal Society Open Science**. 5(3): 172021.

Pereira, C., Silva, A. R., Carvalho, A. P., Pires, J., and Freire, C. (2008). Vanadyl acetylacetonate anchored onto amine-functionalised clays and catalytic activity in the epoxidation of geraniol. **Journal of Molecular Catalysis A: Chemical**. 283(1-2): 5-14.

Qiao, B., Wang, T.-J., Gao, H., and Jin, Y. (2015). High density silanization of nano-silica particles using γ-aminopropyltriethoxysilane (APTES). **Applied Surface Science**. 351: 646-654.

Shi, L. Y., Ji, A., Gao, L., and Wang, Y. (2005). Direct synthesis of water-resistant basic mesoporous material HT/SBA-15. **Studies in Surface Science and Catalysis**. 158: 549-556.

Shircliff, R. A., Martin, I. T., Pankow, J. W., Fennell, J., Stradins, P., Ghirardi, M. L., Cowley, S. W., and Branz, H. M. (2011). High-resolution X-ray photoelectron spectroscopy of mixed silane monolayers for DNA attachment. **ACS Applied Materials & Interfaces**. 3(9): 3285-3292.

Shylesh, S., and Singh, A. P. (2004). Synthesis, characterization, and catalytic activity of vanadium-incorporated, -grafted, and -immobilized mesoporous MCM-41 in the oxidation of aromatics. **Journal of Catalysis**. 228(2): 333-346.

Shylesh, S., and Singh, A. P. (2006). Heterogenized vanadyl cations over modified silica surfaces: a comprehensive understanding toward the structural property and catalytic activity difference over mesoporous and amorphous silica supports. **Journal of Catalysis**. 244(1): 52-64.

Yang, Y., Hao, S., Zhang, Y., and Kan, Q. (2011). Oxovanadium(IV) and dioxomolybdenum(VI) salen complexes tethered onto amino-functionalized SBA-15 for the epoxidation of cyclooctene. **Solid State Sciences**. 13(11): 1938-1942.

Zhao, D., Feng, J., Huo, Q., Melosh, N., Fredrickson, G. H., Chmelka, B. F., and Stucky, G. D. (1998). Triblock copolymer syntheses of mesoporous silica with periodic 50 to 300 angstrom pores. **Science**. 279(5350): 548-552.

CHAPTER IV

ULTRASOUND-ASSISTED GRAFTING OF SILICA GEL

BY AMINOPROPYLTRIETHOXYSILANE FOR ALDOL

CONDENSATION OF FURFURAL AND ACETONE

4.1 Abstract

This chapter focuses on the development of a simple method to prepare heterogeneous catalysts with tunable basicity and stability for aldol condensation of furfural and acetone. Silica gel was grafted by aminopropyltriethoxysilane (APTES) with 20, 30, 40, and 50 wt. % of APTES using probe-type ultrasonicator with a power of 130 W and a frequency of 20 kHz. The grafted samples were studied by XRD, SEM, N_2 sorption, FTIR, XPS, CHN and TG analysis, and CO_2-TPD. The sonication facilitated the bond formation between APTES and the silica gel with less pore-blocking than the conventional grafting method. The basicity of the samples was tunable with the quantity of APTES loading. The grafted samples were active catalysts for aldol condensation of furfural and acetone at 60 ℃. The catalyst with 30 wt. % APTES grafting (30APS-U) provided a nearly complete furfural conversion and high furfurylbutenone selectivity. The conversion and selectivity increased with time and reached the highest values at 24 h. Thus, the catalysts with tunable basicity prepared by ultrasound-assisted grafting of silica with various APTES amounts were effective in furfural valorization.

4.2 Introduction

Among solid base materials, organocatalysts derived from chitosan are proposed to enhance the conversion of furfural (Kayser et al., 2012; Kuhbeck, Saidulu, Reddy, and Diaz, 2012). These catalysts provide surface amino group to promote the dehydration of furfurylhydroxybutanone (FHB) towards furfurylbutenone (FB). However, the preparation of chitosan through the deacetylation of chitin was carried out under an alkaline condition and the treated chitosan was dried under the flow of supercritical fluid CO_2. These procedures lead to an environmental issue from the alkaline wastewater and high operation cost from the supercritical fluid treatment. To overcome these problems, surface functionalization by aminosilane is proposed.

Surface functionalization could be classified into co-condensation and grafting (Maria Chong, and Zhao, 2003). Grafting method is preferable because it provides hydrolytic and structural stability (Zhu, Li, Zheng, Xu, and Li, 2012). For instance, a precipitated silica was grafted with 3-aminopropyltriethoxysilane (APTES) using a mechanical mixing and two-step aging for 60 h (Quang, Hatton, and Abu-Zahra, 2016). In addition, zeolite X was modified with APTES solution with an aging period of 40 h (Yutthalekha et al., 2017). This method results in the chemical formation between the aminosilane and supports. However, the conventional grafting is time-consuming. Hence, ultrasound-assisted grafting is proposed to reduce the long aging time.

Theoretically, acoustic cavitation is from an ultrasonic irradiation providing the formation, growth, and collapse of hot gas bubbles (Mohammadnezhad, Abad, Soltani, and Dinari, 2017). This increases temperature and pressure which enhances diffusion of the grafting precursor (Soltani, Dinari, and Mohammadnezhad, 2018; Suslick, and Flannigan, 2008). Recently, mesoporous MCM-41 was grafted with APTES by

ultrasound (Mohammadnezhad et al., 2017; Soltani et al., 2018). The ultrasound promotes grafting of the aminosilane on the porous support.

This work is aimed to compare the properties of catalysts prepared by ultrasound-assisted and conventional grafting. Physicochemical properties of the samples with various APTES and catalytic activity in aldol condensation of furfural and acetone are studied.

4.3   Experimental

4.3.1   Preparation of APTES-grafted silica gel

Silica gel with particle size of 60-200 μm, absolute ethanol, acetone, furfural and isopropanol (all from Carlo Erba) and APTES (Acrōs Organics) were used as received. Silica gel was grafted with APTES with a method from the literature (Quang et al., 2016) with sonication. In brief, 8 g of ethanol containing a desired amount of APTES was added to 2 g of silica gel, pre-dried at 80 ℃ for 6 h in a hot air oven. Then, the mixture was sonicated for 1 h at an ambient atmosphere with on-off pulses every five seconds using 130-Watt Ultrasonic Processor with a probe size of 6 mm (Sonics Vibra-Cell: VCX 130). The sample after ultrasonication was dried in a rotary evaporator at 40 ℃ with a reduced pressure of 100 mbar. Then, it was further dried in a hot air oven at 90 ℃ for 6 h. The samples containing 20, 30, 40, and 50 wt. % were named nAPS-U where n = wt. % of APTES and U = ultrasound. They were evaluated in the reaction testing. Then, the best catalyst was compared with the conventional impregnation with a similar loading. For comparison, silica gel was impregnated by a similar procedure without ultrasound. The prepared samples were named nAPS-C where C = conventional.

4.3.2 Characterization techniques

Phase characteristics of bare and grafted silica samples were studied by X-ray diffraction (XRD) using a Bruker XRD-D8 Advance with Cu K_α radiation. Morphologies were evaluated by field emission scanning electron microscopy (FE-SEM) using a JEOL JSM 7800F operating at the accelerated voltage of 15 kV. For the comparison between ultrasound-assisted grafting and conventional impregnation, the textural properties determined by the N_2 gas sorption measurement were used to explain the differences between both methods. N_2 sorption was performed using BELSORP-mini II. Samples were degassed at 150 ℃. Specific surface area and pore volume were calculated using the Brunauer-Emmett-Teller (BET) method. Pore size and pore size distribution were computed from an adsorption branch using the Barrett-Joyner-Halenda (BJH) approach.

Functional groups were analyzed by Fourier transform infrared spectrometry (FTIR) using the Bruker Vertex 70+RamII FTIR spectroscope manipulated in an attenuated total reflectance (ATR) mode with a resolution of 4 cm^{-1} and the scan number of 64. Chemical state of surface species was identified by X-ray photoelectron spectroscopy (XPS) using ULVAC-PHI PHI5000 VersaProbe II with Al K_α radiation. Elemental concentrations of C, H, and N were determined using TruSpec Micro CHNS elemental analyzer. Thermal properties were confirmed by thermogravimetric analysis in Mettler Toledo TGA/DSC1 to determine a suitable temperature for basicity measurement.

Basicity of catalysts was investigated by temperature-programmed desorption of carbon dioxide (CO_2-TPD) using a BELCAT-B chemisorption analyzer. Each sample of approximately 50 mg was loaded into a glass cell supported by quartz

wool and heated at 120 ℃ under He gas flow with a rate of 50 mL/min for 60 min. After it was cooled down to 75 ℃, a gas mixture of 10 % CO_2/He with a flow rate of 50 mL/min was introduced to the sample cell for 60 min. After that, an unabsorbed CO_2 was removed under He gas flow with a rate of 50 mL/min. The TPD process was performed in a temperature range of 35 to 150 ℃ with a temperature ramp of 10 ℃/min and holding time of 30 min under He flow with a rate of 30 mL/min.

4.3.3 Catalytic testing in aldol condensation of furfural and acetone

A catalyst amount of 500 mg, ethanol solution of 10 mL and acetone of 10 mL were added consecutively into a round bottom flask and stirred at 60 ℃ for 1 h under static N_2 atmosphere. Then, furfural of 960 mg was added dropwise to the flask. The reaction was held at 60 ℃ for a desired period. After cooling down, the reaction mixture was separated by centrifugation. All solution samples were quantitatively analyzed by gas chromatography with a Hewlett Packard HP 6890 Plus equipped with an FID detector using a 30 m long Innowax HP-1 capillary column with isopropanol as an internal standard. Catalyst activities including furfural conversion and selectivity of furanylbutenone (FB) were expressed in the following equations:

$$\text{Furfural conversion (mol\%)} = \frac{\text{moles of consumed furfural}}{\text{moles of initial furfural}} \times 100 \tag{4.1}$$

$$\text{FB selectivity (mol\%)} = \frac{\text{moles of produced FB}}{\text{moles of consumed furfural}} \times 100 \tag{4.2}$$

4.4 Results and discussion

4.4.1 Characterization of APTES-grafted silica gels

XRD patterns of all APS-U catalysts show the same broad peak at 22º as shown in **Figure 4.1** indicating the amorphous phase characteristic of silica gel as a support of the APS-U catalysts which did not change after the ultrasound-assisted grafting (Sarmah, Sahu, and Das, 2012). Their SEM images in **Figure 4.2** show similar morphology consistent with the XRD result. Moreover, aggregates of silica particles after the preparation are not observed due to the potential effect of acoustic cavitation generated by ultrasound irradiation during the grafting (Soltani et al., 2018).
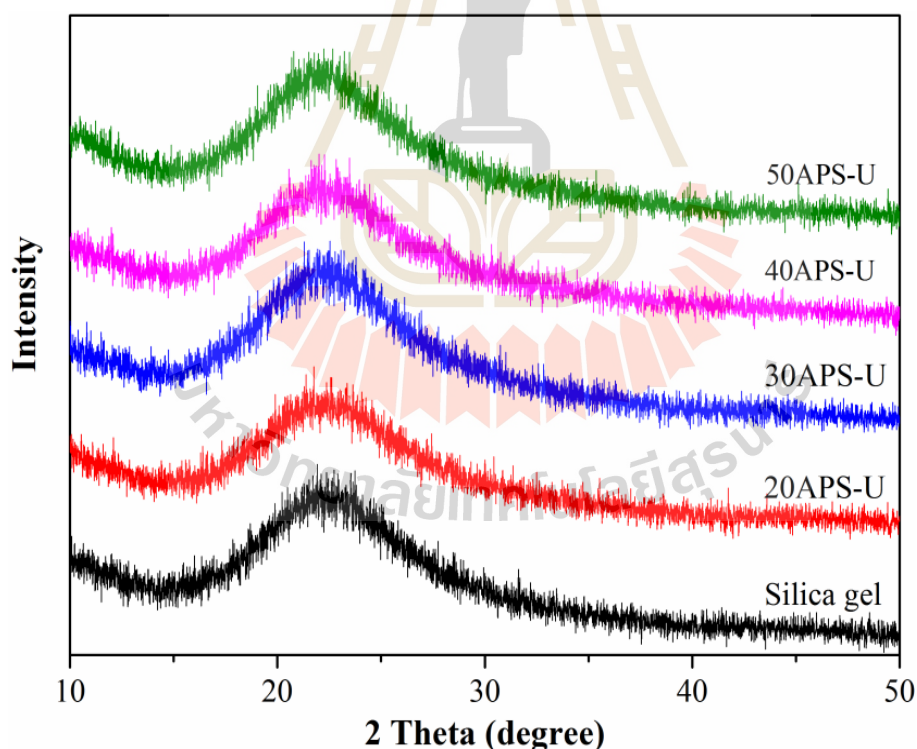
Figure 4.1 XRD patterns of the parent and silica gel grafted with various APTES loading.
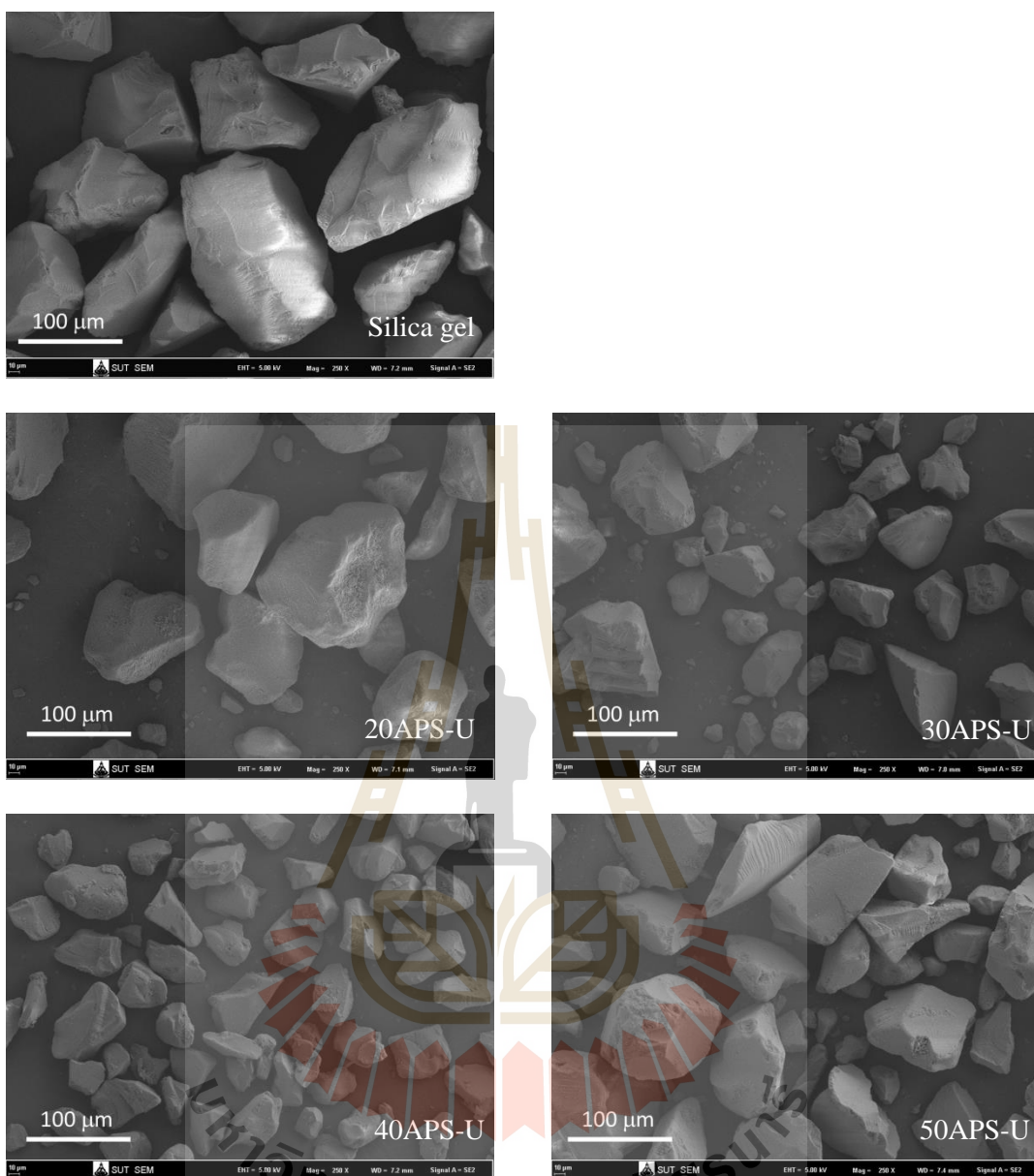
Figure 4.2 SEM images of the parent and silica gel grafted with various APTES.

N$_2$ sorption isotherms of all samples are displayed in **Figure 4.3**. According to the IUPAC classification (Thommes et al., 2015), all samples exhibits type IV(a) adsorption isotherm which is a characteristic of mesoporous materials and which includes the formation of monolayer and multilayer on the mesopore walls

before the pore condensation. In addition, all samples show a type H1 hysteresis loop which indicates a narrow range of uniform mesopores wider than 4 nm (Thommes et al., 2015). In the relative pressure range between 0.45 – 0.85, the size of hysteresis loops decreased with the loading of APTES. A result from the conventional method indicated the smallest loop. A steep desorption branch at the relative pressure between 0.45 – 0.50 implied an effect of pore-blocking due to the presence of the aminopropyl group in the silica cavity similar to the previous report (Jeong, Lim, Jin, and Park, 2012).
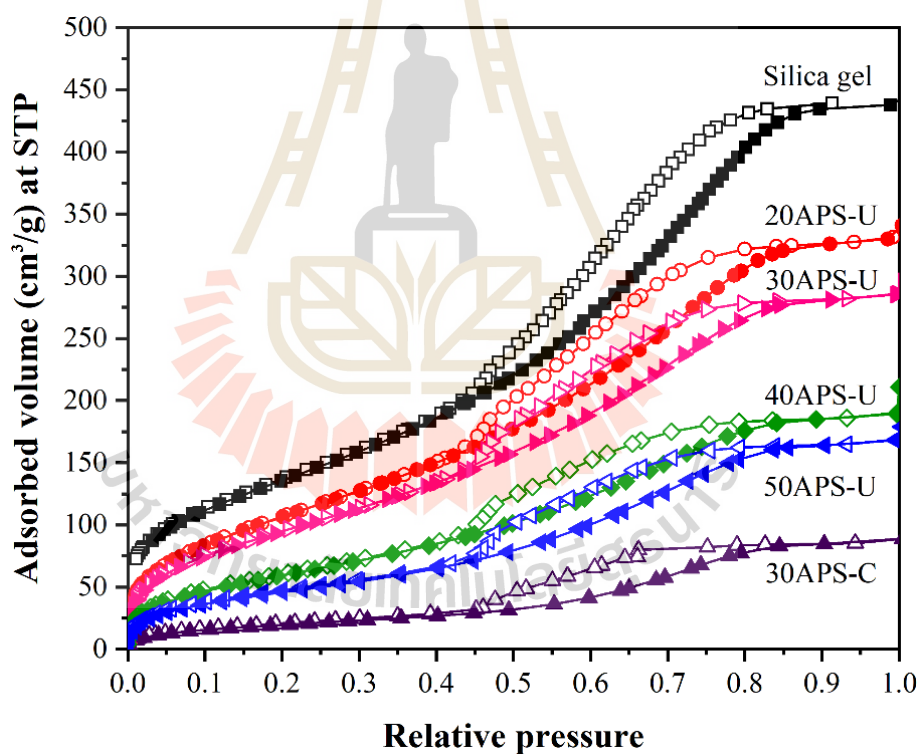
Figure 4.3 Nitrogen sorption isotherms of the parent and silica gel grafted with various APTES loading prepared by ultrasound-assisted grafting (U) and conventional method (C); filled symbols = adsorption, hollow symbols = desorption.

In comparison of two distinct preparation approaches with the same aminosilane loading of 30 wt. % as shown in **Table 4.1**, the sample from the ultrasound-assisted method (30APS-U) had almost 5-fold larger surface area and 4-fold larger pore volume indicating less pore-blocking than that from the conventional method (30APS-C). The result confirmed that the ultrasound-assisted grating provided better diffusion of aminosilane species into the pores than that of the conventional impregnation method.

Table 4.1 BET surface areas, pore volumes, and diameters of the parent silica gel and silica gel grafted with various amounts of APTES by ultrasound-assisted (U) and conventional (C) method.

Sample	BET surface area (m^2/g)	BJH pore volume (cm^3/g)	BJH pore diameter (nm)
Silica gel	505	0.67	4.76
20APS-U	415	0.52	3.28
30APS-U	370	0.44	3.28
30APS-C	75	0.14	5.41
40APS-U	233	0.30	3.71
50APS-U	177	0.27	4.19

FTIR spectra of all samples are shown in **Figure 4.4**. The vibration peaks of parent silica at 3418 and 798 cm^{-1} were assigned to O-H bond stretching and bending while the peaks at 1064 and 969 cm^{-1} were attributed to Si-O bond vibration (Quang et al., 2016). The shoulder peak at 3627 cm^{-1} was related to the vibration of the hydrogen-bonded silanol group on the silica gel surface (Britcher, Rahiala, Hakala, Mikkola, and Rosenholm, 2004). After grafting process by APTES, the major peaks of

both O-H and Si-OH decrease implying the replacement of surface silanol by the grafted aminopropyl (Quang et al., 2016). Moreover, the presence of new surface species was confirmed by the additional bands at 3365 and 3303 cm^{-1} assigned to N-H (Pasternack, Rivillon Amy, and Chabal, 2008; Quang et al., 2016; Sanaeepur, Kargari, and Nasernejad, 2014) while 1567 and 693 cm^{-1} were related to Si-C bond (Pasternack et al., 2008; Sanaeepur et al., 2014). The peaks at 2972 and 2910 cm^{-1} involved the vibration of propyl branch (Soltani et al., 2018). In comparison, the FTIR spectrum of 30APS-C is different from 30APS-U but similar to 50APS-U. The conventional impregnation provided the poorer diffusion of APTES into the pore leading to coverage on silica surface and blockage of the pore consistent with the N$_2$ sorption result.
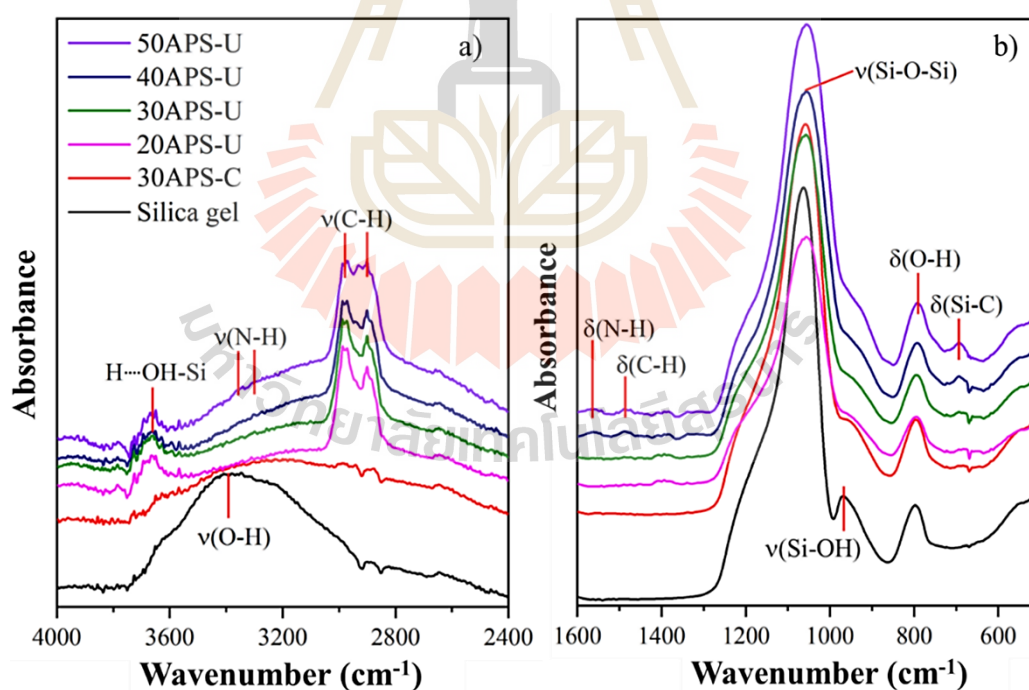
Figure 4.4 FTIR spectra of the silica gel grafted with various APTES loading prepared by ultrasound-assisted grafting (U) and conventional method (C).

To support the FTIR results of new functional groups by ultrasound-assisted grafting, wide-scan XPS spectra collected from as-prepared samples are shown in **Figure B.1** in Appendix B. The XPS spectra of Si 2p, O 1s, C 1s, and N 1s for APS-U samples compared to parent silica gel are shown in **Figure 4.5,** and their peak assignments are demonstrated in **Figure B.2 – B.5** in Appendix B. Identification and peak area of surface species are summarized in **Table 4.2**. The C 1s signal on silica gel arose from an adventitious carbon. After the ultrasound-assisted grafting, the peak shift of C 1s spectra was related to the appearance of APTES structure. Furthermore, total peak areas of all elements were obviously intensified with the increase of grafting concentration. The intensities of Si 2p and O 1s spectra of prepared samples shift to lower binding energy compared to the parent material according to the increase of APTES concentration (Jakša, Štefane, and Kovač, 2013). For 20APS-U, Si 2p peak at 103.38 eV presented a characteristic of Si-O-Si bond belonging to parent silica gel. This implied that its surface was partially occupied by APTES, and it decreased with higher APTES amount than 30 wt. % corresponding to deconvoluted results in **Table B.1** in Appendix B. Particularly, the peak intensities of both C 1s and N 1s raise as a result of bond formation of the APTES species on silica surface. In addition, the N 1s intensity of 30APS-U is similar to that of 20APS-U. This indicated the silica surface was not fully grafted with aminopropyl species which could interact with silanol to form ammonium species ($C-NH_3^+$) (Bezerra et al., 2014) leading to reduction of peak intensity of amine group ($C-NH_2$).
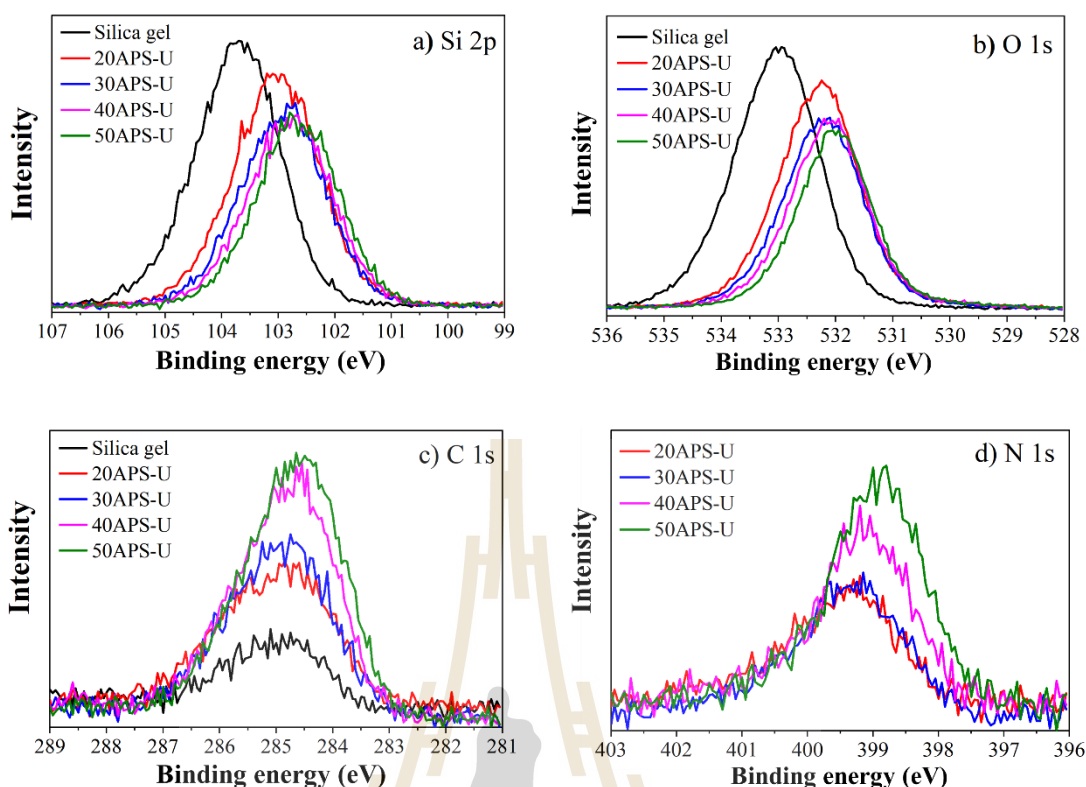
Figure 4.5 XPS spectra of the parent and silica gel grafted with various APTES loading;
a) Si 2p, b) O 1s, c) C 1s and d) N 1s.

The result of XPS atomic concentrations including C, N, O, and Si on
modified material surfaces is summarized in **Table 4.2**. The surface atomic
concentration of all elements increased with the increment of the aminopropyl loading.
Moreover, the atomic ratio of Si to N clearly increased corresponding to the APTES
loading. For consideration in the case of full surface occupation, the N/Si ratio of
aminopropyl silane molecule should approach one because there was only grafting
species on the surface. Interestingly, the obtained value was lower than one indicating
the dispersion of surface moiety was improved by ultrasound-assisted grafting.

Moreover, CHN analysis via combustion method was employed to ensure the elemental concentration of each sample.

Table 4.2 Relative atomic concentration of elements by XPS from the parent and silica gel grafted with various APTES loading.

Sample	XPS atomic concentration (%)				
	C 1s	N 1s	O 1s	Si 2p	N/Si
Silica gel	5.17	0	65.01	29.81	0
20APS-U	13.04	2.69	55.67	28.61	0.09
30APS-U	17.82	3.61	51.72	26.85	0.13
30APS-C	15.27	2.71	51.23	30.80	0.09
40APS-U	21.94	4.33	49.13	24.60	0.18
50APS-U	25.81	5.29	44.27	24.63	0.21

In **Table 4.3**, The aminopropyl branch was only considered after the combustion in air because both Si and O atoms were expected to be a part of the silica framework which was thermally stable (Talavera-Pech et al., 2016). This shows the content of each elemental had similar trend with an XPS result. Theoretically, the C/N molar ratio of aminopropyl moiety ($NH_2C_3H_6$–Si≡) after a complete condensation with three surface silanols was 3. Experimentally, the molar ratio of as-prepared samples was in the range of 3.58 – 4.14 which was higher than that of the calculated ratio. This could be assumed that the aminopropyl species was chemically grafted on the support, whereas either unhydrolyzed ethoxy branches (Parida, and Rath, 2009) or physically adsorbed ethanol was on the catalyst surface. Thus, this evidence could confirm the presence of aminopropyl group on the silica gel support. However, this also suggested the condensation of aminopropyl precursor with the surface silanol group was limited during the catalyst preparation.

Table 4.3 Elemental composition by CHN analysis and basicity by CO_2-TPD of the parent and silica gel grafted with various APTES

loading.

Sample	C (wt. %)		H (wt. %)		N (wt. %)		C/N (mole ratio)		Basicity
	Calc.[a]	Found	Calc.	Found	Calc.	Found	Calc.	Found	(mmol CO_2/g)
Silica gel	0	0.40 ± 0.006	0	1.22 ± 0.132					0.054
20APS-U	3.25	3.87 ± 0.009	0.72	1.88 ± 0.051	1.26	1.09 ± 0.026	3.00	4.14	0.104
30APS-U	4.88	5.49 ± 0.136	1.08	2.19 ± 0.100	1.90	1.66 ± 0.040	3.00	3.85	0.139
40APS-U	6.50	8.50 ± 0.037	1.45	2.78 ± 0.048	2.53	2.59 ± 0.058	3.00	3.87	0.431
50APS-U	8.13	9.04 ± 0.183	1.81	2.95 ± 0.078	3.16	2.95 ± 0.024	3.00	3.58	0.476

[a] Calc. abbreviates from a calculated value which is defined by the mass distribution of an element in the APTES loading as shown in

equation B.2 – B.4 in the Appendix B.

The grafted samples were analyzed by TGA to confirm the amounts of aminopropyl moieties on the silica gel. The thermograms are shown in **Figure 4.6** and the numeric details are in **Table B.2** in Appendix B. The weight loss from silica gel occurred mainly in two regions. The loss around 5 wt. % before reaching 150 ℃ was from the removal of physisorbed gases such as water and CO_2 on the surface (Kulkarni, Mirji, Mandale, and Vijayamohanan, 2006). The further loss of approximately 4 wt. % at the higher temperature was from the desorption of chemisorbed-water and dehydroxylation of the silanol groups (Quang et al., 2016).
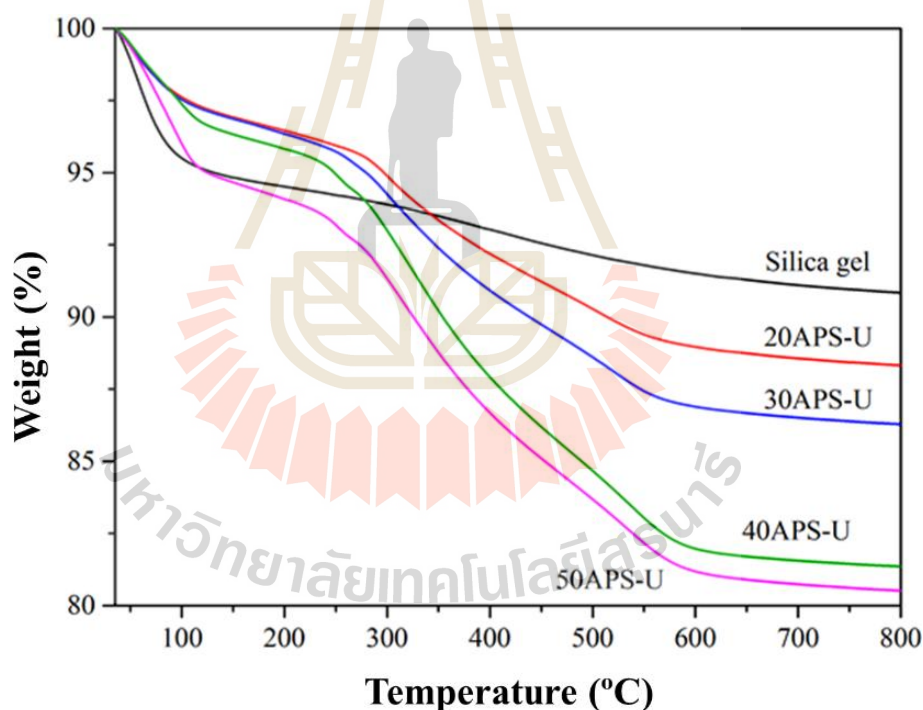
Figure 4.6 TGA profiles of the parent and silica gel with various APTES loading.

From the grafted samples, there were three ranges of weight loss. The first region was similar to that of the parent. The second range from 150 to 600 ℃ was assigned to the decomposition of grafted species. These results agree with the degradation of amine-grafted SBA-15 in air (Khatri, Chuang, Soong, and Gray, 2006). The loss over 600 ℃ corresponded to the condensation of framework silanol (Ivaldi et al., 2019). The TGA results suggested that the maximum temperature for further CO_2-TPD study was 150 ℃ to prevent the decomposition of the surface aminopropyl during the sample pretreatment and desorption process.

Basicity of the amino-modified materials obtained from CO_2 TPD is depicted in **Figure 4.7**. The result indicated that the parent silica was of the lowest basic value because of the physisorption of the CO_2 molecule. Meanwhile, the basicity of modified samples remarkably increased in accordance with the increment of aminopropyl concentration as shown in **Table 4.3**. Theoretically, the CO_2 gas molecule could chemically react with the surface amino species to generate thermally-desorbable carbamate or carbonate group (Quang et al., 2016). Moreover, when the surface aminopropyl moieties were located in an accessible pore, the introduced CO_2 gas could simply diffuse to react with the active site. This also indicated that there was the absence of pore-blocking corresponding to the result of N_2 sorption. Thus, the basic property of prepared catalysts could be enhanced by the increase of amino grafting content.
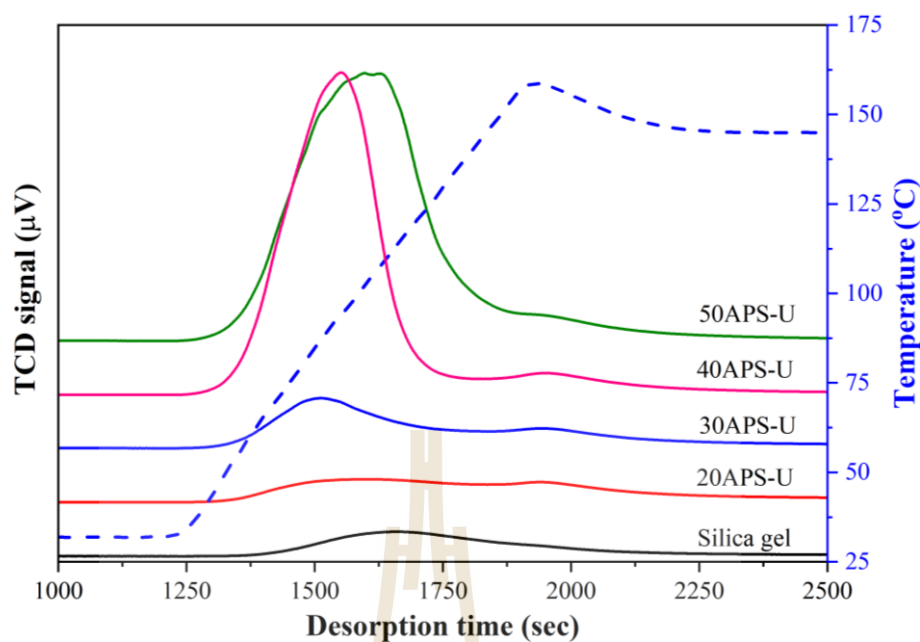
Figure 4.7 CO_2-TPD profiles of the parent and silica gel grafted with various APTES loading.

According to the characterization results, aminopropyl-modified silica gel was successfully prepared by a simple ultrasound-assisted method with shorter period compared to the conventional method and a previous report (Quang et al., 2016). Furthermore, the grafting pathway of 3-aminopropylethoxysilane on silica surface in ethanol was proposed in **Scheme 4.1**. The aminopropyl moiety covalently condensed with surface silanol group of silica gel followed by the elimination of ethanol to form new siloxane bond (Si-O-Si) (Quang et al., 2016). Nevertheless, there was the presence of uncondensed ethoxy groups due to limitation of aminopropyl silane grafting in the operated condition. In addition, the surface aminopropyl played a key role in the active basic species to facilitate aldol condensation of furfural and acetone.
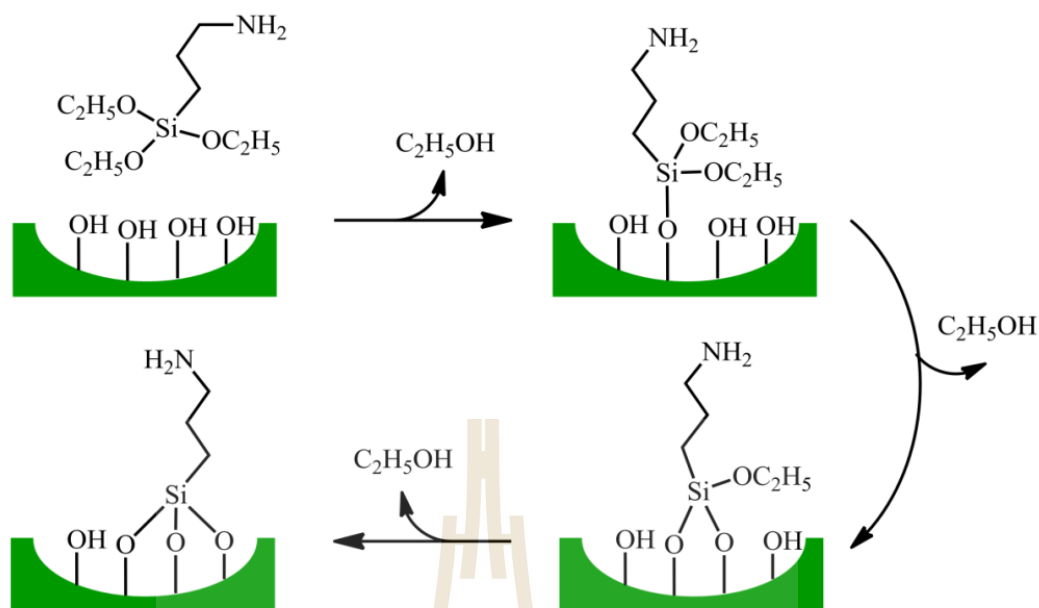
Scheme 4.1 Proposed pathway of APTES grafting on silica gel surface under ultrasound irradiation.

4.4.2 Catalytic activity on the aldol condensation

4.4.2.1 Effect of aminopropyl group loading

A comparison of an aminopropyl concentration effect on the catalytic activity was illustrated in **Figure 4.8**. The silica gel as a reference possessed a poor active basic site in nature as a result of the lowest performance in the reaction. According to the aforementioned basicity determination by CO_2-TPD methodology, all aminopropyl-grafted samples provided almost complete conversion of furfural as a starting reagent as well as the good yield and selectivity towards furfurylbutenone as a desired product. This evidence clearly indicated that the accessible surface aminopropyl moiety facilitated the successive dehydration of furfurylhydroxybutanone as a minor aldol adduct to form the desired product (Kayser et al., 2012). In addition, the grafted

amount of the aminopropyl precursor exhibited less effect on the change of the catalytic

activity. However, the higher loading concentration than that of 40 wt. % showed the

reduction of product variation. This was presumably due to the physicochemical

deposition of some product or intermediate species on surface-active site. In accordance

with the aforementioned results, 30APS-U sample was suitable for further reaction

study.
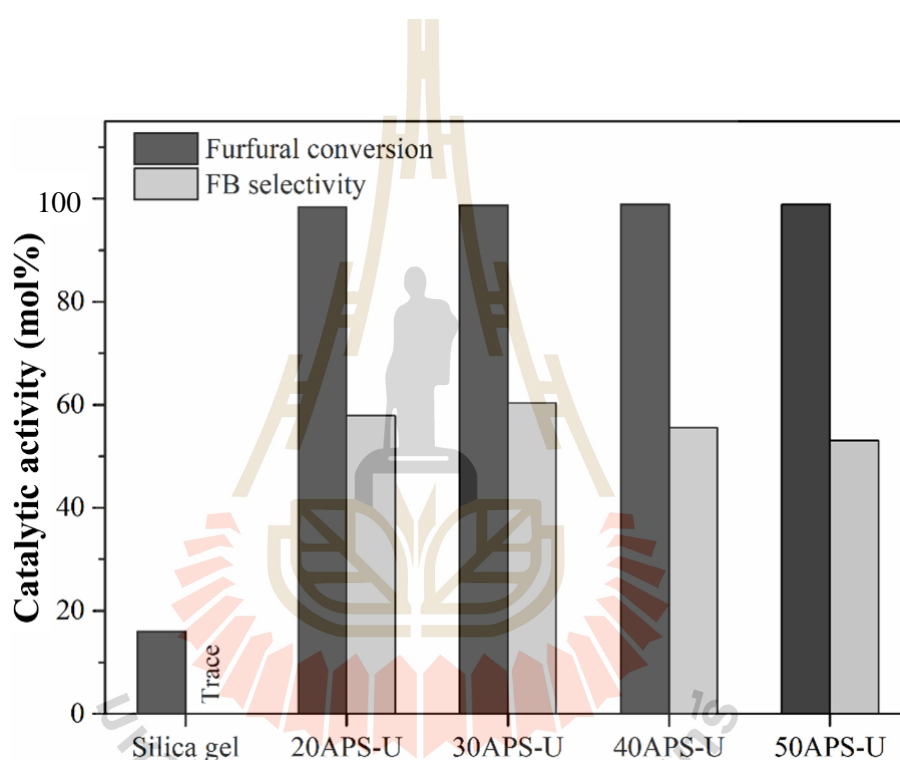
Figure 4.8 Effect of APTES loading on the catalytic activity for the aqueous aldol

condensation of furfural and acetone at 60 ºC for 24 h.

4.4.2.2 Effect of reaction time

Catalytic activities including furfural conversion and FB selectivity with reaction time on 20APS-U catalyst are shown in **Figure 4.9**. The reaction activities increase with the reaction time until 24 h. Whereas FB yield gradually intensified until the reaction time of 24 h, this might be due to the dehydration of furfurylhydroxybutanone as a minor product. At the same reaction time of 24 h, all variations were slightly constant, while there was no appreciable change along further the operation time.
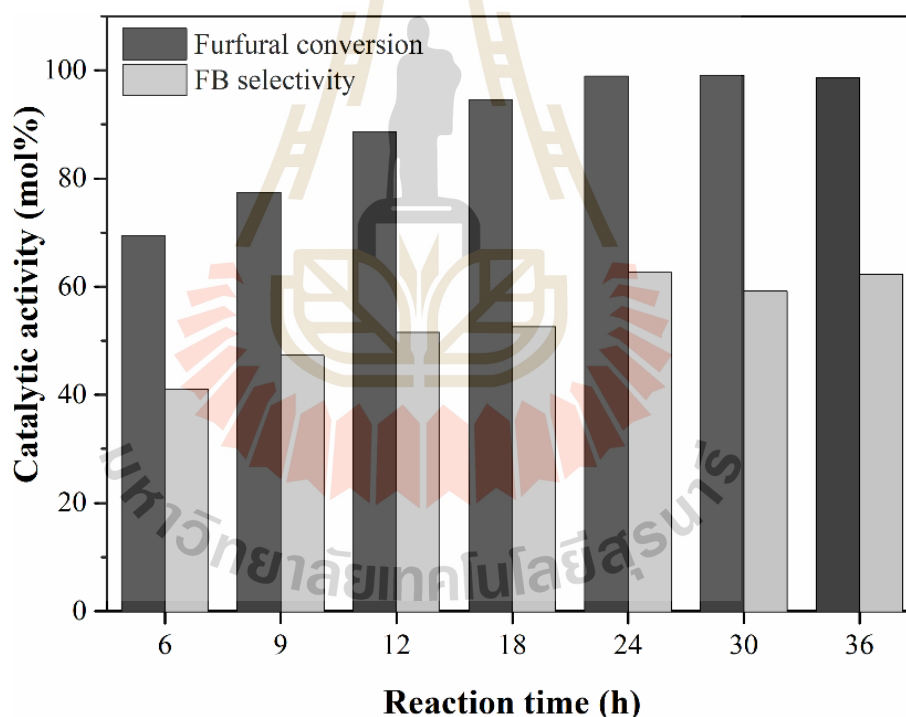
Figure 4.9 Effect of reaction time on performance of 30APS-U catalyst for the aldol condensation of furfural and acetone at 60 °C.

The catalytic activity of aminopropyl-grafting silica gel in this work was compared to previous researches as summarized in **Table 4.4**. In the case of short reaction time, 30APS-U performed better furfural conversion and product selectivity than those of other catalysts operated at similar conditions. For long-term reaction at mild temperature, it still provided greater furfural conversion than that of other samples with stronger basic active species e.g. K_2O. Especially, when compared to the similar amine active site in chitosan gel, it still showed higher activity at lower temperatures. Therefore, the aminopropyl-grafting silica provided better furfural conversion and considerable FB selectivity at a milder condition compared to inorganic catalysts reported in literature (Kayser et al., 2012; Kikhtyanin et al., 2018a; Kikhtyanin, Ganjkhanlou, Kubička, Bulánek, and Čejka, 2018b; Kikhtyanin, Kelbichová, Vitvarová, Kubů, and Kubička, 2014; Nguyen Thanh et al., 2016).
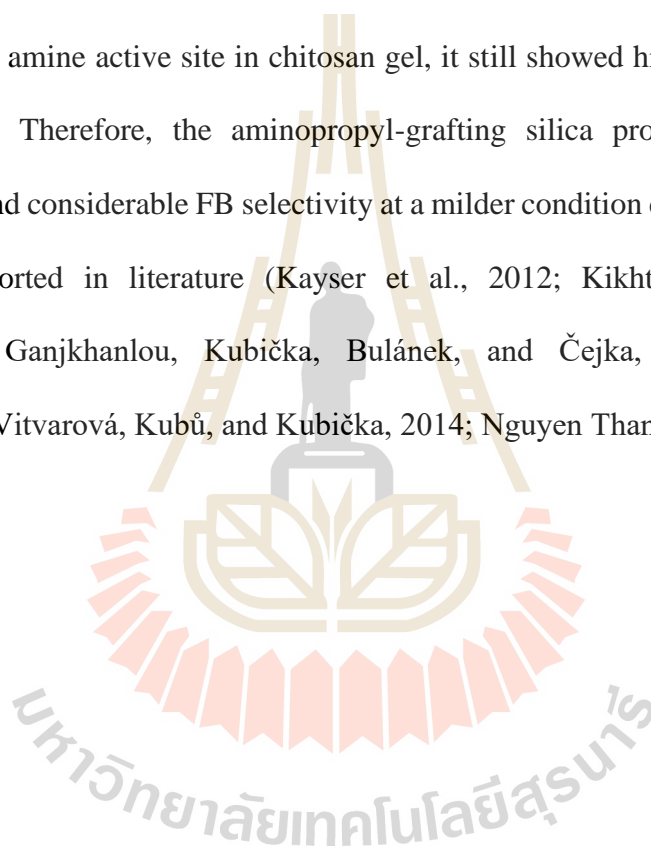
Table 4.4 Comparison of the testing conditions and catalytic activity of aldol condensation between furfural and acetone from literature and this work.

Catalyst	Reaction condition			Furfural Conversion	FB Selectivity	Reference
	Temperature (°C)	Time (h)	Reactor	(%)	(%)	
Nanosized TiO$_2$	50	6	Glassware	25	72	Nguyen Thanh et al. (2016)
MgGa-4R10[a]	50	2	Glassware	59.7	9.3	Kikhtyanin et al. (2018a)
HBEA[b]	60	2	Autocalve	19.8	80.2	Kikhtyanin et al. (2014)
30APS-U	60	6	Glassware	69.5	41.1	This work
30APS-U	60	24	Glassware	98.9	62.7	This work
Dried chitosan gel	90	12	Glassware	<1	58	Kayser et al. (2012)
K-IE-Y(2.5)[c]	100	2	Autocalve	8.3	94.6	Kikhtyanin et al. (2018b)
K-IMP-Y(15)[d]	100	2	Autocalve	44.1	35	Kikhtyanin et al. (2018b)

[a] MgGa-4R10 is MgGa mixed oxide with Mg/Ga = 4 prepared by rehydration for 10 times.

[b] HBEA is Zeolite BEA in a proton (H$^+$) form.

[c] K-IE-Y(2.5) is Zeolite Y (Si/Al = 2.5) ion-exchanged by KNO$_3$.

[d] K-IMP-Y is Zeolite Y (Si/Al = 15) impregnated by KNO$_3$.

4.5 Conclusions

Silica gel was grafted with various amounts of APTES by the simple ultrasonic-assisted method. The grafting did not change the characteristic phase of the silica support, and the grafted samples did not aggregate. The ultrasonic-assisted method enhanced the diffusion of grafting species into the pores of silica gel leading to better dispersion and less pore blocking. The APTES reacted with the silanol groups of silica gel to form new siloxane bonds. The basicity of the grafted silica increased with the amount of APTES. From catalytic testing in aldol condensation between furfural and acetone, all grafted silica samples provided nearly complete furfural conversion. The sample prepared from APTES loading of 30 wt. %, 30APS-U, provided the highest product selectivity after a reaction time of 24 h. This performance was among the best materials as previously reported in the literature. Therefore, the grafted silica gel prepared by the ultrasound-assisted method could serve as a promising catalyst to enhance the production of value-added chemicals.

4.6 References

Bezerra, D. P., Silva, F. W. M. d., Moura, P. A. S. d., Sousa, A. G. S., Vieira, R. S., Rodriguez-Castellon, E., and Azevedo, D. C. S. (2014). CO_2 adsorption in amine-grafted zeolite 13X. **Applied Surface Science**. 314: 314-321.

Britcher, L., Rahiala, H., Hakala, K., Mikkola, P., and Rosenholm, J. B. (2004). Preparation, characterization, and activity of silica supported metallocene catalysts. **Chemistry of Materials**. 16(26): 5713-5720.

Ivaldi, C., Miletto, I., Paul, G., Giovenzana, G. B., Fraccarollo, A., Cossi, M., Marchese, L., and Gianotti, E. (2019). Influence of silicodactyly in the preparation of hybrid materials. **Molecules**. 24(5): 848.

Jakša, G., Štefane, B., and Kovač, J. (2013). XPS and AFM characterization of aminosilanes with different numbers of bonding sites on a silicon wafer. **Surface and Interface Analysis**. 45(11-12): 1709-1713.

Jeong, E.-Y., Lim, C.-R., Jin, H., and Park, S.-E. (2012). trans-1,2-Diaminocyclohexane mesoporous silica for asymmetric catalysis: enhancement of chirality through confinement space by the plug effect. **Chemical Communications**. 48(25): 3079-3081.

Kayser, H., Müller, C. R., García-González, C. A., Smirnova, I., Leitner, W., and Domínguez de María, P. (2012). Dried chitosan-gels as organocatalysts for the production of biomass-derived platform chemicals. **Applied Catalysis A: General**. 445-446: 180-186.

Khatri, R. A., Chuang, S. S. C., Soong, Y., and Gray, M. (2006). Thermal and chemical stability of regenerable solid amine sorbent for CO_2 capture. **Energy & Fuels**. 20(4): 1514-1520.

Kikhtyanin, O., Čapek, L., Tišler, Z., Velvarská, R., Panasewicz, A., Diblíková, P., and Kubička, D. (2018a). Physico-chemical properties of MgGa mixed oxides and reconstructed layered double hydroxides and their performance in aldol condensation of furfural and acetone. **Frontiers in Chemistry**. 6(176).

Kikhtyanin, O., Ganjkhanlou, Y., Kubička, D., Bulánek, R., and Čejka, J. (2018b). Characterization of potassium-modified FAU zeolites and their performance in

aldol condensation of furfural and acetone. **Applied Catalysis A: General**. 549: 8-18.

Kikhtyanin, O., Kelbichová, V., Vitvarová, D., Kubů, M., and Kubička, D. (2014). Aldol condensation of furfural and acetone on zeolites. **Catalysis Today**. 227: 154-162.

Kuhbeck, D., Saidulu, G., Reddy, K. R., and Diaz, D. D. (2012). Critical assessment of the efficiency of chitosan biohydrogel beads as recyclable and heterogeneous organocatalyst for C-C bond formation. **Green Chemistry**. 14(2): 378-392.

Kulkarni, S. A., Mirji, S. A., Mandale, A. B., and Vijayamohanan, K. P. (2006). Thermal stability of self-assembled octadecyltrichlorosilane monolayers on planar and curved silica surfaces. **Thin Solid Films**. 496(2): 420-425.

Maria Chong, A. S., and Zhao, X. S. (2003). Functionalization of SBA-15 with APTES and characterization of functionalized materials. **The Journal of Physical Chemistry B**. 107(46): 12650-12657.

Mohammadnezhad, G., Abad, S., Soltani, R., and Dinari, M. (2017). Study on thermal, mechanical and adsorption properties of amine-functionalized MCM-41/PMMA and MCM-41/PS nanocomposites prepared by ultrasonic irradiation. **Ultrasonics Sonochemistry**. 39: 765-773.

Nguyen Thanh, D., Kikhtyanin, O., Ramos, R., Kothari, M., Ulbrich, P., Munshi, T., and Kubička, D. (2016). Nanosized TiO_2-A promising catalyst for the aldol condensation of furfural with acetone in biomass upgrading. **Catalysis Today**. 277: 97-107.

Parida, K. M., and Rath, D. (2009). Amine functionalized MCM-41: an active and reusable catalyst for Knoevenagel condensation reaction. **Journal of Molecular Catalysis A: Chemical**. 310(1-2): 93-100.

Pasternack, R. M., Rivillon Amy, S., and Chabal, Y. J. (2008). Attachment of 3-(aminopropyl)triethoxysilane on silicon oxide surfaces: dependence on solution temperature. **Langmuir**. 24(22): 12963-12971.

Quang, D. V., Hatton, T. A., and Abu-Zahra, M. R. M. (2016). Thermally stable amine-grafted adsorbent prepared by impregnating 3-aminopropyltriethoxysilane on mesoporous silica for CO_2 capture. **Industrial & Engineering Chemistry Research**. 55(29): 7842-7852.

Sanaeepur, H., Kargari, A., and Nasernejad, B. (2014). Aminosilane-functionalization of a nanoporous Y-type zeolite for application in a cellulose acetate based mixed matrix membrane for CO_2 separation. **RSC Advances**. 4(109): 63966-63976.

Sarmah, C., Sahu, D., and Das, P. (2012). Anchoring palladium acetate onto imine-functionalized silica gel through coordinative attachment: an effective recyclable catalyst for the Suzuki–Miyaura reaction in aqueous-isopropanol. **Catalysis Today**. 198(1): 197-203.

Soltani, R., Dinari, M., and Mohammadnezhad, G. (2018). Ultrasonic-assisted synthesis of novel nanocomposite of poly(vinyl alcohol) and amino-modified MCM-41: a green adsorbent for Cd(II) removal. **Ultrasonics Sonochemistry**. 40(Pt A): 533-542.

Suslick, K. S., and Flannigan, D. J. (2008). Inside a collapsing bubble: sonoluminescence and the conditions during cavitation. **Annual Review of Physical Chemistry**. 59(1): 659-683.

Talavera-Pech, W. A., Esparza-Ruiz, A., Quintana-Owen, P., Vilchis-Nestor, A. R., Carrera-Figueiras, C., and Ávila-Ortega, A. (2016). Effects of different amounts of APTES on physicochemical and structural properties of amino-functionalized MCM-41-MSNs. **Journal of Sol-Gel Science and Technology**. 80(3): 697-708.

Thommes, M., Kaneko, K., Neimark Alexander, V., Olivier James, P., Rodriguez-Reinoso, F., Rouquerol, J., and Sing Kenneth, S. W. (2015). Physisorption of gases, with special reference to the evaluation of surface area and pore size distribution (IUPAC Technical Report). **Pure and Applied Chemistry**. 87(9-10): 1051-1069.

Yutthalekha, T., Suttipat, D., Salakhum, S., Thivasasith, A., Nokbin, S., Limtrakul, J., and Wattanakit, C. (2017). Aldol condensation of biomass-derived platform molecules over amine-grafted hierarchical FAU-type zeolite nanosheets (zeolean) featuring basic sites. **Chemical Communications**. 53(90): 12185-12188.

Zhu, Y., Li, H., Zheng, Q., Xu, J., and Li, X. (2012). Amine-functionalized SBA-15 with uniform morphology and well-defined mesostructure for highly sensitive chemosensors to detect formaldehyde vapor. **Langmuir**. 28(20): 7843-7850.

CHAPTER V

BASICITY OF CATALYST FROM HEAT TREATED

NATURAL MARL AND PERFORMANCE IN

TRANSESTERIFICATION OF PALM OIL

5.1   Abstract

This chapter aims to demonstrate the preparation of calcium catalysts from natural marl in Thailand using a thermal treatment at 600, 700, 800, 900, and 1000 ℃. Physicochemical properties of these samples were studied by XRD, XRF, XPS, FTIR, FE-SEM, and N_2 sorption. Calcium carbonate species is transformed to hydroxide and oxide after treating at 800 and 1000 ℃, respectively. The treatment also affected the elemental contribution on the sample surfaces. Both morphologies and surface properties were also developed by decarbonation during the calcination. The basicity was studied by the conversion of 2-methylbut-3-yn-2-ol (MBOH). The base strength increased with the calcination temperatures. The base strength of calcined samples was further studied by the conversion of palm oil with methanol through transesterification at 60 ℃ for 3 h. The test reaction could distinguish the base strength between carbonate and hydroxide more effectively than the decomposition of MBOH. A catalyst with the higher base strength gave the higher conversion of palm oil. From the reaction, the marl calcined at 800 ℃ was the most suitable catalyst.

5.2 Introduction

According to the current transesterification process to produce biodiesel, homogeneous base catalysts such as NaOH and KOH are widely used due to the operation at a low temperature and high biodiesel production. However, there are several disadvantages; for example, a lot of wastewater produced from a neutralization step and the difficulty in catalyst reusability (Rakmae et al., 2016). Hence, heterogeneous base catalysts are proposed to overcome these drawbacks.

Up to date, a number of research works have focused on the synthesis and improvement of solid base catalysts for transesterification. Among several types of calcium-rich materials, e.g., dolomite, coral fragment, and hydrated lime, Thai natural marl is considered as a low-cost raw material. (Jaiyen, Naree, and Ngamcharussrivichai, 2015; Ngamcharussrivichai, Nunthasanti, Tanachai, and Bunyakiat, 2010; Ngamcharussrivichai, Wiwatnimit, and Wangnoi, 2007; Roschat, Kacha, Yoosuk, Sudyoadsuk, and Promarak, 2012; Roschat, Siritanon, Yoosuk, and Promarak, 2016). It is one of carbonate-rich compounds with a small amount of alumina and silica and can be found in many areas of Thailand.

Although calcium carbonate ($CaCO_3$) is the main species in these raw materials, it gives low conversion of triglycerides and requires a high temperature to accomplish a high reaction activity due to a poor base strength (Ngamcharussrivichai et al., 2007). This literature suggested that the base strength of calcium-based catalysts is a predominant effect on the activity of base-catalyzed transesterification. Hence, heterogeneous catalysts require specific and precise techniques to investigate a base property after a preparation process.

So far, temperature-programmed desorption of carbon dioxide (CO_2-TPD) is commonly used to determine the basicity of several solid samples (Jaiyen et al., 2015; Ngamcharussrivichai et al., 2010; Ngamcharussrivichai et al., 2007; Roschat et al., 2016). Although this technique provides highly accurate information and convenient operation, the serious problems is the strong interaction of CO_2 on surface base sites (Supamathanon, Wittayakun, Prayoonpokarach, Supronowicz, and Roessner, 2012). According to the limitation of the thermal property of carbonate-rich materials, the basicity could not be measured due to the decomposition of the carbonate at a desorption temperature higher than 800 ℃ (Ngamcharussrivichai et al., 2010). Thus, the decomposition of 2-methylbut-3-yn-2-ol (MBOH) has been considered as a test reaction to evaluate the base strength by consideration of obtained products catalyzed by different active sites (Kulawong, Prayoonpokarach, Roessner, and Wittayakun, 2015; Supamathanon et al., 2012). The benefits of this method consist of an operation temperature lower than that of the decomposition of carbonate compounds (less than 180 ℃) and classification of surface-active species in nature.

Therefore, this research is aimed to prepare calcium catalysts from Thai natural marl by a thermal treatment with different calcination temperatures. Then, the base strength of these calcined samples is studied by conversion of palm oil as a proposed test reaction compared with the decomposition of MBOH as a reference method. Finally, all catalysts are tested in transesterification of palm oil.

5.3   Experimental

5.3.1   Preparation of calcium catalysts through a thermal treatment

A natural Thai marl was purchased from a convenient store in Nakhon Ratchasima province, Thailand. It was treated thermally according to the literature (Ngamcharussrivichai et al., 2010). The raw material of 5 g was ground and sieved by a mesh size of 80 to obtain the fine powder. Then, it was pre-dried in a hot air oven at a temperature of 80 ℃ overnight and calcined at a temperature range between 600 to 1000 ℃. Finally, the sample was kept in a desiccator to prevent adsorption of atmospheric gases e.g. H_2O and CO_2 causing an inert surface for further study. The prepared sample is denoted as Mx when x is a calcination temperature. For example, M600 is the sample calcined at 600 ℃.

5.3.2   Characterization techniques

Phase characteristics of the parent and marl samples calcined at various temperatures were studied by X-ray diffraction (XRD) using a Bruker XRD-D8 Advance with Cu K_α radiation. The relative elemental concentration of the raw material was determined by wavelength dispersive X-ray fluorescence spectroscopy using a PANalytical AXIOS^{mAX} XRF spectrometer with a rhodium (Rh) X-ray source. XRF results were quantified by an OMNION mode. Relative atomic concentrations of surface species were identified by X-ray photoelectron spectroscopy (XPS) using a ULVAC-PHI PHI5000 VersaProbe II with Al K_α radiation.

Functional groups of bulk samples were analyzed by Fourier transform infrared spectrometry (FTIR) using a Bruker Tensor21 spectroscope manipulated in an attenuated total reflectance (ATR) mode with a resolution of 4 cm^{-1} and the scan

number of 64. Morphologies were evaluated by field emission scanning electron microscopy (FE-SEM) using a JEOL JSM 7800F operating at the accelerated voltage of 15 kV. Adsorption-desorption isotherms, surface area, and pore volume were determined by an N_2 gas sorption analysis using a BELSORP-mini II. Sample powder of approximately 0.2 g was loaded into a glass tube and further degassed at a temperature of 150 ℃ overnight. Specific surface area and pore volume were calculated by a Brunauer-Emmett-Teller (BET) method using an adsorption branch.

5.3.3   Evaluation of base strength by the decomposition of MBOH

Basicity of the calcium catalysts was evaluated through the decomposition of 2-methylbut-3-yn-2-ol (MBOH). The test reaction was performed in a fixed bed reactor equipped with an HP 5890 Series II gas chromatograph (GC) as shown in **Scheme 5.1** below modified from the literature (Novikova, Roessner, Belchinskaya, Alsawalha, and Krupskaya, 2014). Prior to the measurement, 0.5 g of a sample with a particle size in the range of 200 to 315 µm was packed into a tubular reactor and pretreated at 350 ℃ under an N_2 gas flow. Then, the reactor was cooled down to 150 ℃ and flushed with a vaporized mixture with a mass ratio of 95:5 between MBOH and toluene as an internal standard under N_2 gas flow of 10 mL/min. A conversion of MBOH and product selectivity were calculated according to **equations C1 – C3** in Appendix C.
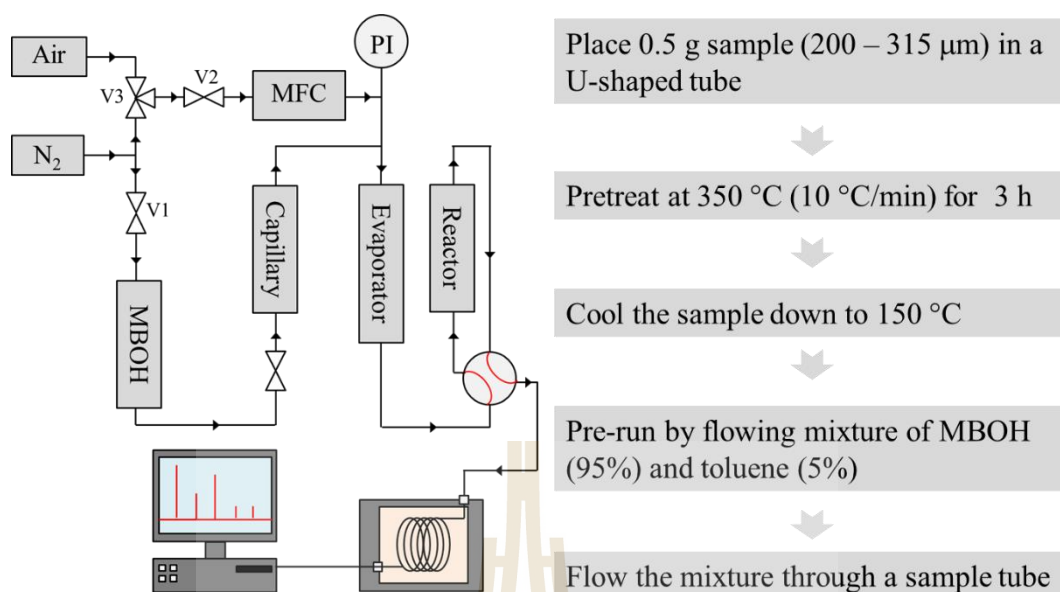
Scheme 5.1 Systematic diagram of the decomposition of 2-methylbut-3-yn-2-ol

(MBOH) as a test reaction for the evaluation of acid-base properties.

5.3.4 Conversion of palm oil by base-catalyzed transesterification

Palm oil (Morakot Industries PCL., Thailand) was purchased from a

convenience store in Nakhon Ratchasima province. A methanol-to-oil molar ratio in

the reaction was 15:1. For the conversion of palm oil via a base-catalyzed

transesterification, a desired amount of marl-derived catalysts was mixed with

methanol and stirred in a three-necked round bottom flask at 60 °C for 30 min. Then,

palm oil contained in a glass dropping funnel was slowly added dropwise under a

vigorous stirring for 3 h at the same temperature. After the completion of the reaction,

the solid is immediately removed by filtration. The filtrate is further separated, washed

with deionized water and dried with anhydrous sodium sulfate salt (Na_2SO_4). The

conversion of palm oil was determined by a thin layer chromatography (TLC) plate

using a mobile phase mixture of petroleum ether-to-diethyl ether-to-glacial acetic acid with a volume ratio of 85:15:1 (Manadee et al., 2017).

5.4 Results and discussion

5.4.1 Characterization of the parent and Thai natural marl calcined at different temperatures

XRD patterns of the parent and marl samples calcined at various temperatures are shown in **Figure 5.1**. From the parent, M600 and M700, the main phase was calcite ($CaCO_3.xH_2O$) (JCPDS database number 2004-05-0586). There was a slight difference in cell parameters in between M600 and M700 due to a peak shift. From M800, the main phase was calcium hydroxide ($Ca(OH)_2$), also called portlandite (JCPDS number 2004-44-1481). The change includes the decarboxylation and the hydroxylation by water in the calcite framework to generate the hydroxide species. The result was similar to a TGA result of calcite decarbonation at 820 ℃ reported by Vance et al. (2015). From M900, the main phase was a mixed-phase between $Ca(OH)_2$ and CaO. From M1000, the only phase observed was CaO (JCPDS number 2004-04-0777). Therefore, the thermal treatment converts the phase of the Thai marl from $CaCO_3$ to $Ca(OH)_2$ and CaO.

Elemental composition by XRF of the as-received Thai natural marl is listed in **Table 5.1**. Calcium carbonate ($CaCO_3$) or calcite is the major component with a small amount of oxides such as Al_2O_3, SiO_2, Fe_2O_3, and MgO. These oxides were not detected by XRD. With the rich of crystalline $CaCO_3$, the natural marl is a suitable material for calcium catalysts.
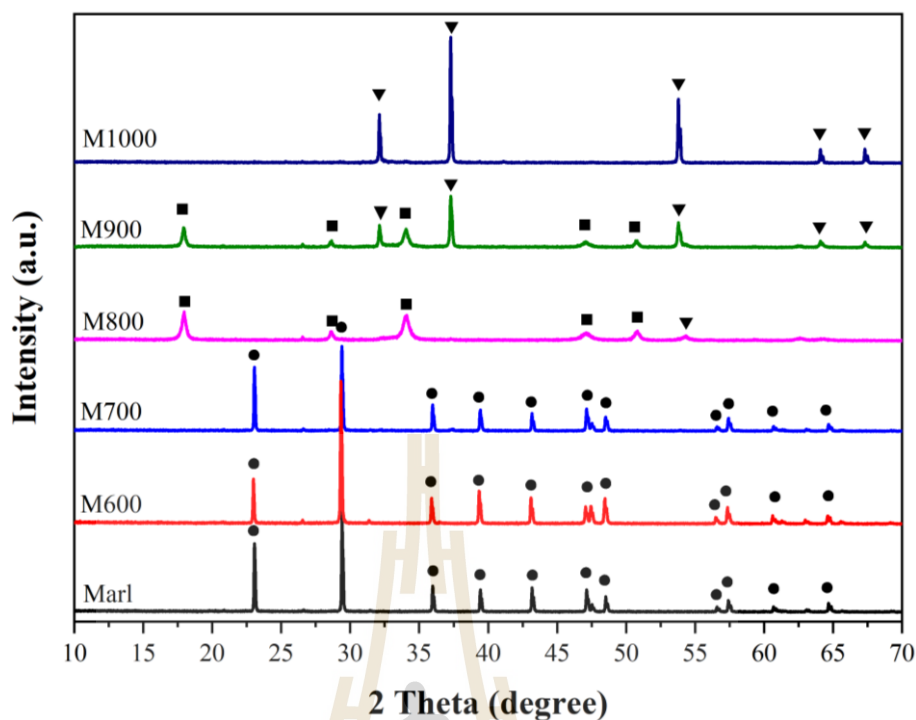
Figure 5.1. XRD patterns of samples calcined at various temperatures resulting in different calcium phases; Symbol ● = $CaCO_3$ (JCPDS 2004-05-0586), ■ = $Ca(OH)_2$ (JCPDS 2004-44-1481), and ▼ = CaO (JCPDS 2004-04-0777).

Table 5.1 Elemental composition of as-received natural marl determined by XRF.

Elemental composition (wt. %)							
$CaCO_3$	SiO_2	Al_2O_3	Fe_2O_3	MgO	TiO_2	MnO_2	P_2O_5
95.88	2.89	0.58	0.34	0.19	0.06	0.05	0.01

The relative surface atomic concentration was determined by XPS. The relative atomic concentration of the parent and the marl samples calcined at various temperatures is listed in **Table 5.2**. There are four major elements including Ca, C, O, and Si. The samples from the higher calcination temperature had a larger amount of Ca.

This result is in good agreement with the study by Sasaki, Qiu, Hosomomi, Moriyama, and Hirajima (2013) that the Ca amount increased owing to the decarbonation by a heat treatment. Theoretically, the carbon constituents should be completely eliminated after the calcination above 800 ℃. On the other hand, there was the presence of carbon species on the surface of the calcined samples. The result indicated that both calcium hydroxide and oxide phases from the calcined samples could adsorb carbon dioxide (CO_2) and water from the atmosphere to generate new surface species. This finding is similar to the literature by Sasaki et al. (2013) and Granados et al. (2007). Thus, the XPS results confirmed the change of atomic distribution on the sample surfaces which agree with the XRD results.

Table 5.2 Relative atomic concentration by XPS of the parent and Thai natural marl calcined at different temperatures.

Sample	Relative atomic concentration (atom %)				
	Ca	C	O	Si	Total
Marl	3.01	9.75	67.61	19.64	100.00
M600	8.65	14.13	63.07	14.15	100.00
M700	12.70	13.60	63.00	10.71	100.00
M800	16.31	18.66	59.70	5.32	100.00
M900	18.98	12.66	63.37	4.99	100.00
M100	17.87	14.79	61.07	6.27	100.00

Both XRD and XPS results above indicated the change of chemical phases and bulk compositions. Hence, an FTIR technique was further employed to confirm the functional groups of the marl samples calcined at various temperatures compared to their raw material. FTIR spectra are shown in **Figure 5.2** and their

functional groups were assigned according to the literature (Roschat et al., 2016; Sasaki et al., 2013; Ylmén, and Jäglid, 2013). Like the as-received marl, a functional group of M600 and M700 was mainly carbonate species indicated by the four vibration modes consisting of in-plane bending ($\nu_4(CO_3^{2-})$), out-of-plane bending ($\nu_2(CO_3^{2-})$), symmetric stretching ($\nu_1(CO_3^{2-})$), and asymmetric stretching ($\nu_3(CO_3^{2-})$). In addition, there was a presence of silica contained in the bulk indicated by the stretching modes ($\nu(Si-O)$) of the silica framework. From M800 and M900, the characteristic FTIR peaks of carbonate groups were not observed indicating the complete transformation of the carbonate species $Ca(OH)_2$ consistent with the XRD results. From M900, the major functional group was hydroxide indicated by the vibration of hydroxyl group ($\nu(Ca-O-H)$). Although the XRD pattern of M900 confirmed the presence of calcium oxide phase, this species is IR inactive. From M1000, the carbonate was thoroughly converted to the CaO phase indicated by the disappearance of a stretching mode of $Ca(OH)_2$.

In addition, the contaminant silica was not removed by the calcination, as indicated by the silica stretching in all calcined samples. Although the XRD results suggested the carbonate phase was completely transformed to either the hydroxide or oxide at a temperature above 800 ℃, the characteristic of carbonate was still observed by FTIR. This was a result of the re-carbonation of the calcined samples from an atmospheric CO_2 (Sasaki et al., 2013). Hence, the FTIR findings confirmed that carbonate was fully transformed to the calcium hydroxide and oxide phase at the temperature higher than 800 ℃ and 900 ℃, respectively.
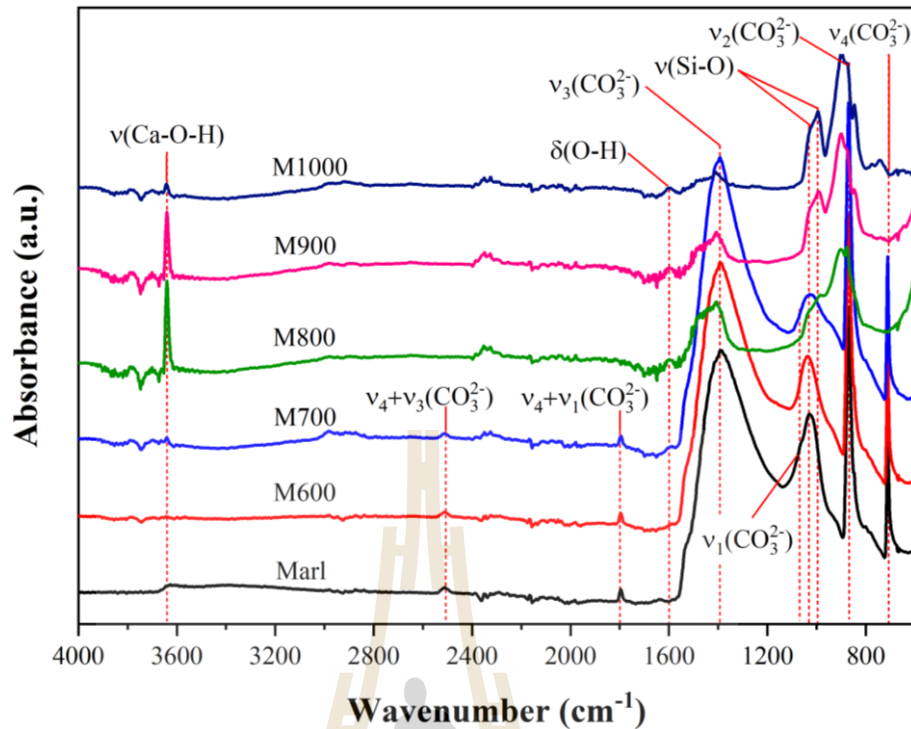
Figure 5.2 FTIR spectra of calcium samples calcined at various temperatures compared with the parent marl.

SEM images of the parent and the marl calcined at different temperatures are shown in **Figure 5.3-5.5**. The geometry of parent marl is rhombohedral with a wider size distribution. There is plenty of calcite sheets with approximately 1 µm in length covering over the specimen surface. The calcined samples lost its rhombohedral morphologies within the thermal treatment. The results suggested that the higher calcination temperature led to a larger degree of deconstruction. Additionally, the presence of surface roughness is observed at a calcination temperature above 600 ℃ as shown in **Figure 5.4-5.5**. This phenomenon was also observed in the calcination of natural dolomite consisting of $CaMg(CO_3)_2$ studied by Ngamcharussrivichai et al. (2010). The literature proposed that the increment of surface roughness might be a

result of decarbonation of bulk carbonate components during the calcination process. According to the above XRD and FTIR results, the paradigm shift of chemical-phase characteristics in the parent marl affected the morphological properties in terms of both shape and roughness changes.
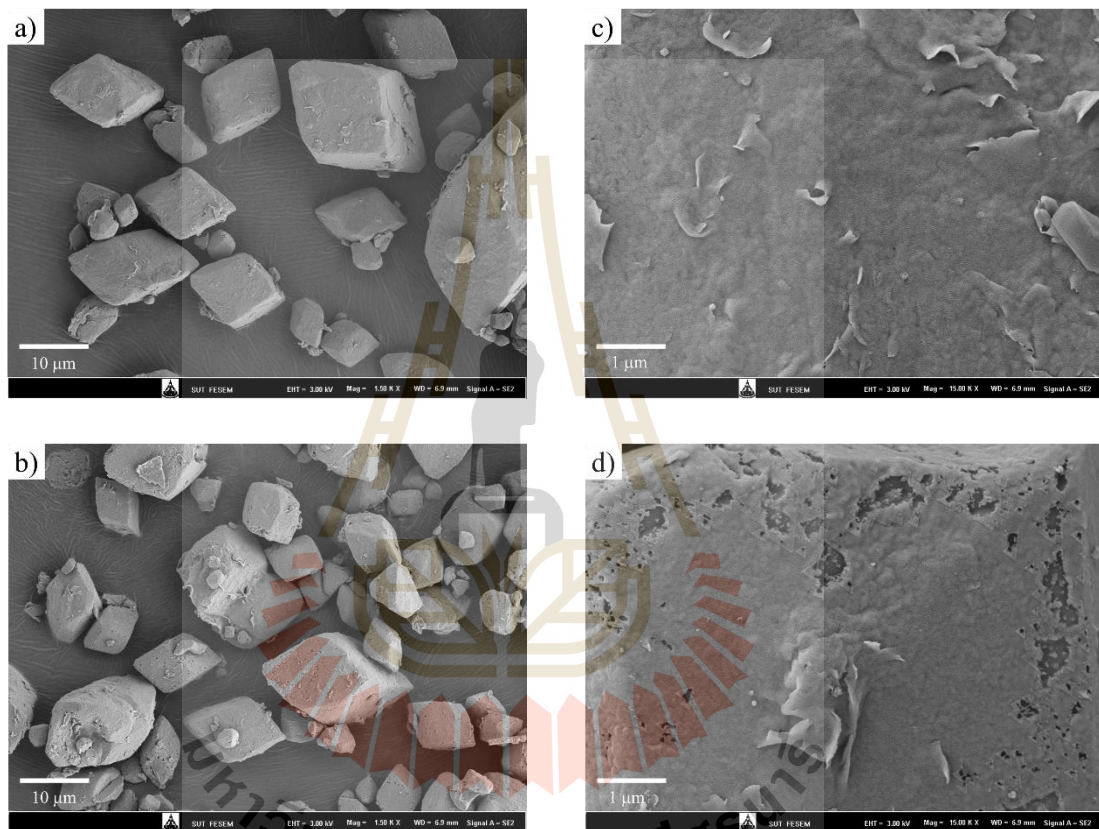
Figure 5.3 SEM images of the marl samples calcined at different temperatures with the magnification of 1500; a) Marl and b) M600 and with the magnification of 15,000; c) Marl and d) M600
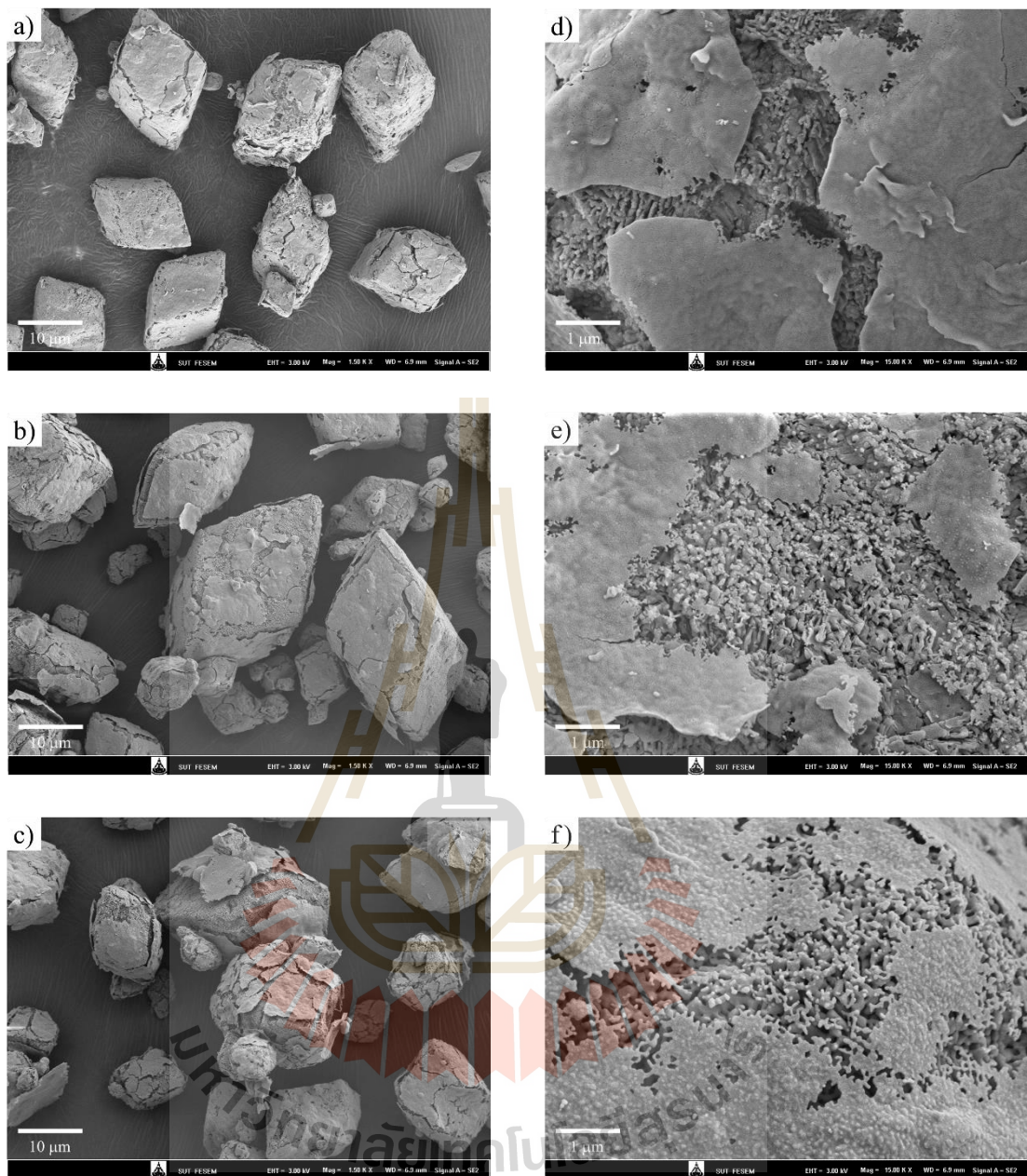
Figure 5.4 SEM images of the marl samples calcined at different temperatures with the magnification of 1500; a) M700, b) M800, and c) M900 and with the magnification of 15,000; d) M700, e) M800, and f) M900.
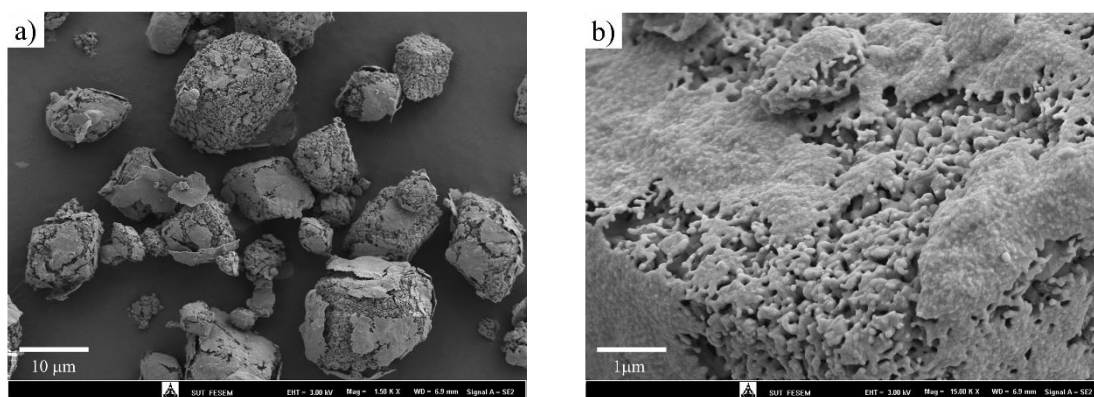
Figure 5.5 SEM images of M1000 with the magnification of 1500 a) and 15,000 b).

N$_2$ adsorption-desorption isotherms of the parent and calcined marl samples are displayed in **Figure 5.6**. At a calcination temperature lower than 700 ℃, the samples show a type II isotherm as a result of unrestricted monolayer-multilayer adsorption up to a high relative pressure according to the IUPAC classification (Thommes et al., 2015). These isotherms indicate that these carbonate-rich are nonporous or macroporous solids. At calcined at the temperature higher than 800 ℃, the samples show a type IV(a) isotherm, a characteristic of mesoporous materials caused by monolayer-multilayer adsorption on the mesopore walls. In addition, these samples show a type H1 hysteresis loop indicating a narrow range of uniform mesopore as a result of the occurrence of capillary condensation. Indeed, the presence of mesopores might not occur thorough the bulk, but the external surface only possessed the pores caused by the sintering effect of the surface carbonate species at high calcination temperatures (Ngamcharussrivichai et al., 2010; Oates, 1980). The BET surface areas and pore volumes are listed in **Table 5.3**. The result suggested that the higher calcination temperature could enhance the larger surface areas and pore volumes

in agreement with both the morphological change by SEM and the literature (Sasaki et al., 2013).
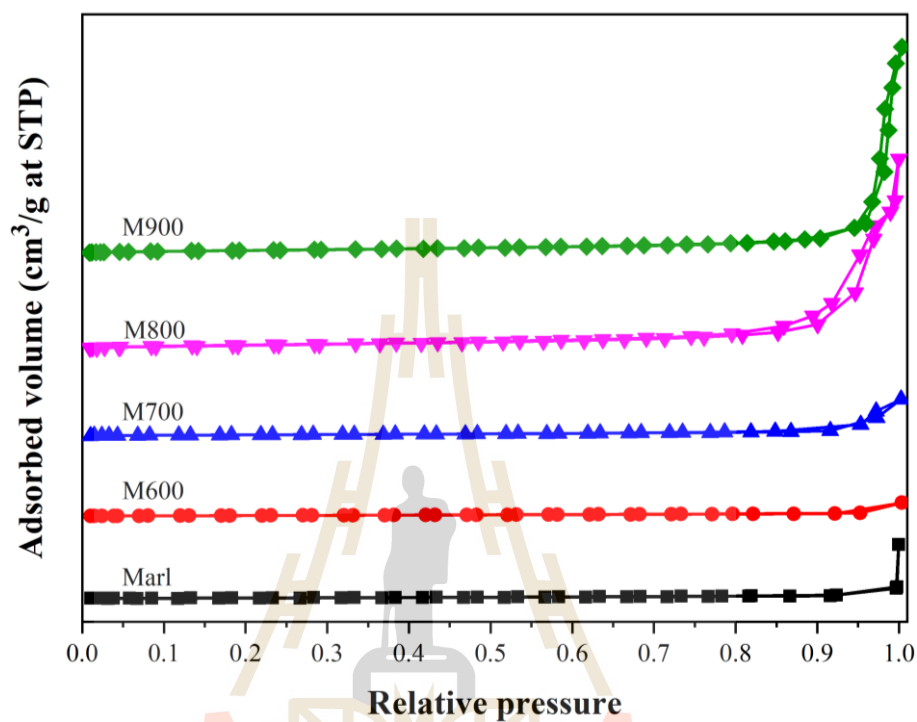
Figure 5.6 N_2 sorption isotherms of the parent and the natural marl calcined at various temperatures.

Table 5.3 BET Surface area and pore volume of the parent and the marl samples calcined at different temperatures.

Sample	Calcination temperature (ºC)	BET surface area (m^2/g)	Pore volume (cm^3/g)
Marl	-	1	0.01
M600	600	2	0.01
M700	700	3	0.02
M800	800	12	0.11
M900	900	9	0.12

5.4.2   Basicity evaluation by the decomposition of MBOH

There are many effects on the catalytic process, for example, intrinsic properties, base strength, porosity, and surface species. Among these properties, basicity plays an important role in a base-catalyzed transesterification. A test reaction of MBOH decomposition is considered to differentiate acidic, basic active and defect sites (Kulawong et al., 2015) in terms of the selectivity of obtained products. For instance, 3-methylbut-3-en-1-yne (MBYNE) and 3-methylbut-2-enal (prenal) are produced from an acid-catalyzed pathway. 3-Methylbut-3-en-2-one (MIPK) and 3-hydroxy-3-methylbutan-2-one (HMB) are produced by a defect-site-catalyzed pathway. On the other hand, a base-catalyzed route provides both acetylene and acetone. Thus, the basicity of the marl calcined at different temperatures could be compared directly from the conversion of MBOH and the selectivity to obtained products.

The conversion of MBOH at the reaction temperature of 150 ºC against time on stream catalyzed by the marl samples calcined at different temperatures is shown in **Figure 5.7**. The activity of MBOH decomposition was in the following order: Marl < M600 < M700 ≈ M800 ≈ M900 ≈ M1000. This result implied that the higher calcination temperature could enhance the better base strength. The results indicated that the carbonate species had the lowest basicity.
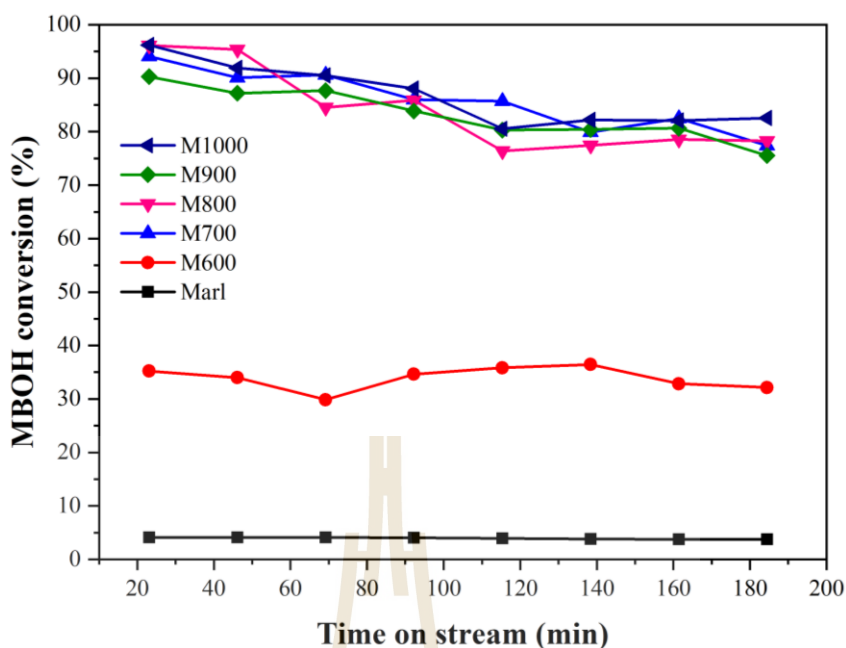
Figure 5.7 Conversion of MBOH against time on stream over the parent and the marl samples calcined at different temperatures.

The catalytic behavior of surface species preferred a base-catalyzed pathway indicated by the selectivity to acetone and acetylene as shown in **Figure 5.8** and **5.9**, respectively. The summary of product selectivity at the time on stream of 140 ℃ is also listed in **Table 5.4**. Although the marl and M600 gave based-catalyzed products, a small number of an acid-catalyzed product was obtained. This implied that the contaminants such as Al_2O_3, SiO_2, and Fe_2O_3 could facilitate the conversion of MBOH through the acid-catalyzed route. This could be an indication both marl and M600 were basic. The samples calcined at the temperature higher than 700 ℃ gave base-catalyzed products indicating that the active sites were basic. The evaluation of base strength provided a similar result from the MBOH conversion over hydrotalcite treated at different temperatures reported by Tanner et al. (2005).
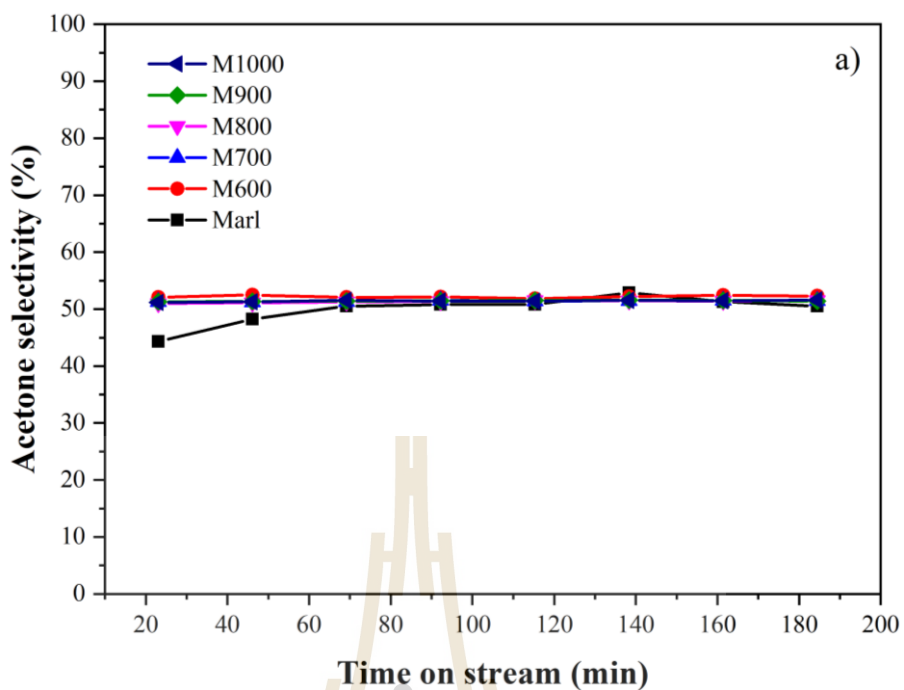
Figure 5.8 Selectivity to acetone against different time on stream.
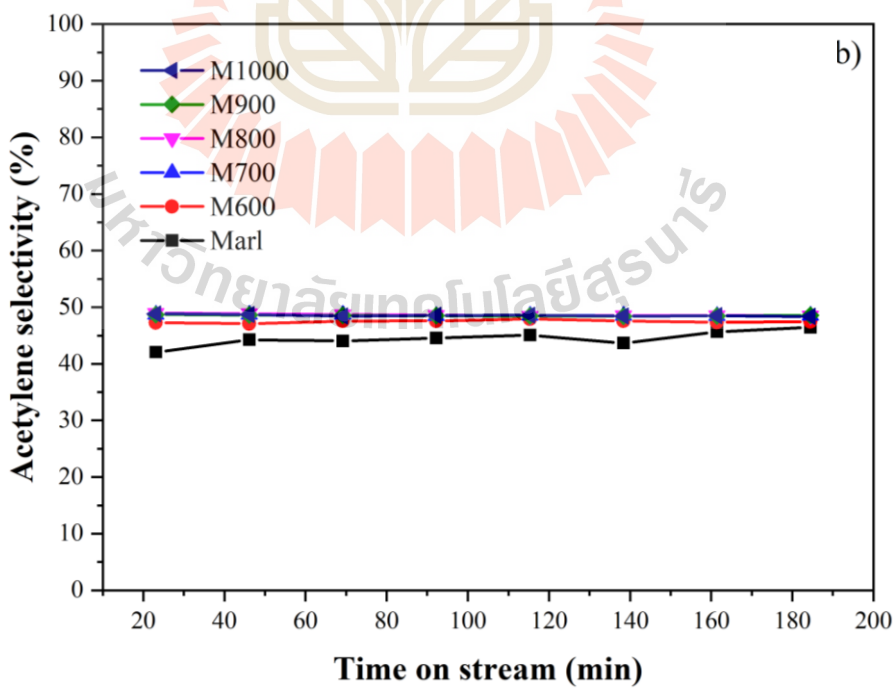
Figure 5.9 Selectivity to acetylene against different time on streams.

Table 5.4 Selectivity to the obtained products through the decomposition of MBOH at

the time on stream of 140 min for the evaluation of base strength.

Sample	Conversion of MBOH at the time on stream of 140 min (%)	Product selectivity (%)	
		Base-catalyzed products	Acid-catalyzed product
Marl	3.82	96.55	3.45
M600	36.45	99.80	0.20
M700	79.88	100.00	0
M800	77.46	100.00	0
M900	80.41	100.00	0
M1000	82.19	100.00	0

5.4.3 Conversion of palm oil through transesterification

Differentiation of the base strength of M700, M800, M900, and M100

by the decomposition of MBOH was limited. Thus, the conversion of palm oil through

base-catalyzed transesterification was considered to distinguish the basic strength of

the samples calcined at different temperatures. Herein, two reaction parameters

consisting of the effect of calcination temperature and a catalyst loading were studied.

The base strength of the calcined samples was indicated in terms of the conversion of

palm oil monitored by a thin-layer chromatography (TLC) plate.

5.4.3.1 Effect of the calcination temperature

The TLC results of the effect of calcination temperature on the

conversion of palm oil with methanol at the reaction temperature of 60 °C are shown in

Figure 5.10. The marl and M600 samples show a conversion of palm oil to methyl

esters (ME) poorer than the others due to the presence of inactive carbonate species.

This finding is in a good agreement with the results from MBOH conversion.

Meanwhile, the M700 sample provides a partial conversion of palm oil due to the presence of both palm oil and ME products. At a calcination temperature higher than 800 ℃, these samples give a complete conversion of palm oil related to the presence of $Ca(OH)_2$ and CaO. Hence, this result indicated that the base strength obtained from the test transesterification was in the following order: Marl < M600 < M700 < M800 ≈ M900 ≈ M1000. This finding was in accordance with the literature (Ngamcharussrivichai et al., 2010; Ngamcharussrivichai et al., 2007; Roschat et al., 2016). Additionally, in a point of view in the transesterification of palm oil, the calcination temperature at 800 ℃ was suitable for the production of a strong base catalyst.
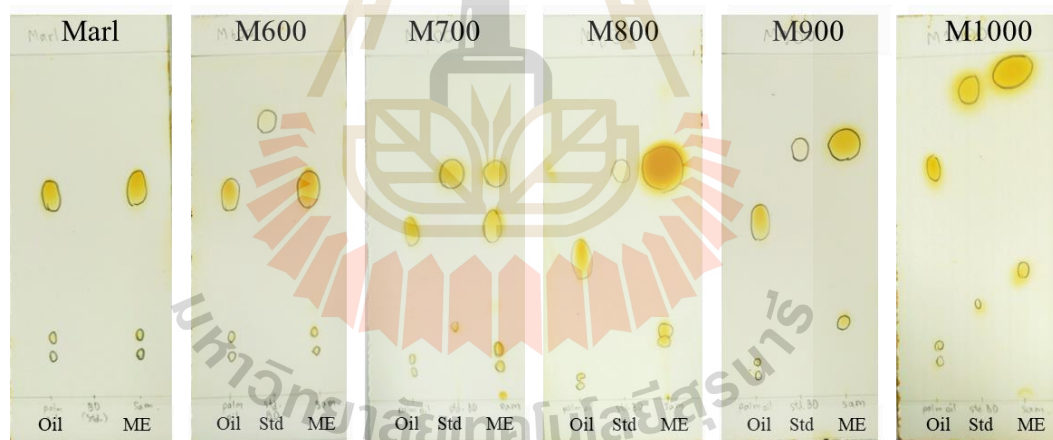
Figure 5.10 The results of thin-layer chromatography (TLC) from various calcium samples calcined at different temperatures: Oil = palm oil, Std = methyl ester standard and ME = methyl ester obtained from the conversion of palm oil at 60 ℃.

5.4.3.2 Effect of catalyst loading

The TLC results of the effect of catalyst loading on the conversion of palm oil are illustrated in **Figure 5.11**. After the completion of the transesterification at the reaction time for 3 h, all loading of M800 sample in the range of 1 – 9 wt. % provided the full conversion of palm oil to ME. This result indicated that the lowest catalyst loading of 1 wt. % was optimal for the conversion of palm oil According to the literature, Roschat et al. (2016) studied the transesterification between palm oil and methanol catalyzed by hydrated lime-derived calcium samples calcined at a temperature range from 700 to 900 ℃. The work suggested that a catalyst loading higher than 6 wt. % no longer increased the reaction activity because of the increment of system viscosity and a limitation of mass transfer.

Figure 5.11 The results of thin-layer chromatography (TLC) from various M800 loadings.

5.5 Conclusions

Calcium catalysts with various phases were successfully produced through the thermal treatment of Thai natural marl, a carbonate-rich source. At a calcination temperature of 600, 700, 800, and above 900 ºC, the characteristic calcium phases of the raw material were changed to dehydrated carbonate, hydroxide, and oxide forms, respectively. The increment of calcination temperature also varied the elemental composition by the increase of calcium contents in a bulk component indicated by XRF and XPS techniques. These changes affected the bulk functional group by the reduction of the carbonate group as a major species on the raw sample studied by FTIR. The characteristic rhombohedral shape of the marl was destructed while the surface roughness increased after the calcination observed by SEM imaging. The change of morphologies also increased the surface area and pore volume analyzed by N_2 sorption. Both different chemical and physical properties of samples greatly impacted a catalytic reaction. The higher calcination temperature increased the base strength indicated by the test reaction of MBOH decomposition. The conversion of palm oil with methanol through a base-catalyzed transesterification as a proposed tool for the evaluation of base strength also confirmed that a basicity of calcium hydroxide and oxide was greater than the carbonate. The base strength of the calcined catalysts increased with the following series; Marl < M600 < M700 < M800 ≈ M900 ≈ M1000. With 1 wt. % loading, the M800 catalyst provided a complete conversion of palm oil.

5.6 References

Granados, M. L., Poves, M. D. Z., Alonso, D. M., Mariscal, R., Galisteo, F. C., Moreno-Tost, R., Santamaría, J., and Fierro, J. L. G. (2007). Biodiesel from sunflower oil by using activated calcium oxide. **Applied Catalysis B: Environmental**. 73(3-4): 317-326.

Jaiyen, S., Naree, T., and Ngamcharussrivichai, C. (2015). Comparative study of natural dolomitic rock and waste mixed seashells as heterogeneous catalysts for the methanolysis of palm oil to biodiesel. **Renewable Energy**. 74: 433-440.

Kulawong, S., Prayoonpokarach, S., Roessner, F., and Wittayakun, J. (2015). Acidity of modified mordenites synthesized from rice husk silica and catalytic transformation of methylbutynol. **Química Nova**. 38: 191-195.

Manadee, S., Sophiphun, O., Osakoo, N., Supamathanon, N., Kidkhunthod, P., Chanlek, N., Wittayakun, J., and Prayoonpokarach, S. (2017). Identification of potassium phase in catalysts supported on zeolite NaX and performance in transesterification of Jatropha seed oil. **Fuel Processing Technology**. 156: 62-67.

Ngamcharussrivichai, C., Nunthasanti, P., Tanachai, S., and Bunyakiat, K. (2010). Biodiesel production through transesterification over natural calciums. **Fuel Processing Technology**. 91(11): 1409-1415.

Ngamcharussrivichai, C., Wiwatnimit, W., and Wangnoi, S. (2007). Modified dolomites as catalysts for palm kernel oil transesterification. **Journal of Molecular Catalysis A: Chemical**. 276(1-2): 24-33.

Novikova, L., Roessner, F., Belchinskaya, L., Alsawalha, M., and Krupskaya, V. (2014). Study of surface acid-base properties of natural clays and zeolites by the conversion of 2-methylbut-3-yn-2-ol. **Applied Clay Science**. 101: 229-236.

Oates, J. A. H. (1980). *Calcination of Limestone*. New York: John Wiley & Sons.

Rakmae, S., Keawkumay, C., Osakoo, N., Montalbo, K. D., de Leon, R. L., Kidkhunthod, P., Chanlek, N., Roessner, F., Prayoonpokarach, S., and Wittayakun, J. (2016). Realization of active species in potassium catalysts on zeolite NaY prepared by ultrasound-assisted impregnation with acetate buffer and improved performance in transesterification of palm oil. **Fuel**. 184: 512-517.

Roschat, W., Kacha, M., Yoosuk, B., Sudyoadsuk, T., and Promarak, V. (2012). Biodiesel production based on heterogeneous process catalyzed by solid waste coral fragment. **Fuel**. 98: 194-202.

Roschat, W., Siritanon, T., Yoosuk, B., and Promarak, V. (2016). Biodiesel production from palm oil using hydrated lime-derived CaO as a low-cost basic heterogeneous catalyst. **Energy Conversion and Management**. 108: 459-467.

Sasaki, K., Qiu, X., Hosomomi, Y., Moriyama, S., and Hirajima, T. (2013). Effect of natural dolomite calcination temperature on sorption of borate onto calcined products. **Microporous and Mesoporous Materials**. 171: 1-8.

Supamathanon, N., Wittayakun, J., Prayoonpokarach, S., Supronowicz, W., and Roessner, F. (2012). Basic properties of potassium oxide supported on zeolite y studied by pyrrole-TPD and catalytic conversion of methylbutynol. **Química Nova**. 35: 1719-1723.

Tanner, R., Enache, D., Wells, R. P. K., Kelly, G., Casci, J., and Hutchings, G. J. (2005). Comments on the use of 2-methylbut-3-yn-2-ol decomposition as a probe reaction for the potential reactivity Mg-Al hydrotalcites as base catalysts. **Catalysis Letters**. 100(3-4): 259-265.

Thommes, M., Kaneko, K., Neimark, A. V., Olivier, J. P., Rodriguez-Reinoso, F., Rouquerol, J., and Sing, K. S. W. (2015). Physisorption of gases, with special reference to the evaluation of surface area and pore size distribution (IUPAC Technical Report). **Pure and Applied Chemistry**. 87(9-10): 1051-1069.

Vance, K., Falzone, G., Pignatelli, I., Bauchy, M., Balonis, M., and Sant, G. (2015). Direct carbonation of $Ca(OH)_2$ using liquid and supercritical CO_2: implications for carbon-neutral Cementation. **Industrial & Engineering Chemistry Research**. 54(36): 8908-8918.

Ylmén, R., and Jäglid, U. (2013). Carbonation of portland cement studied by diffuse reflection Fourier transform infrared spectroscopy. **International Journal of Concrete Structures and Materials**. 7(2): 119-125.

CHAPTER VI

CONCLUSIONS

AP-SBA-15 and VAP-SBA-15 are prepared by grafting with aminopropyl-triethoxysilane (APTES) and successively anchored by vanadyl acetylacetonate (VO(acac)$_2$) by conventional method for in situ aldol condensation between furfural and acetone. The conventional preparation did not affect the characteristic geometry, morphologies, and pore topologies of the parent SBA-15. In AP-SBA-15, the APTES species chemically bonded with the silica gel surface. In VAP-SBA-15, the further anchoring provided the bond formation between VO(acac)$_2$ species and AP-SBA-15. From aldol condensation between furfural and acetone monitored by the in situ ATR-FTIR, AP-SBA-15 was the suitable catalyst with the reaction temperature for the in situ aldol condensation was 40 ℃.

To simplify the conventional grafting and reduce the preparation cost, silica gel was grafted with various amounts of APTES by the ultrasonic-assisted method. The grafting preserved the characteristic phase and reduced aggregation of the silica support. The APTES species diffused effectively into the silica pores with a better surface species dispersion and less pore blocking. In comparing the conventional method, the ultrasound assistance facilitated the chemical bonding between the APTES and the surface silanol of silica gel with a shorter operation time. The basicity of the grafted silica gel was tunable with the APTES loading. From aldol condensation between furfural and acetone, all samples gave nearly complete furfural conversion.

The silica gel with the APTES loading of 30 wt. %, 30APS-U, was the suitable catalyst for the reaction in 24 h.

For the development of calcium base catalysts from Thai natural marl, the thermal treatment at different temperatures converted calcium carbonate phases to hydroxide at 800 °C, and oxide above 900 °C. This method improved the concentration of calcium contents and affected both morphologies and surface roughness with the calcination temperature. The test reaction of MBOH decomposition at 150 °C indicated the calcined samples contained the active basic site with the base strength in the order Marl < M600 < M700 ≈ M800 ≈ M900 ≈ M1000. The transesterification of palm oil with methanol at 60 °C further suggested that a base strength of M800 higher than M700. The M800 catalyst at least 1 wt. % was optimal.
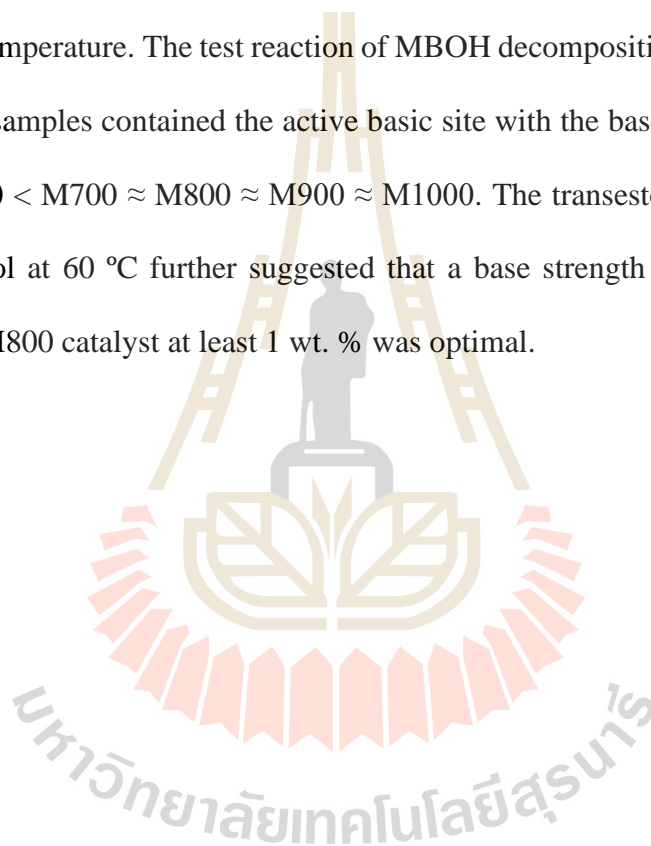
APPENDICES
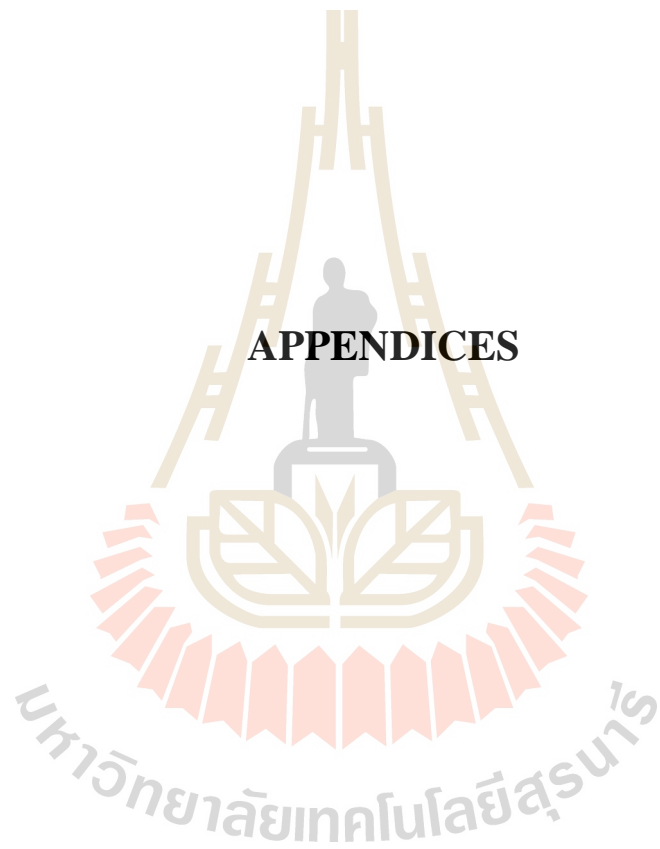
APPENDIX A

ADDITIONAL CHARACTERIZATION RESULTS OF

SBA-15 GRAFTED WITH APTES AND

OXOVANADIUM COMPLEX

A.1 Calculation of structural parameters by results of low angle XRD technique

Table A.1 Structural parameters calculated from XRD patterns for SBA-15 grafted with APTES (AP-SBA-15) and oxovanadium complex (VAP-SBA-15).

Sample	2θ	θ	λ (Cu K_α), Å	$\sin \theta$	$d_{(100)}$, Å [a]	$d_{(100)}$, nm	A_o (nm) [b]
SBA-15	0.8272	0.4136	1.54058	0.007219	106.7	10.67	12.32
AP-SBA-15	0.8476	0.4238	1.54058	0.007397	104.1	10.41	12.02
VAP-SBA-15	0.8681	0.4340	1.54058	0.007575	101.7	10.17	11.74

[a] $d_{(100)}$ is interplanar spacing at (100) plane calculated from the equation 3.2 in Chapter III.

[b] A_o is a unit cell parameter calculated from equation 3.1 in Chapter III.

## A.2   Distribution of pore diameter and wall thickness by TEM
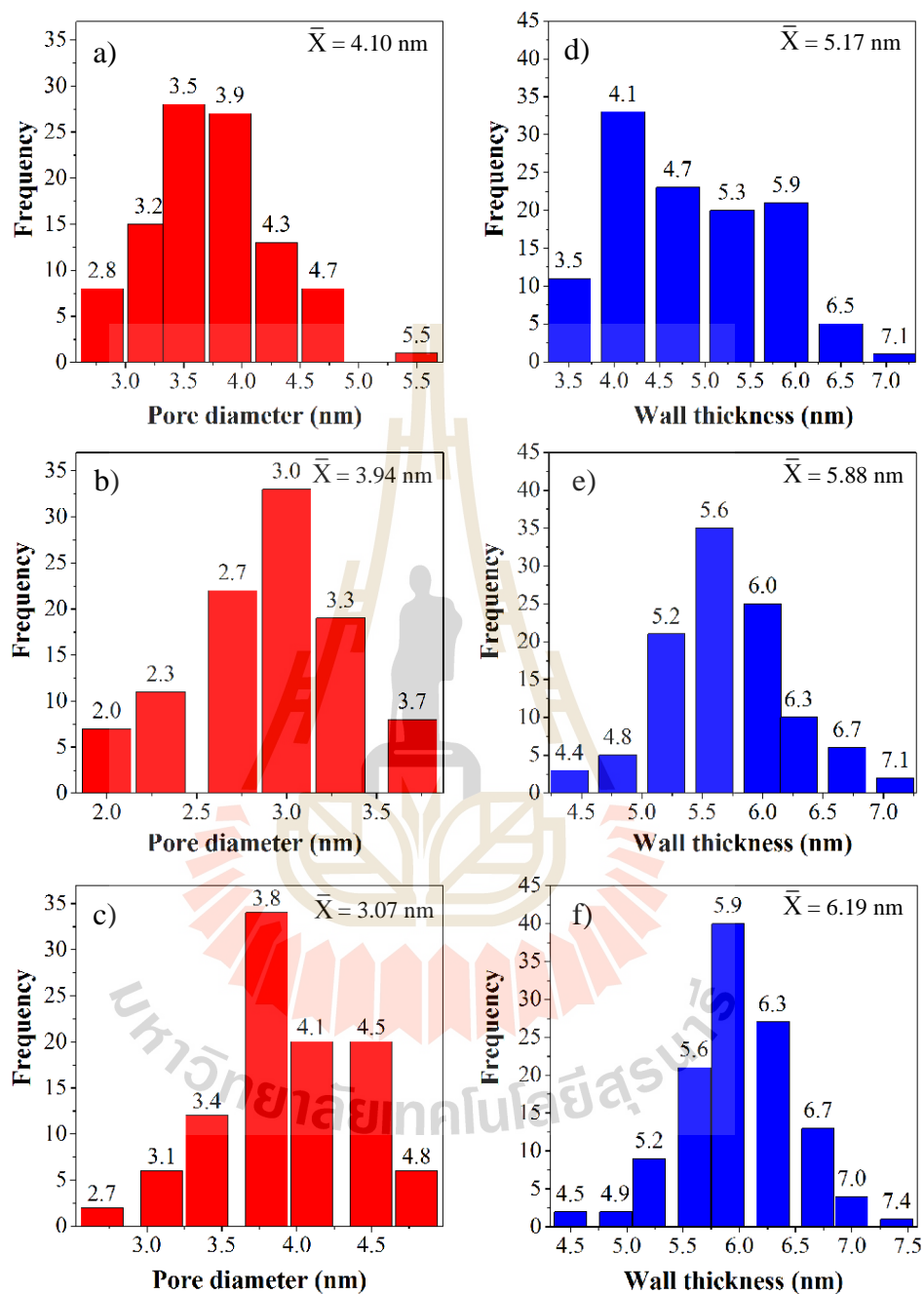
Figure A.1 Pore diameter distribution of a) SBA-15, b) AP-SBA-15 and c) VAP-SBA-15 and wall thickness distribution of d) SBA-15, e) AP-SBA-15 and f) VAP-SBA-15.

A.3 Assignment of functional groups from FTIR results

Table A.2 Assignment of functional groups of SBA-15 grafted with APTES (AP-SBA-15) and oxovanadium complex (VAP-SBA-15).

Wavenumber (cm^{-1})			Assignment	Reference
SBA-15	AP-SBA-15	VAP-SBA-15		
444 s	447 s	447 s	δ(Si-O-Si)	(Di Giuseppe et al., 2013)
-	697 w	696 w	δ(N-H)	(Di Giuseppe et al., 2013)
807 m	799 m	799 m	ν_s(Si-O-Si)	(Di Giuseppe et al., 2013; Shylesh, and Singh, 2004)
-	-	959 w	ν(V=O)	(Ferrer, Salinas, Correa, Vrdoljak, and Williams, 2005)
970 w	970 w	-	ν(Si-OH)	(Di Giuseppe et al., 2013)
1060 s	1065 s	1059 s	ν_{as}(Si-O-Si)	(Di Giuseppe et al., 2013)
-	1414 w	1413 w	δ(Si-CH$_2$)	(Majoul, Aouida, and Bessaïs, 2015)
-	1450 w	1445 w	δ(C-H)	(Park, Celedonio, Seo, Park, and Ko, 2015)
-	1475 w	1470 w	δ(C-H)	(Park et al., 2015)
-	-	1556 w	(C=N)	(Li et al., 2012)
-	1568 w	-	ν_s(N-H)	(Yang, Hao, Zhang, and Kan, 2011)
-	-	1612 w	ν(C=C)	(Ferrer et al., 2005)
1633 w	1641w	1632 w	δ(O-H)	(Di Giuseppe et al., 2013)
-	2867 w	2885	ν(CH$_2$)	(Park et al., 2015)
-	2941 w	2942	ν(C-H)	(Lee, Lin, and Mou, 2003)
3697-2955 w	3700-2987 w	3712-2981 w	Adsorbed H$_2$O	(Park et al., 2015)
-	3306 w	-	ν_s(NH$_2$)	(Srikanth, and Chuang, 2013)
3743 w	3728 w	3727	ν(Si-OH)	(Shylesh, and Singh, 2004)
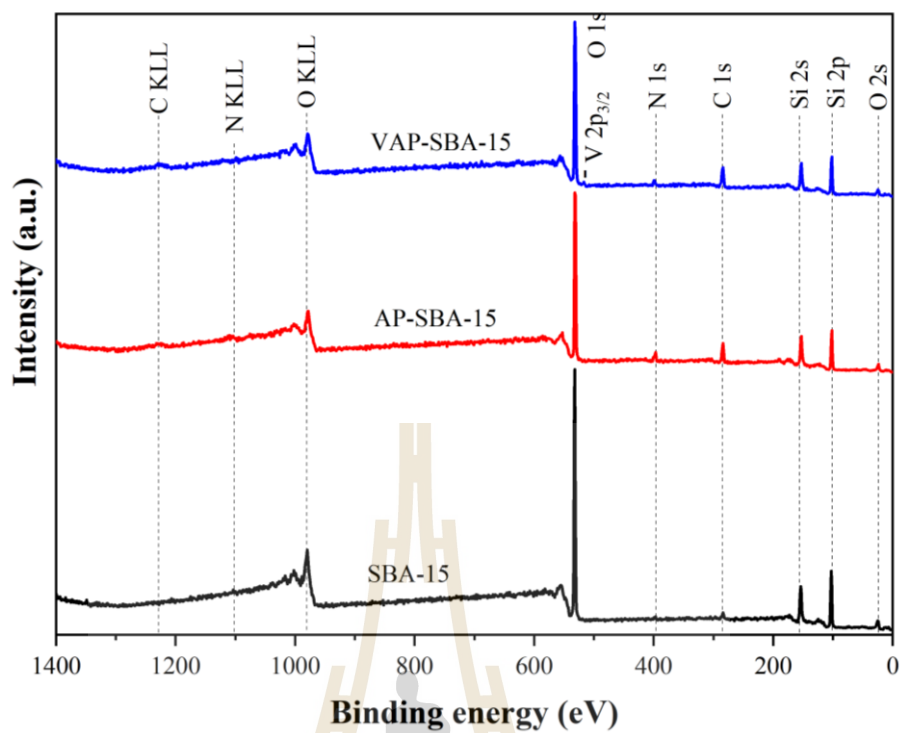
Figure A.2 Wide-scan spectra from SBA-15, AP-SBA-15, and VAP-SBA-15.
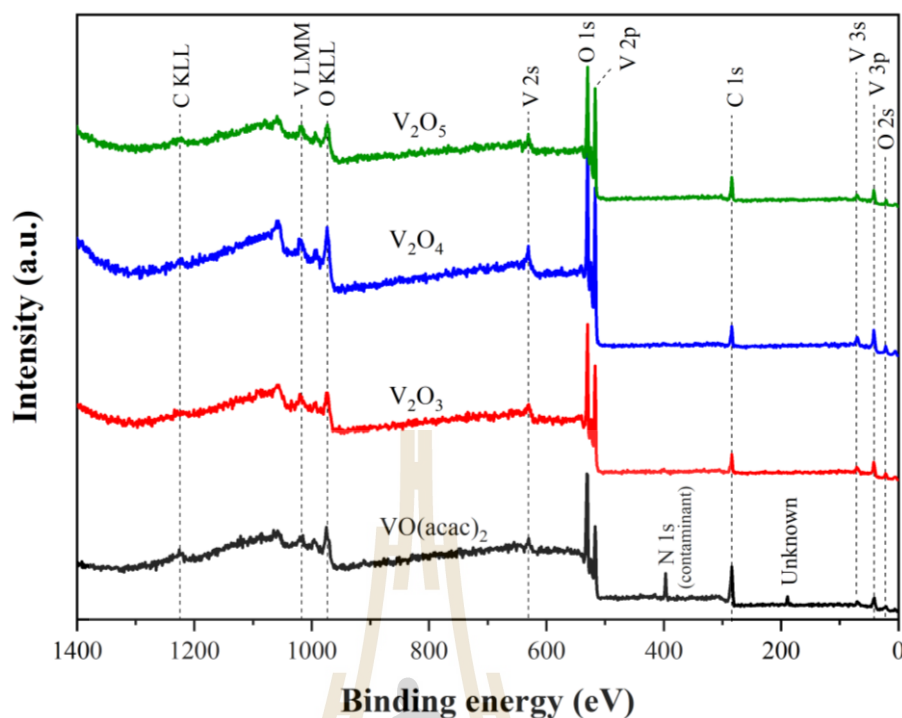
Figure A.3 Wide-scan spectra from various references of vanadium compounds.

A.5 References

Di Giuseppe, A., Di Nicola, C., Pettinari, R., Ferino, I., Meloni, D., Passacantando, M., and Crucianelli, M. (2013). Selective catalytic oxidation of olefins by novel oxovanadium(IV) complexes having different donor ligands covalently anchored on SBA-15: a comparative study. **Catalysis Science & Technology**. 3(8): 1972-1984.

Ferrer, E. G., Salinas, M. V., Correa, M. J., Vrdoljak, F., and Williams, P. A. (2005). ALP inhibitors: vanadyl (IV) complexes of ferulic and cinnamic acid. **Zeitschrift für Naturforschung B**. 60(3): 305-311.

Lee, C.-H., Lin, T.-S., and Mou, C.-Y. (2003). $(VO)^{2+}$ ions immobilized on functionalized surface of mesoporous silica and their activity toward the

hydroxylation of benzene. **The Journal of Physical Chemistry B**. 107(11): 2543-2551.

Li, Z., Liu, L., Hu, J., Liu, H., Wu, S., Huo, Q., Guan, J., and Kan, Q. (2012). Epoxidation of styrene with molecular oxygen catalyzed by a novel oxovanadium(IV) catalyst containing two different kinds of ligands. **Applied Organometallic Chemistry**. 26(5): 252-257.

Majoul, N., Aouida, S., and Bessaïs, B. (2015). Progress of porous silicon APTES-functionalization by FTIR investigations. **Applied Surface Science**. 331: 388-391.

Park, J. H., Celedonio, J. M., Seo, H., Park, Y. K., and Ko, Y. S. (2015). A study on the effect of the amine structure in CO_2 dry sorbents on CO_2 capture. **Catalysis Today**.

Shylesh, S., and Singh, A. P. (2004). Synthesis, characterization, and catalytic activity of vanadium-incorporated, -grafted, and -immobilized mesoporous MCM-41 in the oxidation of aromatics. **Journal of Catalysis**. 228(2): 333-346.

Srikanth, C. S., and Chuang, S. S. C. (2013). Infrared study of strongly and weakly adsorbed CO_2 on fresh and oxidatively degraded amine sorbents. **The Journal of Physical Chemistry C**. 117(18): 9196-9205.

Yang, Y., Hao, S., Zhang, Y., and Kan, Q. (2011). Oxovanadium(IV) and dioxomolybdenum(VI) salen complexes tethered onto amino-functionalized SBA-15 for the epoxidation of cyclooctene. **Solid State Sciences**. 13(11): 1938-1942.

APPENDIX B

ADDITIONAL CHARACTERIZATION RESULTS FOR

SILICA GEL GRAFTED WITH VARIOUS APTES

LOADING BY ULTRASOUND-ASSISTED (U)

AND CONVENTIONAL METHOD (C)

B.1 Identification of surface species by X-ray photoelectron spectroscopy (XPS)

The XPS data interpretation was processed with a freeware XPSPEAK 4.1 using a combined Gaussian-Lorentzian function with a Shirley background correction (Acres et al., 2012). All binding energy (BE) peaks were calibrated corresponding to the standard C 1s peak at 284.8 eV from an adventitious carbon (Jakša, Štefane, and Kovač, 2013; Qiao, Wang, Gao, and Jin, 2015; Shircliff et al., 2011).
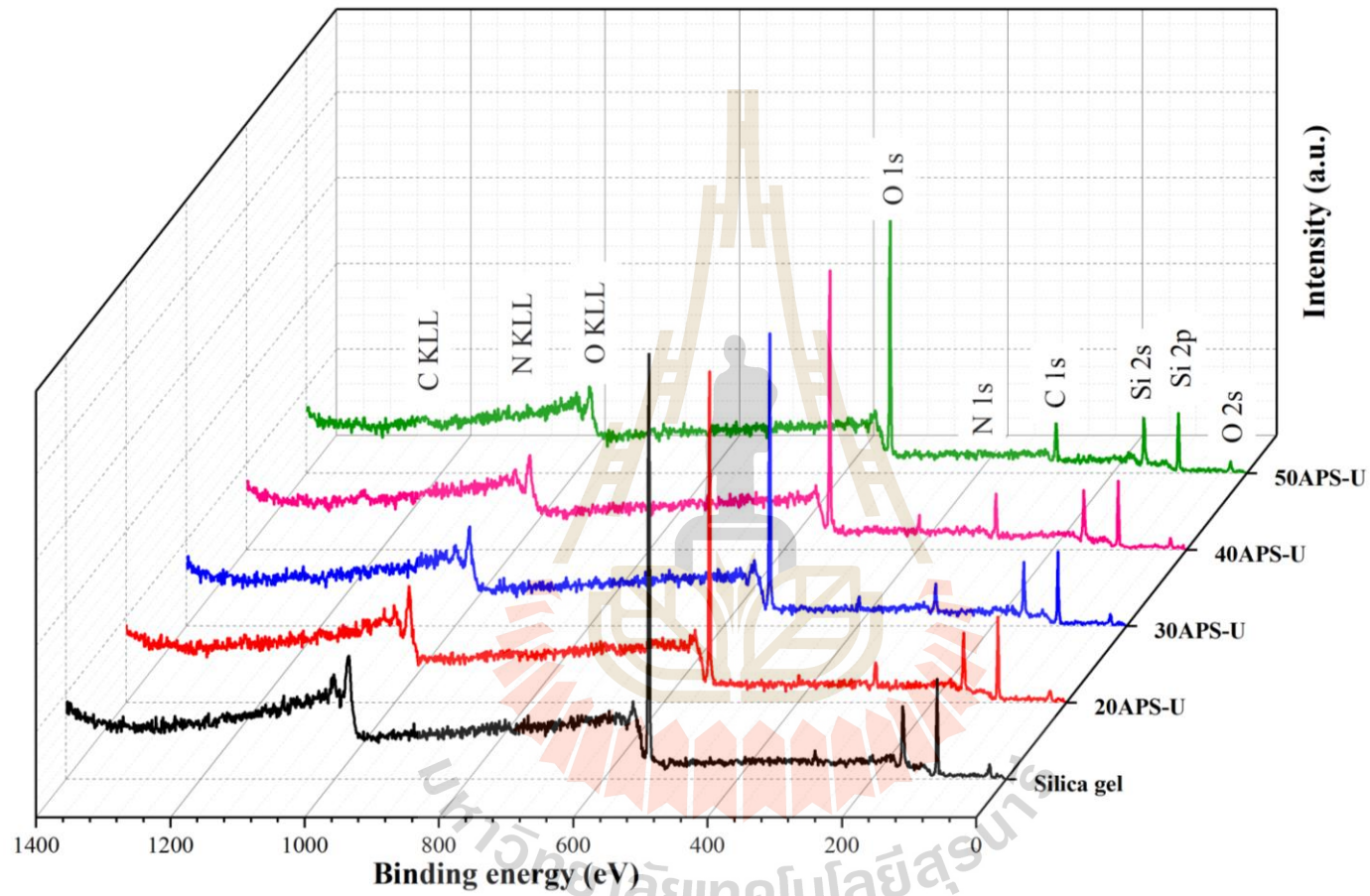
Figure B.1 Wide-scan spectra of the parent and silica gel grafted with various APTES loading.
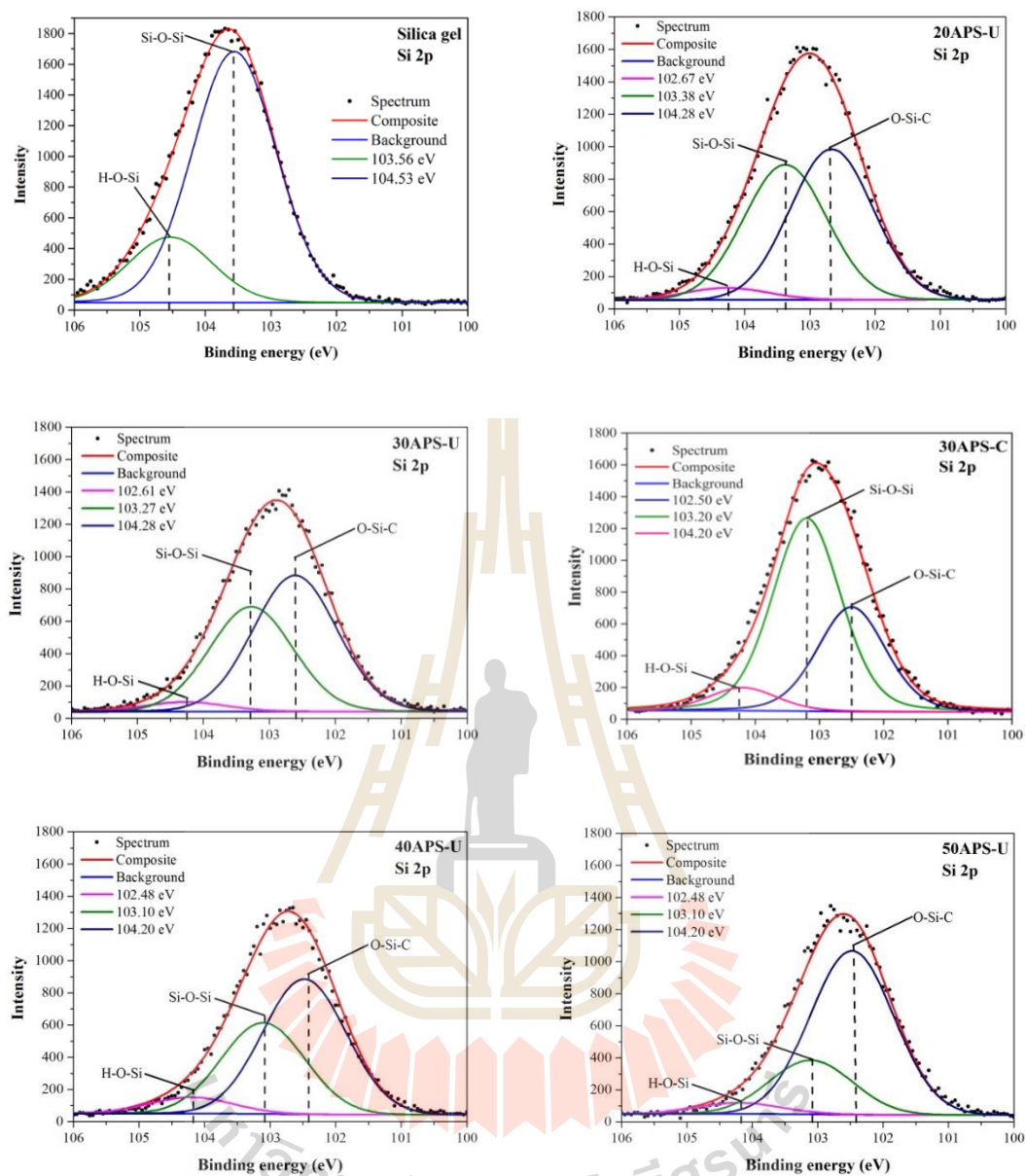
**Figure B.2** Si 2p spectra and surface species classification.
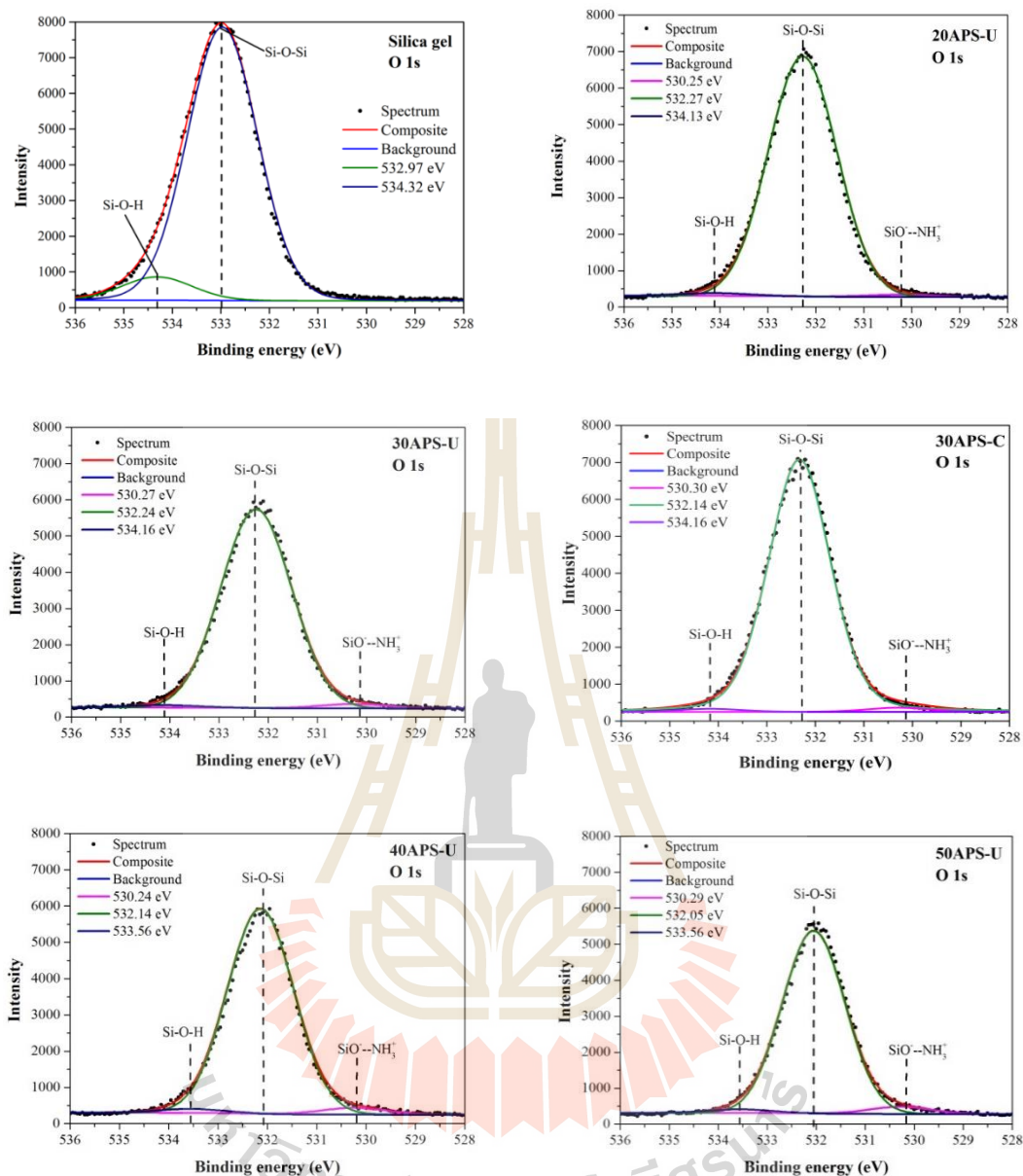
**Figure B.3** O 1s spectra and surface species classification.
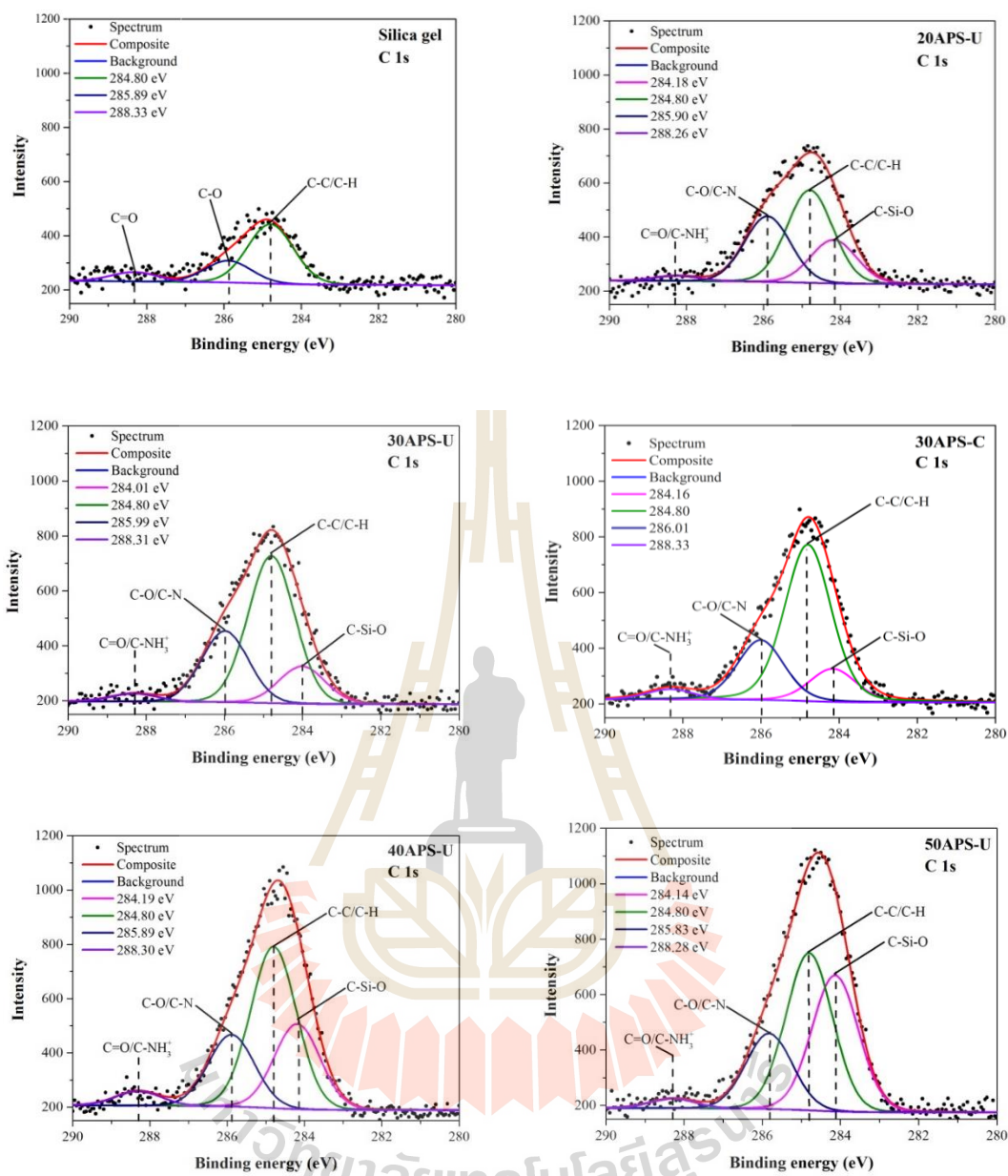
**Figure B.4** C 1s spectra and surface species classification.
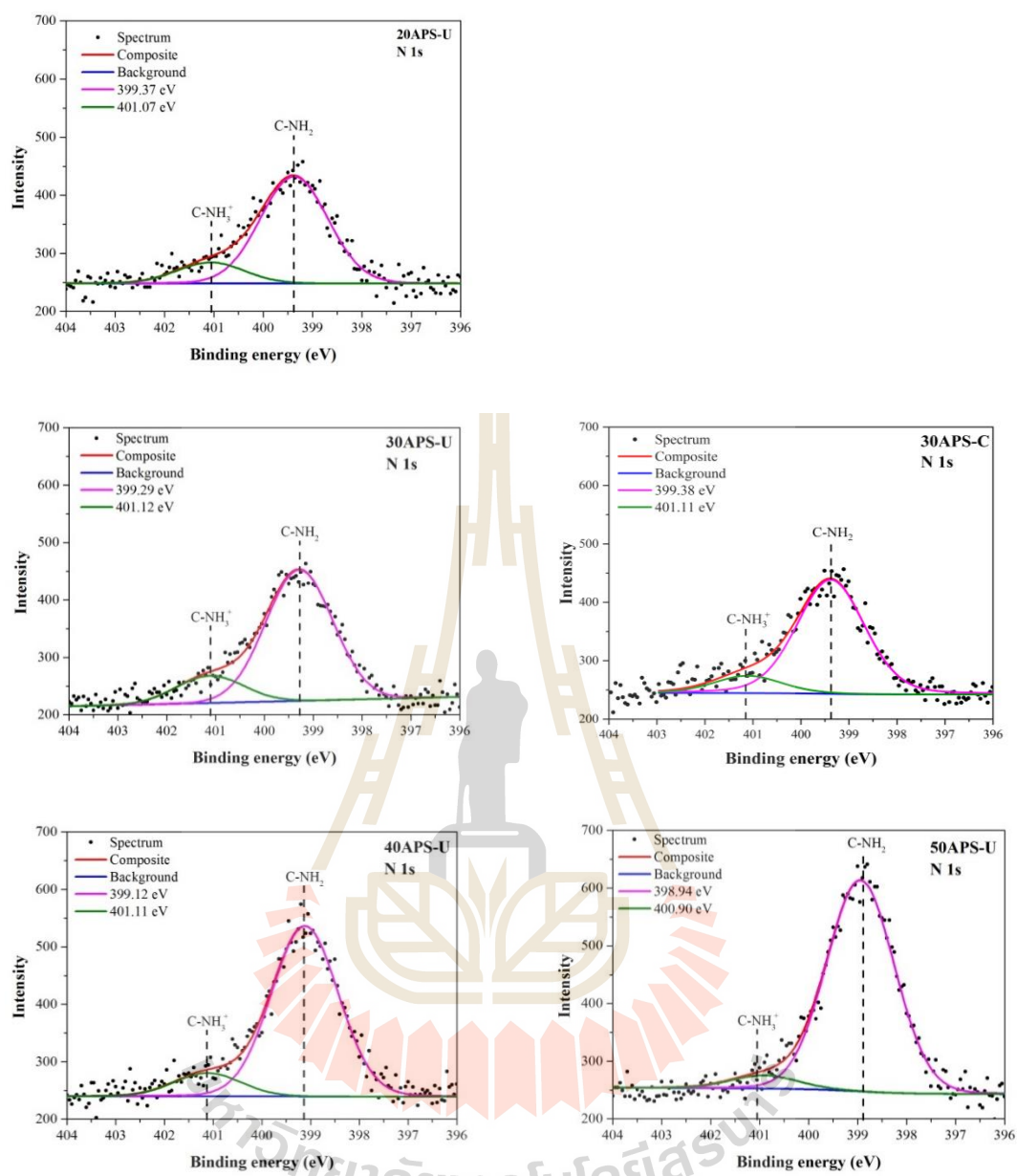
Figure B.5 N 1s spectra and surface species classification.

Table B.1 Classification of surface species on silica gel grafted with various amounts of APTES based on binding energy (BE) and peak area from deconvolution of XPS spectra.

Surface species	Silica gel BE (eV)	Silica gel Area (%)	20APS-U BE (eV)	20APS-U Area (%)	30APS-U BE (eV)	30APS-U Area (%)	30APS-C BE (eV)	30APS-C Area (%)	40APS-U BE (eV)	40APS-U Area (%)	50APS-U BE (eV)	50APS-U Area (%)	Reference
Si 2p													
O-Si-C			102.67	50.38	102.61	54.43	102.50	32.61	102.48	55.69	102.48	71.47	Lecoq et al. (2013); Shang, Zhu, and Li (2017)
Si-O-Si	103.56	79.27	103.38	45.54	103.27	41.70	103.20	60.18	103.10	37.59	103.10	23.61	Jakša et al. (2013); Kulkarni, Mirji, Mandale, and Vijayamohanan (2006)
Si-O-H	104.53	20.73	104.28	4.08	104.28	3.87	104.20	7.20	104.20	6.72	104.20	4.92	Acres et al. (2012)
C 1s													
C-Si-O			284.18	21.06	284.01	14.21	284.16	12.75	284.19	25.60	284.14	36.08	Shang et al. (2017)
C-C/C-H	284.80	65.74	284.80	44.76	284.80	55.80	284.80	60.24	284.80	48.47	284.80	41.49	Bezerra et al. (2014); Jakša et al. (2013)
C-O/C-N	285.89	24.04	285.90	31.68	285.99	26.96	286.01	23.05	285.89	21.61	285.83	19.92	Bezerra et al. (2014); (Lecoq et al., 2013)
$C=O/C-NH_3^+$	288.33	10.22	288.26	2.50	288.31	3.03	288.33	3.96	288.30	4.33	288.28	2.51	Lecoq et al. (2013)
N 1s													
NH_2-C			399.37	83.55	399.29	82.86	399.38	86.78	399.12	87.93	398.94	94.11	Bezerra et al. (2014); Lecoq et al. (2013)
NH_3^+-C			401.07	16.45	401.12	17.14	401.11	13.22	401.11	12.07	400.90	5.89	Bezerra et al. (2014); Golczak, Kanciurzewska, Fahlman, Langer, and Langer (2008)
O 1s													
$SiO^-\!\!-NH_3^+$			530.25	0.91	530.27	2.15	530.30	1.63	530.24	3.21	530.29	3.78	Martins, Hölderich, Hammer, and Cardoso (2010)
Si-O-Si	532.97	92.16	532.27	97.96	532.24	96.67	532.33	97.15	532.14	94.95	532.05	94.30	Martins et al. (2010)
Si-O-H	534.32	7.84	534.13	1.13	534.16	1.18	534.16	1.22	533.56	1.84	533.56	1.92	Golczak et al. (2008)

B.2 Thermal analysis

Theoretical losses of aminopropyl skeleton for TGA measurement were calculated by the following equation:

$$\text{Weight loss of } C_3H_8N \text{ (wt. \%)} \quad = \quad \frac{\%\text{APTES loading}}{\text{Mw of APTES}} \times \text{Mw of } C_3H_8N \tag{B1}$$

Table B.2. Evaluation of weight loss of the parent and silica gel grafted with various APTES loading prepared by ultrasound-assisted (U) and conventional method (C).

Sample	Weight loss (wt. %)			Calculated weight loss of C_3H_8N (wt. %)
	35 – 150 ℃	151 – 600 ℃	601 – 800 ℃	
Silica gel	5.17	3.32	0.67	0
20APS-U	3.08	7.95	0.65	5.24
30APS-U	3.13	9.98	0.61	7.86
40APS-U	3.67	14.36	0.62	10.48
50APS-U	5.33	13.49	0.67	13.10

The analytical weight percentages of C, H and N were compared to theoretical values from the decomposition of the surface aminopropyl group (C_3H_8N) calculated from the equation:

$$\text{C content (wt. \%)} \quad = \quad \frac{\%\text{APTES loading}}{\text{Mw of APTES}} \times \text{Mw of 3C in } C_3H_8N \tag{B2}$$

$$\text{H content (wt. \%)} \quad = \quad \frac{\%\text{APTES loading}}{\text{Mw of APTES}} \times \text{Mw of 8H in } C_3H_8N \tag{B3}$$

$$N \text{ content (wt. \%)} \quad = \quad \frac{\%\text{APTES loading}}{\text{Mw of APTES}} \times \text{Mw of N in } C_3H_8N \qquad (B4)$$

Mw is a molecular weight.

B.3   References

Acres, R. G., Ellis, A. V., Alvino, J., Lenahan, C. E., Khodakov, D. A., Metha, G. F., and Andersson, G. G. (2012). Molecular structure of 3-aminopropyltriethoxysilane layers formed on silanol-terminated silicon surfaces. **The Journal of Physical Chemistry C**. 116(10): 6289-6297.

Bezerra, D. P., Silva, F. W. M. d., Moura, P. A. S. d., Sousa, A. G. S., Vieira, R. S., Rodriguez-Castellon, E., and Azevedo, D. C. S. (2014). CO_2 adsorption in amine-grafted zeolite 13X. **Applied Surface Science**. 314: 314-321.

Golczak, S., Kanciurzewska, A., Fahlman, M., Langer, K., and Langer, J. (2008). Comparative XPS surface study of polyaniline thin films. **Solid State Ionics**. 179(39): 2234-2239.

Jakša, G., Štefane, B., and Kovač, J. (2013). XPS and AFM characterization of aminosilanes with different numbers of bonding sites on a silicon wafer. **Surface and Interface Analysis**. 45(11-12): 1709-1713.

Kulkarni, S. A., Mirji, S. A., Mandale, A. B., and Vijayamohanan, K. P. (2006). Thermal stability of self-assembled octadecyltrichlorosilane monolayers on planar and curved silica surfaces. **Thin Solid Films**. 496(2): 420-425.

Lecoq, E., Duday, D., Bulou, S., Frache, G., Hilt, F., Maurau, R., and Choquet, P. (2013). Plasma polymerization of APTES to elaborate nitrogen containing

organosilicon thin films: influence of process parameters and discussion about the growing mechanisms. **Plasma Processes and Polymers**. 10(3): 250-261.

Martins, L., Hölderich, W., Hammer, P., and Cardoso, D. (2010). Preparation of different basic Si–MCM-41 catalysts and application in the Knoevenagel and Claisen–Schmidt condensation reactions. **Journal of Catalysis**. 271(2): 220-227.

Qiao, B., Wang, T.-J., Gao, H., and Jin, Y. (2015). High density silanization of nano-silica particles using γ-aminopropyltriethoxysilane (APTES). **Applied Surface Science**. 351: 646-654.

Shang, X., Zhu, Y., and Li, Z. (2017). Surface modification of silicon carbide with silane coupling agent and hexadecyl iodiele. **Applied Surface Science**. 394: 169-177.

Shircliff, R. A., Martin, I. T., Pankow, J. W., Fennell, J., Stradins, P., Ghirardi, M. L., Cowley, S. W., and Branz, H. M. (2011). High-resolution X-ray photoelectron spectroscopy of mixed silane monolayers for DNA attachment. **ACS Applied Materials & Interfaces**. 3(9): 3285-3292.

APPENDIX C

SUPPLEMENTARY INFORMATION FOR THE

EVALUATION OF BASIC STRENGTH OF THAI

MARL-DERIVED CALCIUM CATALYSTS

FOR CONVERSION OF PALM OIL

C.1 Decomposition of 2-methylbut-3-yn-2-ol

A conversion of MBOH and product selectivity from the decomposition of MBOH are calculated according to equations reported in literature (Supamathanon, Wittayakun, Prayoonpokarach, Supronowicz, and Roessner, 2012).

$$\text{MBOH conversion (\%)} = \left[1 - \frac{A_{MBOH}rRF_{MBOH} / Mw_{MBOH}}{\sum_i (A_i rRF_i / Mw_i)}\right] \times 100 \tag{C1}$$

$$\text{Product yield (\%)} = \frac{A_p rRF_p / Mw_p}{\sum_i (A_i rRF_i / Mw_i)} \times 100 \tag{C2}$$

$$\text{Product selectivity (\%)} = \frac{\text{Product yield}}{\text{MBOH conversion}} \times 100 \tag{C3}$$

Where A_{MBOH} = Peak area of MBOH

      rRF_{MBOH} = Response factor of MBOH

      Mw_{MBOH} = Molecular weight of MBOH

      A_p = Peak area of product

      rRF_p = Relative response factor of product

      Mw_p = Molecular weight of product

      A_i = Peak area of all components

      rRF_i = Relative response factor of each component

      Mw_i = Molecular weight of each component

A response factor is expressed by an equation below. Each effective carbon number for a GC with flame ionization detector (FID) is shown in **Table C.1** below.

$$rRF_i = \frac{Mw_i}{Mw_{toluene}} \times \frac{ECN_{toluene}}{ECN_i} \tag{C4}$$

Where Mw_i = Molecular weight of all components

      ECN_i = Effective carbon number

      $Mw_{toluene}$ = Molecular weight of all components

      $ECN_{toluene}$ = Effective carbon number

Table C.1 An effective carbon number of each chemicals involving the decomposition of MBOH detected by GC-FID.

Compound	ECN_i	MW_i	rRF_i
acetylene	1.95	26.04	1.01
MBYNE	5.50	66.10	0.91
acetone	2.00	58.08	2.21
toluene	7.00	92.14	1.00
MBOH	5.35	84.12	1.19

C.2 References

Supamathanon, N., Wittayakun, J., Prayoonpokarach, S., Supronowicz, W., and Roessner, F. (2012). Basic properties of potassium oxide supported on zeolite y studied by pyrrole-TPD and catalytic conversion of methylbutynol. **Química Nova**. 35: 1719-1723.

CURRICULUM VITAE

NARONGRIT SOSA

Education

2013   B.Sc. in Chemistry (First Class Honors), Ubon Ratchathani

                     University, Faculty of Science, Thailand

2013 – 2019   Ph.D. candidate in Chemistry, Suranaree University of

                     Technology, Institute of Science, Thailand

Scholarship

2010 – 2018   Science Achievement Scholarship of Thailand (SAST)

Publications

1. <u>N. Sosa</u>, N. Chanlek, J. Wittayakun, **Ultrason. Sonochem.**, 62 (2020) 104857.

2. C. Keawkumay, W. Rongchapo, <u>N. Sosa</u>, S. Suthirakun, I.Z. Koleva, H.A. Aleksandrov, G.N. Vayssilov, J. Wittayakun, **Mater. Chem. Phys.**, 238 (2019) 121824.

3. M. Pimsuta, <u>N. Sosa</u>, K. Deekamwong, C. Keawkumay, Y. Thathong, S. Rakmae, S. Junpirom, S. Prayoonpokarach, J. Wittayakun, **Suranaree J. Sci. Technol.**, 25 (2018) 177-190.

4. N. Osakoo, C. Pansakdanon, <u>N. Sosa</u>, K. Deekamwong, C. Keawkumay, W. Rongchapo, N. Chanlek, J. Jitcharoen, S. Prayoonpokarach, J. Wittayakun, **Mater. Chem. Phys.**, 193 (2017) 470-476.